Development of advanced human intestinal *in vitro* models

***

Entwicklung von erweiterten humanen intestinalen *in vitro* Modellen

Doctoral thesis for a doctoral degree
at the Graduate School of Life Sciences,
Julius-Maximilians-Universität Würzburg,
Section Clinical Sciences

submitted by

Matthias Oliver Schweinlin

from Lörrach

Würzburg 2016

Submitted on: ....

Members of the *Promotionskomitee*:

Chairperson: Prof. Dr. Thomas Hünig

Primary Supervisor: Prof. Dr. Heike Walles

Supervisor (Second): Prof. Dr. Stefan Störk

Supervisor (Third): PD Dr. Beate Niesler

Date of Public Defence: ....

Date of Receipt of Certificates: ....

Table of contents

List of figures

List of tables

Abbreviations

Table 1: List of abbreviations

Abbreviation	long term
%	percent
®	registered
°C	degrees centigrade
Ø	average
µg	microgram
µl	microliter
µm	micrometer
2D	two-dimensional
3D	three-dimensional
3Rs	replacement, reduction and refinement
ABC	ATP-binding cassette
ADMET	absorption, distribution, metabolism, excretion and toxicity
ADP	adenosine diphosphate
APC	antigen presenting cells
ATP	adenosine triphosphate
AUT	Austria
BCS	biopharmaceutics classification system
BMP	bone morphogenetic protein
BR	bioreactor
BSA	bovine serum albumin
CBC	crypt base columnar
CD-[number]	cluster of differentiation
CD	crohn's disease
CK 18	cytokeratin 18
cm	centimeter
CO_2	carbon dioxide
Da	dalton
DAPT	N-[N-(3,5-Difluorophenacetyl)-l-alanyl]-S-phenylglycine t-butyl ester

Abbreviation	long term
DAPI	4',6-Diamidino-2-phenylindole
DCs	dendritic cells
DE	definitive endoderm
DMEM	dulbecco's modified eagle medium
DMSO	dimethyl sulfoxide
DNA	deoxyribonucleic acid
ECM	extracellular matrix
EDTA	ethylenediaminetetraacetic acid
EGF	epidermal growth factor
ELISA	enzyme-linked immunosorbent assay
ER	Endoplasmic reticulum
ESCs	embryonic stem cells
EtOH	ethanol
Et al.	et alii
FAE	follicle associated epithelium
FDA	Food and Drug Administration
FCS	fetal calf serum
FITC	fluorescein-isocyanate
g	gram
g	gravity
GALT	gut-associated lymphoid tissue
GER	Germany
h	hours
HCl	hydrogen chloride
HBSS	Hanks' Balanced Salt Solution
H&E	haematoxylin and eosin
IBD	inflammatory bowel disease
IECs	intestinal epithelial cells
IHC	immunohistochemistry
iPSCs	induced pluripotent stem cells
ISCs	intestinal stem cells
kDa	kilo Dalton

Abbreviation	long term
kGy	kilo Gray
LGR5	Leu-rich repeat-containing G protein-coupled receptor 5
m	meter
M	molar
M cells	microfold or membranous cells
ManPP-PLGA-NPs	Mannose-PEG-PAGE-PLGA-nanoparticles
Mdr1	multi-drug-resistance-protein 1
MEM	Minimum Essential Medium
mg	milligram
min	minutes
ml	milliliter
mm	millimeter
mM	millimolar
NaCl	sodium chloride
NEAA	non-essential amino acids
NL	the Netherlands
NPs	nanoparticles
OD	optical density
OECD	Organization for Economic Co-operation and Development
OS	orbital shaker
PAGE	poly(allyl glycidyl ether)
PCR	polymerase chain reaction
PBS$^-$	phosphate buffered saline without calcium and magnesium ions
PBS$^+$	phosphate buffered saline containing calcium and magnesium ions
PEG	poly(ethylene glycol)
Pen/Strep	penicillin/streptomycin
PET	polyethylenterephthalat
PFA	paraformaldehyde
PLGA	poly(lactic-co-glycolic acid)
PP-PLGA-NPs	PEG-PAGE-PLGA-nanoparticles

Abbreviation	long term
PPAR-γ	Peroxisome proliferator-activated receptor γ
PSCs	pluripotent stem cells
qPCR	real-time quantitative PCR
rpm	revolutions per minute
RT	room temperature
SEM	scanning electron microscopy
SIS	small intestine mucosa
SIS-muc	small intestine mucosa with mucosa
TA	transit amplifying
TEER	transepithelial resistance
TEM	transmission electron microscopy
TK	toxicokinetics
UC	ulcerative colitis
USA	United States of America

Summary

The main function of the small intestine is the absorption of essential nutrients, water and vitamins. Moreover, it constitutes a barrier protecting us from toxic xenobiotics and pathogens. For a better understanding of these processes, the development of intestinal *in vitro* models is of great interest to the study of pharmacological and pathological issues such as transport mechanisms and barrier function. Depending on the scientific questions, models of different complexity can be applied.

In vitro Transwell® systems based on a porous PET-membrane enable the standardized study of transport mechanisms across the intestinal barrier as well as the investigation of the influence of target substances on barrier integrity. However, this artificial setup reflects only limited aspects of the physiology of the native small intestine and can pose an additional physical barrier. Hence, the applications of this model for tissue engineering are limited.

Previously, tissue models based on a biological decellularized scaffold derived from porcine gut tissue were demonstrated to be a good alternative to the commonly used Transwell® system. This study showed that preserved biological extracellular matrix components like collagen and elastin provide a natural environment for the epithelial cells, promoting cell adhesion and growth. Intestinal epithelial cells such as Caco-2 cultured on such a scaffold showed a confluent, tight monolayer on the apical surface. Additionally, myofibroblasts were able to migrate into the scaffold supporting intestinal barrier formation.

In this thesis, dendritic cells were additionally introduced to this model mimicking an important component of the immune system. This co-culture model was then successfully proven to be suitable for the screening of particle formulations developed as delivery system for cancer antigens in peroral vaccination studies. In particular, nanoparticles based on PLGA, PEG-PAGE-PLGA, Mannose-PEG-PAGE-PLGA and Chitosan were tested. Uptake studies revealed only slight differences in the transcellular transport rate among the different particles. Dendritic cells were shown to phagocytose the particles after they have passed the intestinal barrier. The particles demonstrated to be an effective carrier system to transport peptides across the

intestinal barrier and therefore present a useful tool for the development of novel drugs.

Furthermore, to mimic the complex structure and physiology of the gut including the presence of multiple different cell types, the Caco-2 cell line was replaced by primary intestinal cells to set up a de novo tissue model. To that end, intestinal crypts including undifferentiated stem cells and progenitor cells were isolated from human small intestinal tissue samples (jejunum) and expanded *in vitro* in organoid cultures. Cells were cultured on the decellularized porcine gut matrix in co-culture with intestinal myofibroblasts. These novel tissue models were maintained under either static or dynamic conditions.

Primary intestinal epithelial cells formed a confluent monolayer including the major differentiated cell types positive for mucin (goblet cells), villin (enterocytes), chromogranin A (enteroendocrine cells) and lysozyme (paneth cells). Electron microscopy images depicted essential functional units of an intact epithelium, such as microvilli and tight junctions. FITC-dextran permeability and TEER measurements were used to assess tightness of the cell layer. Models showed characteristic transport activity for several reference substances. Mechanical stimulation of the cells by a dynamic culture system had a great impact on barrier integrity and transporter activity resulting in a tighter barrier and a higher efflux transporter activity.

In Summary, the use of primary human intestinal cells combined with a biological decellularized scaffold offers a new and promising way to setup more physiological intestinal *in vitro* models. Maintenance of primary intestinal stem cells with their proliferation and differentiation potential together with adjusted culture protocols might help further improve the models. In particular, dynamic culture systems and co-culture models proofed to be a first crucial steps towards a more physiological model. Such tissue models might be useful to improve the predictive power of *in vitro* models and *in vitro in vivo* correlation (IVIVC) studies. Moreover, these tissue models will be useful tools in preclinical studies to test pharmaceutical substances, probiotic active organisms, human pathogenic germs and could even be used to build up patient-specific tissue model for personalized medicine.

Zusammenfassung

Die Hauptfunktion des Dünndarms besteht in der Aufnahme von lebenswichtigen Nährstoffen, Wasser und Vitaminen. Zudem stellt er eine Barriere dar, die uns vor toxischen Fremdstoffen und Pathogenen schützt. Um diese Prozesse besser zu verstehen, ist die Entwicklung neuer *in vitro* Modellen des Darms von großem Interesse um pharmakologische und pathologische Studien durchzuführen. Abhängig von der wissenschaftlichen Fragestellung können Modelle von unterschiedlicher Komplexität zur Anwendung kommen.

In vitro Transwell® Systeme basierend auf einer porösen PET-Membran ermöglichen die Untersuchung von Transportmechanismen über die intestinal Barriere und den Einfluss von Wirkstoffen auf deren Integrität. Dieser künstliche Aufbau ähnelt jedoch nur eingeschränkt der Physiologie des Dünndarms und kann eine zusätzliche physikalische Barriere darstellen. Die Anwendungsmöglichkeiten dieses Modells im Tissue Engineering sind daher begrenzt.

Gewebemodelle basierend auf einer dezellularisierten biologischen Matrix hergestellt aus Schweinedarmgewebe haben sich als gute Alternative zum herkömmlichen Transwell® System herausgestellt. Diese Studie zeigt, dass die erhaltenen Komponenten der biologischen Extrazellulärmatrix wie Kollagen und Elastin eine natürliche Umgebung für die Epithelzellen bieten und Zelladhäsion und Wachstum der Zellen fördern. Darmepithelzellen wie Caco-2 Zellen, welche auf einer solchen Matrix kultiviert wurden, bildeten einen konfluenten, dichten Monolayer auf der apikalen Oberfläche aus. Zusätzlich ermöglichte dieser Aufbau die Migration von Myofibroblasten in die Matrix, was die Bildung der intestinalen Barriere unterstützt.

In dieser Doktorarbeit wurden zusätzlich dendritische Zellen als wichtige Komponente des adaptiven Immunsystems in das Modell integriert. Dieses Ko-Kultur Modell erwies sich als geeignet um partikuläre Formulierungen zu testen, welche als Transportsysteme für Tumorantigene entwickelt wurden. Es wurden Partikel basierend auf PLGA, PEG-PAGE-PLGA, Mannose-PEG-PAGE-PLGA und Chitosan untersucht. Aufnahmestudien ergaben nur geringfügige Unterschiede in den Transportraten zwischen den verschiedenen Partikeln. Es konnte ausserdem gezeigt

werden, dass dendritische Zellen die Partikel phagozytieren, nachdem sie die intestinale Barriere überwunden haben. Die Partikel erwiesen sich als effektives Transportsystem um Peptide über die intestinale Barriere zu schleusen und stellen daher ein nützliches Werkzeug für die Entwicklung neuartiger Medikamente dar.

Um die komplexe Struktur und Physiologie des Darms noch besser nachzustellen, wurde für den Aufbau des Modells die Caco-2 Zelllinie durch primäre Darmzellen ersetzt. Die Darmkrypten, welche undifferenzierte Stammzellen und Vorläuferzellen enthalten, wurden aus humanen Dünndarmgewebe, dem Jejunum, isoliert und *in vitro* expandiert. Die Zellen wurden zusammen mit Myofibroblasten auf der dezellularisierten Schweinedarmmatrix, unter statischen und dynamischen Bedingungen, kultiviert.

Die primären Darmepithelzellen bildeten einen konfluenten Monolayer, welcher alle differenzierten intestinalen Zelltypen aufwies, gezeigt durch Zellen positiv für Mucin (Becherzellen), Villin (Enterozyten), Chromogranin A (enteroendokrine Zellen) und Lysozym (Paneth-Zellen). Mit Hilfe von Elektronenmikroskopie ließen sich essentielle funktionelle Einheiten eines intakten Epithels darstellen, wie die Mikrovilli und Tight-Junctions. Um die Dichtigkeit des Epithels zu überprüfen wurde mit FITC-Dextran die Permeabilität bestimmt und TEER-Messungen durchgeführt. Die Modelle zeigten einen charakteristischen Transport für mehrere Referenzsubstanzen. Mechanische Stimulation durch ein dynamisches Kultivierungssystem hatte einen starken Einfluss auf die Barriereintegrität und Transporteraktivität der Modelle, was sich in einer dichteren Barriere und erhöhten Efflux-Transporteraktivität widerspiegelte.

Alles in allem bietet die Verwendung primärer intestinaler Zellen in Kombination mit einer dezellularisierten biologischen Matrix eine neue, vielversprechende Möglichkeit physiologischere *in vitro* Modelle des Darms aufzubauen. Der Erhalt intestinaler Stammzellen mit ihrem Proliferations- und Differenzierungspotential zusammen mit angepassten Protokollen könnte dabei helfen die Modelle weiter zu verbessern. Insbesondere die dynamische Kultivierung und die Ko-Kultur-Modelle erwiesen sich als entscheidender Schritt auf dem Weg zu physiologischeren Modellen. Solche

Gewebemodelle könnten sich als nützlich erweisen, wenn es darum geht die Vorhersagekraft der *in vitro* Modelle, sowie die *in vitro-in vivo* Korrelation zu verbessern. Solche Gewebemodelle können ein nützliches Werkzeuge in der präklinischen Forschung für die Testung von pharmazeutischen Wirkstoffen, probiotisch aktiven Organismen, sowie humaner pathogener Keime sein und sogar zum Aufbau personalisierter Modelle für die regenerative Medizin dienen.

1 Introduction

1.1 The small intestine

1.1.1 Anatomy and physiology of the small intestine

The small intestine is the part of the gastrointestinal tract were enzymatic digestion of the *bolus* takes place and nutrients, important vitamins, and drugs get absorbed. The small intestine starts after the *pyloric sphincter* distally to the stomach and ends in the colon *ascendens*. It can be divided into three parts: duodenum, jejunum and ileum. The transition between the three parts is smooth and differentiation only possible on microscopic scale whereas villi decrease in size from the duodenum to the ileum. The duodenum has the shape of a "C", is about 25 to 30 cm long and shows the highest uptake rate of carbohydrates and proteins of the gut [1]. Brunner´s glands are located in the upper part directly adjacent to the pylorus secreting bicarbonate to neutralize the gastric acid and thereby protecting the intestinal mucosa [2]. The two pancreatic ducts end in the duodenum at the papillae, secreting enzymes for digestion of carbohydrates, lipids and proteins. Additionally the *ductus choledochus* ending in the duodenum allows emulgation of lipids by bile. The jejunum and the ileum together have a length of about 3 m on average, whereas 2/3 belong to the jejunum and 1/3 is part of the ileum. Next to nutrient uptake, vitamins, micronutrients and minerals are absorbed in this part of the small intestine which is supported by a long passage time of the food bolus of 8 to 16 hours (h) [3]. Along this line, the surface of the mucosa is increased to support effective resorption. The gut tube shows circular folds, which reach up to 1 cm in the tube's lumen. The epithelium grows in finger-like structures, the villi; moreover, every enterocyte has its apical surface covered by microvilli to furthermore enlarge the area for absorption [4]. Given a total length of about 3 m, an average diameter of 2.5 cm and a surface enlargement by villi and microvilli of 6.5 to 13 times the calculated surface is between 30-300 m^2 [5, 6]. The whole gut tube is covered by a monolayer of epithelial cells including the mucosa's typical mucus layer, which protects the epithelium from mechanical damage and direct contact with bacteria [7, 8]. The lamina propria, the stroma tissue directly beneath the epithelium, shows a complex system of vascularization and lymphatic vessels to support effective

transport of nutrients. Next to the stromal cells the lamina propria also contains immune and smooth muscle cells [2]. The submucosa tissue with blood vessels and the submucosal (Meissner) nerve plexus consists of collagen and elastic fibers allowing stretching of the gut tube in both, longitudinal and transverse direction. The layer underlying the *muscularis mucosae* contains inner circular and outer longitudinal muscles and the myenteric (Auerbach) nerve plexus allowing for the transport of the chymus by peristaltic movements and intermixture by pendular and segmental movements [3]. The enteric nervous system gives the gut nearly complete functional autonomy, *e.g.* motoric coordination or secretion of glands [2]. With exception of the duodenum, the small intestine is covered with serosa, a thin connective tissue layer and connected to the mesenterium [1].

1.1.2   The intestinal mucosa - cell types and molecular regulation

The intestinal epithelium is known to be a highly regenerative tissue. Each intestinal villus is surrounded by several crypts of Lieberkühn, where stem cells and progenitor cells are located to ensure compensation of natural cell loss and regeneration of injuries. To guarantee an optimal function of the epithelium the cells undergo rapid renewal [9]. At the tip of the villus, cells die by a complex process of cytoskeletal remodelling and are being shed off, while at the same time barrier integrity is being ensured [10]. About 10^{11} new cells have to be generated every day in order to replace dying cells within the intestine [11]. This way, the small intestine renews its complete mucosal surface about every 5 to 6 days [12].
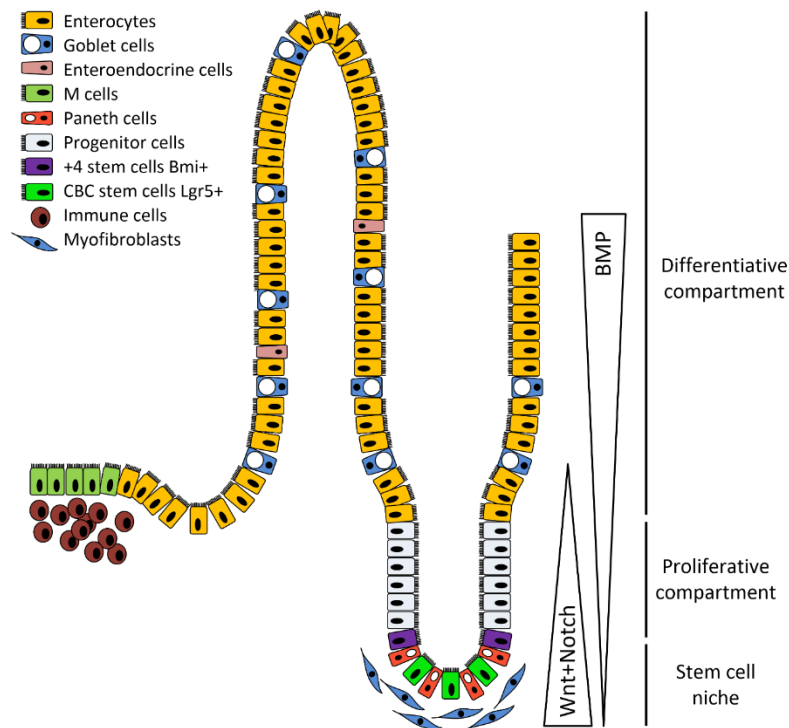
Figure 1: The intestinal epithelium. The bottom of the crypts contains the intestinal stem cells and the highly proliferative progenitor cells which are responsible for regeneration and maintenance of the epithelium. On their way from the crypts up to the top of the villi the cells differentiate into the different cell types with their repective functions. This shift from proliferation towards differentiation is induced by contrariwise signalling of antagonistic pathways. Gradients are created by neighbouring cells such as myofibroblasts which provide signals to the epithelial cells. Peyer patches with the immune cells beneath the epithelium are involved in immune defence and tolerance mechanisms. Adapted from Yeung et al. 2011 [11].

Stem cells of the gut

The intestinal stem cells are located together with the Paneth cells at the bottom of the crypts. Crypt base columnar (CBC) stem cells were shown to highly express Lgr5 (Leu-rich repeat-containing G protein-coupled receptor 5), a Wingless-related integration site pathway (Wnt) target gene [13]. Lgr5 encodes for a seven transmembrane receptor which modulates the Wnt signalling. Binding R-spondin, a Wnt agonist, the Lgr5-receptor is responsible for the amplification of the Wnt-signal and thereby maintains stemness within the niche [14, 15]. Lineage tracing in mice identified these cells as self-renewing multipotent adult stem cells [16]. Lgr5^{+} cells can

generate mini guts (organoids) *in vitro* while negative cells were not able to generate these epithelial organoids [17]. Due to the lack of a specific human anti-Lgr5 antibody clear identification of human Lgr5 positive intestinal stem cells still remains difficult. It has been reported that symmetrical cell division seems to be predominant in the Lgr5$^+$ stem cells, but it is still unknown how cell fate is determined between stem cells or transit amplifying (TA) cells [18]. This could either be a stochastic process or it could likely be the case that local niche and biomechanical factors post-mitotically guide cell fate depending on the position within the niche [9]. Apart from Lgr5, olfactomedin 4 (Olfm4), achaete-scute family bHLH transcription factor 2 (Ascl2), musashi RNA binding protein 1 (Msi1), and SPARC-related modular calcium-binding protein 2 (Smoc2) are reported as markers for CBC stem cells [19-22]. CBC stem cells were shown to have proliferative activity and to be particular sensitive to radiation damage.

Other studies identified cells at position +4 of the crypt as stem cells with the capability of multilineage differentiation and potential of self-renewal [23]. The proto-oncogene, polycomb ring finger (Bmi1), HOP homeobox (Hopx), leucine-rich repeats and immunoglobulin-like domains protein 1 (Lrig1) and telomerase reverse transcriptase (TERT) were reported as markers of +4 cells which were identified to have Bromodeoxyuridine (BrdU) label retaining properties, are damage resistant and more quiescent, slowly dividing cells [24-27]. The contradictory results led to a more plastic model of stem cell identity predicting a two-stem-cell model, where CBC stem cells are active and ensure the daily epithelial homeostasis, while +4 more quiescent cells are "reserve" stem cells responsible for maintenance or compensation of the resident stem cell population in case of an injury [9, 25, 28, 29].

Progenitor cells

Progenitor cells or transit amplifying cells (TA) are located in the crypt above the +4 zone. These fast proliferating progenitor cells are produced by the CBC stem cells and divide 2-3 times per day [30]. On their way migrating up the crypt to the base of the villi the cells differentiate in a step-wise manner towards absorptive or secretory lineage.

Differentiated cells

The vast majority of the intestinal epithelial cells are enterocytes, which are responsible for absorption of nutrients within the gut. These cells are polarized, their apical surface is covered by microvilli and they are connected to each other by tight and adherence junctions. Different digestion enzymes are located on the "brush border" responsible for the terminal digestion steps (*e.g.* maltase, lactase, sucrase, erepsin). Enterocytes show different transporter/channel patterns on the apical and basolateral surfaces, respectively, allowing them to build up ion gradients (Na^+/K^+-ATPase), which are important for various transport mechanisms. Characteristic transporters allow the uptake of sugars (SGLT-1 and GLUT2/5), peptides and amino acids (PepT 1, sodium-dependent and -independent amino acid transporters) [31]. A special transporter found in these cells is the Multidrug-resistance-protein 1 (Mdr1 or P-glycoprotein), which is an efflux transporter having a major impact on the bioavailability of drugs. Characteristic for these cells is also the expression of enzymes of the cytochrome P450 superfamily which can catalyse the biotransformation of endo- and xenobiotics and are responsible for metabolic elimination of 50 % of commonly used drugs [32].

Apart from the enterocytes other cell types of the secretory lineage can be found in the gut: The goblet cells which secrete various mucins to cover the mucosal surface with an adherent mucus layer in order to protect it from mechanical induced injuries and keep bacteria at distance to the epithelium. These cells show typical intracellular mucin loaded vesicles towards the apical membrane, which fuse with the cell membrane and release the mucins into the gut lumen [8]. The mucus secreted in the small intestine primarily consists of mucin 2, a large, negatively charged glycoprotein that binds large amounts of water building a gel-like insoluble layer [33]. The correct folding and organization of these large proteins is controlled by a pH shift induced by bicarbonate secretion of the enterocytes [34]. In the small intestine the mucus is single-layered, whereas in the colon it consists of two layers [35]. The immune system has a strong influence on mucus secretion by the goblet cells confirming the important role of the mucus as first line of defence against intruding pathogens [8].

Another important cell type are Paneth cells, which are located at the base of the crypts in between the Lgr5$^+$ CBC stem cells. In contrast to the other differentiated cells these cells can only be found in the small intestine and directly develop from the Lgr5$^+$ stem cells instead of the progenitors [36]. Characteristic for these cells is the large ER and Golgi networks typical for secretory cells as well as the apical clusters of granules [37]. Paneth cells are part of the innate immunity as they secrete host-defensive components like lysozyme and defensins [38, 39]. Their secreted products protect the host from pathogenic bacteria and largely influence the microbiota [40, 41]. In addition to these immunological functions, the Paneth cells were shown to be important for the CBC Lgr5$^+$ stem cells as they provide essential factors for homeostasis, self-organization, self-renewal and repair after injuries [36, 42]. Gene expression studies showed that these cells produce Epidermal Growth Factor (EGF), Wnt3A, and Delta like ligand 4(Dll4) essential for mini gut development *in vitro* [43]. A recently published study also suggests Paneth cells to be nutrient sensitive and stem cell activity inducing in response to calorie restriction [44].

Enteroendocrine cells within the intestine secrete hormones controlling the activity of the GI-tract. There are two main groups of enteroendocrine cells in the small intestine. The intestinal specific cells, which secret glucose-dependent insulinotropic polypeptide (GIP), Secretin, CCK, Neurotensin, PYY, and glucagon-like peptide-1/-2 (GLP-1/-2) to control, *e.g.* satiety and gastric emptying and secondly, cells producing ghrelin and motilin, which are responsible for hunger and increasing motility of the gut. There are also pan GI-tract cells, which can be differentiated into 5HT- and Substance P- producing cells influencing metabolism and gastrointestinal motility and Somatostatin-secreting cells to control the secretion of mucus [45, 46].

In direct contact with the environment, the gut is exposed to many proteins and microorganisms. In order to maintain a balance between protection and tolerance, the immune system is strongly embedded in this organ in the form of the gut-associated lymphoid tissue (GALT). The follicle-associated epithelium (FAE) is a tissue specialized in sampling antigens from the gut lumen to elicit an immune response, a task mainly accomplished by M cells (microfold or membranous cells) [47]. M cells show a very high capacity for uptake and translocation of antigens to make them accessible for

lymphocytes. Typical for these cells are shorter irregular microvilli and a basolateral pocket for lymphatic cells [48].

1.1.3 Gut homeostasis - regulation/dysregulation

The homeostasis within the intestinal epithelium is mainly regulated by three different pathways which build gradients along the crypt/villus axis, leading to a spatial separation of cell differentiation and proliferation (Fig. 1). Wnt-signalling is the key pathway in driving proliferation and maintaining the stemness within the crypt, with a strong activity on the base and decreasing signal towards the upper part. The Wnt-signal by ligand secretion is mainly provided by the Paneth cells and neighbouring myofibroblasts at the base of the crypt [43, 49]. Beside the Wnt-signal, Notch-signalling was shown to be important for maintenance, proliferation, and differentiation of ISCs and progenitor cells [50]. Inhibition of Notch signalling, *e.g.* by DAPT, leads to differentiation into the secretory lineage [51]. The Notch-signal is provided by cell-cell-interaction with neighbouring cells like CD4+ T-cells due to membrane located ligands like Jagged-1. It has also been shown to play an important role in IEC differentiation and barrier integrity [52]. BMP-signalling counteracts cell proliferation within the intestinal epithelium inducing differentiation of the cells. BMPs (bone morphogenetic proteins) are secreted by subepithelial stromal cells and epithelial cells, while myofibroblasts located next to the stem cells at the base of the crypt express the BMP inhibitor noggin [53].

Imbalance within this fine-tuned regulated system can have serious consequences. Cancer in the intestine predominantly develops in all parts of the colon and rectum and is the third most common cancer in Germany with about 60.000 new cases every year [54]. The colorectal cancer originates from the intestinal epithelium in the colon, in most cases an adenocarcinoma which has glandular origin or characteristics. The change from normal to abnormal cell growth can be caused by several driver mutations in the genome. More than one of these changes are necessary to turn a cell into a cancerous cell. The most common mutation is the one of the Adenomatous polyposis coli gene (APC), which causes increased Wnt-signalling and unnaturally high proliferation. Additional mutations in cell division controlling proteins like P53 or BAX

are typical. Also, mutations in genes encoding deactivating proteins responsible for programmed cell death like TGF-ß and DCC can be found. Oncogenes like KRAS, RAF and PI3K normally stimulate cell division caused by growth factors. Mutations in these proteins lead to over-activation of proliferation. The cause of these mutations can be different factors such as genetic predisposition, exogenous factors, *e.g.* influence of infections or chemicals, as well as life style or age [55].

Inflammatory bowel diseases (IBD) are chronical inflammations of the gastrointestinal tract together with an abnormal bacteria growth. The two most common types are ulcerative colitis (UC) and Crohn´s disease (CD). The latest published studies suggest that chronical disease-related genes, together with environmental factors, may be associated with the outcome of the diseases. The highest number of people with IBDs can be found in northern Europe and North America while Asia shows the lowest incidence and prevalence [56]. Colitis shows an incidence of 1.2 to 20.3 and a prevalence of 7.6 to 246.0 cases per 100.000 per year [57]. The pathogenesis of UC is characterized by dysregulations in the immune system but also genetic variants resulting in reduced expression of peroxisome proliferator–activated receptor γ (PPAR-γ) and abnormal mucus production. While UC is restricted to the colon, CD can occur in the entire gastrointestinal tract from the mouth to the rectum but primarily affects the terminal ileum. The incidence is 0.03 to 15.6 and the prevalence 3.6 to 214.0 cases per 100.000 per year [57]. CD shows a clear genetic background with an increased risk for the next generation [58]. Patients of both diseases show an increased production of proinflammatory cytokines (IL-8, IL-6, TNF-α, IL-1β, TL1A), which leads to pathological alterations and dysfunction of the intestinal epithelium [59].

1.2   The gut barrier - intestinal transport mechanisms

The intestinal lumen is covered by a monolayer of high-prismatic epithelial cells, which build a highly selective barrier sealed by tight junctions between the cells. The epithelial cells show polarization allowing to for the generation of concentration gradients by expression of specific transporters on the apical as well as on the basolateral side, which are separated by the tight junctions. Specific and unspecific transport systems can be distinguished as follows:
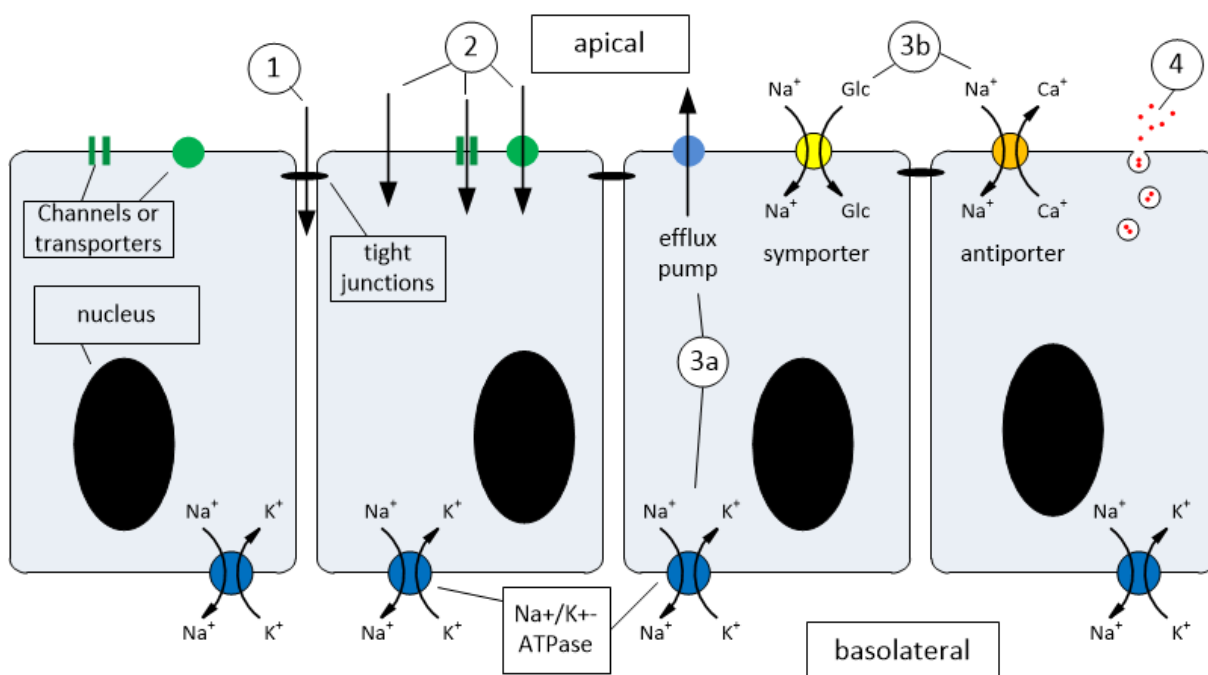
Figure 2: Transport mechanisms through the epithelium. Paracellular transport trough the cellular gap (1), passive transport directly over the cell membrane, through channels and with transporters or carriers (2), primary active transport by Na+/K+ – ATPase and efflux transporter (3a), secondary active transport by symporter and antiporter (3b) and uptake by endocytosis (4).

1.2.1 Paracellular transport

Transport through the intercellular gap between two epithelial cells allows transport of ions, water and a few small molecules. This pathway allows hydrophilic drugs which cannot overcome the lipophilic cellular membrane and have no specific transporter system to pass the intestinal barrier [60]. This passive transport is driven by the concentration gradient and by solvent drag (water flow draging small molecules across the barrier). The tight junctions which gate the paracellular gap allow small molecules with a molecular weight of up to 200 Da to pass but flexibility of the molecule structure seems also important [61].

1.2.2 Transcellular passive/active transport

Diffusion of molecules over the apical cell membrane is called transcellular passive transport. This passive transport requires a concentration gradient and only hydrophobic molecules can pass the lipophilic cell membrane. For ions and molecules

with hydrophilic character there are specific channels, carriers or pumps. All these transmembrane transporters are highly regulated and selective for their specific molecule. Carrier mediated transport along the gradient is called passive facilitated transport which allows specific transport of hydrophilic molecules [2]. For active transport of molecules against a gradient energy is needed. This energy is provided by the hydrolysis of ATP to ADP. The primary active transport allows transport of ions over the cell membrane under usage of ATP to build up gradients. The most important ion pump is the Na^+-/K^+-ATPase which, at the basolateral membrane actively transports Na^+ out and K^+ in the cell. The efflux transporters (1.2.3) of the ATP-binding cassette (ABC) -transporter family, which actively transport drugs out of the cell to protect also belong to the ATP-powered primary active transporters (*e.g.* P-glycoprotein). The secondary active transport is a co-transport of a substrate with ions, which are transported passive along a gradient. It can be distinguished between symporter where both ion and substrate are transported along the gradient (*e.g.* glucose symporter SGLT1) and an antiporter which transports the co-transported substrate in the opposite direction (*e.g.* sodium-calcium-exchanger) [62].

1.2.3 Efflux transport

To protect the human body from harmful cytotoxic molecules the epithelial cells express transporters on the apical membrane to actively pump substances out of the cell towards the gut lumen. Efflux transporters, like the Mdr1 (P-glycoprotein), breast cancer resistance protein (BCRP) and multidrug resistance-associated protein 2 (MRP2), are expressed in the intestinal epithelium [63]. These transporters belong to the group of multi-drug-resistance proteins, which are part of class B of the ABC-transporter family. These transporters are especially of interest in drug development as some drugs are ligands of these efflux transporters which has major impact on their bioavailability [64].

1.2.4 Endocytosis

A totally different kind of active transport is endocytosis, which is the uptake of bigger solved molecules or particles by invagination of cell membrane eventually forming intracellular vesicles. The transport is a specific receptor-mediated process, for ligands

like LDL or transferrin. After binding of the ligand to the transmembrane receptor, clathrin binds to the adaptor proteins. Clathrin by its protein structure promotes a critical impulse for the formation of rounded vesicles for intracellular trafficking [62].

1.3 Preclinical model systems

Knowledge of intestinal absorption and toxicokinetics of individual drugs are mandatory in pre-clinical drug development [65]. So far animal experiments have a long tradition in pre-clinical risk assessment for potential new pharmaceuticals. Although, to reduce animal experiments and to lower the risk of late clinical failure, since 2010, more and more new *in vitro* and *in silico* methods have been approved by the authorities for preclinical testing [66]. Lately there is more and more data indicating a bad correlation between animal derived data and humans due to interspecies differences in physiology, as well as metabolism and biochemical pathways.

1.3.1 In vivo

The classical test by the OECD guideline 417 to determine toxicokinetics (TK) relies on rat based animal testing. Such models require interspecies extrapolation for consideration of species differences in adsorption, distribution, metabolism, excretion and toxicity (ADMET). To look for relevance of *in vivo*, animal derived data in humans, chemical-specific assessment factors are used to take interspecies and intraspecies differences in sensitivity into account. Next to ethical concerns, high cost and low-throughput make people look for non-animal alternatives. The European Union started a policy initiative to reduce animal testing by prohibition of animal studies for cosmetics in 2013 (2003/15/EC).

1.3.2 Ex vivo

Ex vivo models are important to investigate and assess the transport and safety of drugs, cell-cell-communication and interactions with pathogens or xenobiotics. The gut is a highly organized and complex organ which makes it impossible to model all its properties *in vitro*. Freshly excised tissue usually from mice, rats or piglets, provides a model for transport assays with preserved microstructure which closely mimics the *in*

vivo physiology. Compared to common dish culture these models provide a three-dimensional (3D) environment. How substances or microorganisms interact with the mucosa depends on their size, surface properties, solublility or form. All substances and organisms first get into contact with the mucus, which overlies the epithelium, and also the microbiome as an potential factor of metabolism or interaction has to be considered [67]. Particulate substances have a special routing as they get take up by microfold cell (M cells) or directly by dendritic cells and accumulate in Peyer´s patches. A general challenge of *ex vivo* models is to maintain the properties of this complex tissue for a longer time. Due to the high complexity and the lack of vascularization the tissue is not provided sufficiently with nutrients which can lead to rapid changes. Loss of functionality is caused by hypoxia, decreasing viability of the cells and necrosis. Most short duration studies have been conducted using the Ussing chamber and the non-converted gut sac model. The Ussing chamber was first mentioned in 1951 by Ussing and Zehran to study sodium transport in frog skin. Later on, the chamber was discovered as a useful tool to study transport and barrier properties of the intestine. The Ussing chamber has two chambers (apical/basolateral) separated by the mucosa/submucosa which are filled with physiological buffer and are temperature controlled. This construction allows to investigate the transport of various substrates of interest [68]. Additionally, properly installed electrodes can be used to monitor the barrier integrity during the experiment as well as the influence of drugs on the physiology which can give important information on pharmacological properties of a test substances [69]. The non-everted gut sac is a very simple model. A defined length of gut lumen is closed up with a string on one end, then filled the test substance and finally also closed on the other end. Lying in medium, diffusion from the inner to the outer compartment can be tested. Thus, the additional muscle layers (*muscularis mucosa*) which are not removed during the preparation process can lead to an underestimation of the transport.

1.3.3   In vitro

In vitro models are mostly simplified systems to allow high through-put analysis primarily used to gain information about toxicity or uptake of potential drugs, to investigate infections or disease, like cancer or IBD [70, 71]. The models can differ in

complexity from simple two-dimensional (2D) monocultures in a petri dish to 3D co-culture models with different cell types based on different kinds of scaffolds to mimic the niche of the cells [72, 73]. Additionally, bioreactors can be used to induce defined mechanical stress, which can have strong influence on the physiology of the cells [74, 75]. The models can be also interesting for basic research were co-culture models can help to understand the influence of various cell-cell interactions within complex tissues or stem cell cultures to get information about proliferation, regeneration and differentiation processes within the stem cell niche [76]. Different cell sources provide advantages and disadvantages.

Cell lines

The culture of isolated human intestinal epithelial cells is difficult, complex and expensive. Primary cells showing important physiological features however, are limited in their viability. For this reasons, immortalized adenocarcinoma cell lines like Caco-2 and T84 have been commonly used to study toxicity and absorption mechanisms [77, 78]. These cells can be grown on porous PET-membrane Transwell® inserts. They form polarized epithelial monolayers, which show characteristic microvilli on the apical surface [79]. The two cell lines were shown to spontaneously differentiate into cells similar to mature enterocytes expressing tight junctions and an apical brush border with characteristic digestion enzymes [80]. Compared to the T84, the confluent Caco-2 monolayer shows a significantly lower Transepithelial electrical resistance (TEER) which correlates with an increased permeability of the intestinal epithelial cells and, if decreased, is also used as indicator for cell toxicity. While Caco-2 cells only represent the enterocytes, T84 cells also secrete mucin in cell culture which more closely reflects the *in vivo* situation in the gut [78]. Also, T84 cells respond to external stimuli to activate the innate immune responses analogous to the human intestinal surface [81]. For evaluation of the barrier function serval endpoints are utilized. This can be, for example, the TEER, changes in gene expression of several junction proteins, viability or proliferation of the cells. Supernatants or cell lysate are analyzed to look for example for inflammatory factors, activation proteins, drug concentrations and other parameters. While these immortalized cells offer many advantages, the correlation data generated by using these cell lines and *in vivo* data is

difficult [80]. The cells have a cancerogenic background as they were isolated from tumors and are therefore show differences compared to the true physiological environment [82].

Primary cells

With respect to the limitations of cell line-based models, researchers started working on primary cell based *in vitro* models. In the year 2009, the Clevers group published a new culture method which for the first time allowing the culture of primary intestinal epithelial cells [17]. Providing a 3D environment using Matrigel and the addition of certain growth factors mimics the stem cell niche, the crypt, and therefore allows to maintain stem cell properties and capacity. These intestinal stem cells (ISCs) have the potential to differentiate into all cell types of the intestinal epithelium, the absorptive enterocytes and M cells as well as into secreting cells, like goblet cells, enteroendocrine cells and Paneth cells [17, 83].

The crypts can be isolated from small intestine and colon tissue containing the undifferentiated proliferative cell population of intestinal epithelium, the Lgr5+ stem cells and the progenitor cells [23]. After isolation, the crypts get embedded in Matrigel drops, which are placed in well-plates. Matrigel consists of the basal lamina components such as Collagen IV, Laminin and Fibronectin and provides a 3D environment. For expansion of the cells, growth factors and inhibitors get added to mimic the natural environment at the base of the crypt where Wnt-, EGF and Notch-signals are secreted by Paneth cells and neighbouring mesenchymal cells to promote stemness and proliferation [84]. Cells form organoids with protruding crypt-like structures growing out or cystic roundish spheres. These organoids represent "miniguts" with a lumen and a polarized epithelium containing all characteristic cell populations of the intestinal epithelium [17]. Moving up the crypt, proliferation signals get down-regulated while differentiation is induced by BMP- and Notch-signals. For directed differentiation into the secretory lineage, Notch-signal is reduced by the γ-secretase inhibitor (DAPT) and reduction of Wnt3A [51].

The culture and differentiation of intestinal epithelial cells (IECs) as organoids has been shown for mouse as well as for human cells [17, 85]. Success and yield of isolation

are also dependent on the donor tissue. The age, region of the gut where the tissue was excised, health of the donor and time from tissue extraction to isolation may influence the outcome. The organoid culture presents a nice tool to investigate and understand basic mechanisms of cell biology within the gut [76].

In respect to the development new test systems with broad usage, a monolayer is needed to evaluate the barrier function and perform transport studies. Few models based on transwells with different cell sources are known so far [72, 86-89].

Pluripotent cells - ESCs and iPSCs

Looking more closely at the embryonic development pluripotent stem cells can differentiate into all the three embryonic germ layers. The gut arises from the endodermal germ layer. The endoderm then divides into foregut, midgut and hindgut. The midgut gives rise to the small intestine while the colon develops from hindgut [90]. Differentiation into the intestinal lineage is guided by Wnt- and Notch-signalling [91].

To obtain intestinal epithelial cells, the efficiency of PSCs differentiating into definitive endoderm is the first critical step. Differentiating of both embryonic stem cells (ESCs) and induced pluripotent stem cells (iPSCs) with Activin A and using small molecules to inhibit Wnt- and BMP-signalling results in up to 90 % definitive endoderm (DE) [92]. The characteristic markers for DE, SOX17 and FOXA2 get up-regulated while pluripotent markers like OCT3/4 and Nanog are down-regulated. Mid/hindgut differentiation is promoted by FGF- and Wnt-signalling. Obtained mid/hindgut organoids get embedded in Matrigel which mimics the intestinal stem cell niche by its 3D environment of basal matrix components. For further differentiation into the intestinal lineage and expansion, R-Spondin (Wnt-agonist), EGF and Noggin (BMP-antagonist) are required [93]. These factors of the stem cell niche are produced *in vivo* by the Paneth cells and surrounding mesenchymal cells. To differentiate these undifferentiated cells into the four different epithelial cell types, Wnt-signalling has to be blocked and the Notch-signal inhibited by the γ-secretase inhibitor (DAPT) [94, 95]. The fully differentiated cells are polarized epithelial cells showing characteristic morphology and protein expression. The composition of the different cell types can be

compared to the *in vivo* gut. However, unlike mature adult cells, these cells still show more embryonal immature characteristics.

Pluripotent stem cells (PSCs), either ESCs or iPSCs from mice or humans, provide a promising defined cell source for intestinal models and regenerative medicine [86, 96]. Because these cells can be gained in big numbers from the same source, these cells seem to be good for building up standardized test systems for absorption and toxicity studies.

1.3.4 *In silico* modelling

Computational (*in silico*) modelling is an important tool for early stage screening in drug development and of great financial interest for the pharmaceutical industry. Such systems support the development of tailored drug design optimized to overcome the intestinal barrier. The models are designed to predict ADMET of potential drug candidates which may help to reduce the number of substances and the risk for failure in late clinical trials [97]. Additionally, libraries containing information about ADMET as well as molecular structure, metabolic stability and medical chemistry are set up [98]. Known sets of substances with known characteristics are used to train neural networks which then allow to predict properties of new compounds [99]. Such neural network give the possibility to extend the "Lipinski's rules of five" (which states that for oral activity, a drug should have $\leq$ 5 hydrogen bond donors, $\leq$ 10 hydrogen bond acceptors, a molecular weight of $\leq$ 500 daltons, and maximum logP value of 5) to any other needed factor [100]. In many aspects, proteins are the drug candidates of choice because of their many advantages such as high selectivity, good response to treatment and fewer side effects, while on the other hand they are instable, too big and relatively hydrophilic which makes it hard to cross the cell membrane [101]. For selection of peptides crossing the intestinal barrier, neural networks have been established to predict the permeability based on the peptide-sequence [102]. Despite all the progress made in this field a good prediction of human bioavailability is still not possible. There are several in silico and *in vitro* prediction studies with models based on Caco-2 data showing no correlation with human *in vivo* permeability [103].

1.4 Tissue engineering

Tissue engineering combines cell culture with biomaterial science and bioreactor engineering in order to develop tissue models that mimic the human physiology. Different sources of cells with individual advantages and disadvantages can be used (1.4). Cells have to be expanded and characterized before setting up tissue models. To differentiate and maintain the properties of certain cell types they have to be provided with a specific environment mimicking the natural niche of the cell. These can be a co-culture with neighbour cells which secrete factors stimulating growth or differentiation of the cells or produce a specific matrix. For more defined conditions single recombinant factors or small molecules can be added to the culture medium. Those factors normally build fine regulated gradients *in vivo* which is difficult to implement in such a model. To support the cells in adherence and give the tissue a structure, extracellular matrix (ECM) proteins like collagens, elastin, laminin and fibronectin are used. This can be a porous plastic membrane (PET) coated with ECM proteins [75], a scaffold produced be electrospinning [104], a 3D-printed hydrogel [105] or a decellularized matrix [106]. Another important factor can be mechanical stimulation typical for the cells. This can be for example a pressure force for cartilage cells [107] or shear stress on endothelial or epithelial cells. Put together, this knowledge can help to develop more predictive *in vitro* models which allow us to screen potential drugs or gain new information about the interaction of cells and their environment in basic research. Improved models could help to lower the costs of drug development by decreasing the risk of failure in late phase of clinical trials due to better prediction and also reduce animal testing within the principles of the 3Rs (Replacement, Reduction and Refinement) [108]. Finally, it also opens the possibility to generate tissue for transplantation in patients. This has been already done for more simple structured tissues like skin and cartilage. The transplants can be autografts (same person), allografts (human/human) and xenografts (animal/human). New generation transplants using smart biomaterials aim to integrate a structure with specific function that is slowly taken over by the body and finally completely replaced by own tissue [109]. To generate whole organ transplants the biggest challenge in the field of tissue engineering remains the vascularization of

bigger tissues as cells die because of insufficient supply with nutrients, thus there has been progress made which gives hope to solve that main problem [110].
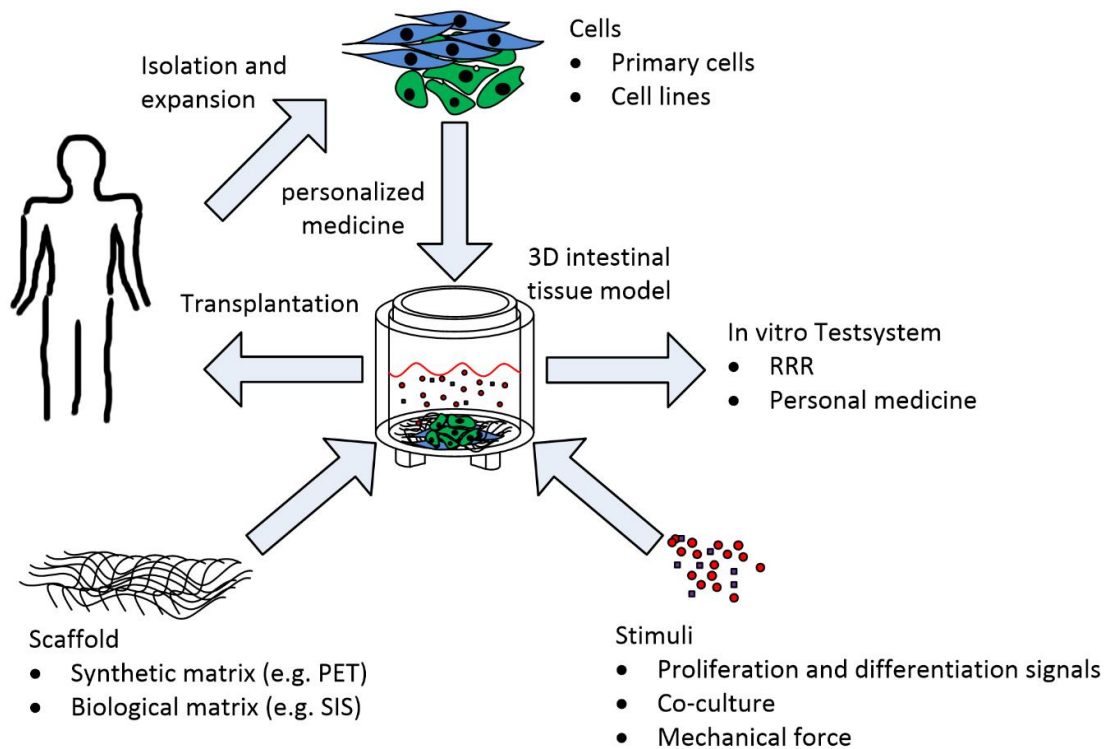
Figure 3: Concept of tissue engineering. Basic methods and components of tissue engineering starting with cell isolation, expansion of the cells and culture in 3D environment under defined conditions.

1.5 Applications of peroral test systems in biomedical research

Intestinal *in vitro* models provide a tool to investigate the ability of potential perorally administered pharmaceutical substances to cross the intestinal barrier which is represented by the epithelial monolayer. The permeability rate of the drug may later on have great impact on the bioavailability of the substance. Compared to animal studies, *in vitro* models allow easy handling and sample analysis. Additionally, human cells can be used to setup the models leading to higher predictive power. Such *in vitro* models also have their limitations. Some models develop very tight or very low non-physiological barriers, the cells lack expression of important transport and metabolic enzymes or the models show no mucus layer, depending on the cells used and the culture conditions [80].

Furthermore, the influence of substances regarding barrier integrity can be looked at by TEER measurement, impedance spectroscopy or reference substances. Also dose depended cytotoxicity can be determined.

For more efficient drug development, pharmaceutical substances can be classified by the Biopharmaceutics Classification System (BCS) of the FDA. Substances are classified by their properties regarding solubility, permeability and dissolution in four categories (Class I-IV). This classification system can be used to estimate bioavailability and bioequivalence by *in vitro* testing and waive or reduce *in vivo* studies [111].

Human intestinal tissue models also provide the possibility to do infection studies to closer investigate the mechanisms of pathogen and host-cell interactions. This is particularly interesting as some pathogens are restricted to humans *e.g. Salmonella Typhi* [112]. Additionally, co-culture models with cells of the immune system allow to study the immune reaction caused by the infection or perorally administered vaccines [113].

2 Scope of thesis

The aim of this doctoral thesis was to develop novel, more physiological and predictive tissue models of the human small intestine. Existing, commonly used cell line-based models like the Caco-2 model have a number of limitations as the cells differ in morphology, cell polarity, have altered gene expression due to their cancerogenic origin and show different barrier function compared to the *in vivo* physiology of the gut. To overcome these limitations we used primary intestinal epithelial cells and fibroblasts from fresh human jejunal tissue of different donors, expanded them and built up co-culture models. Furthermore, we applied a decellularized porcine matrix from the gut providing a more physiological environment supporting the cells in growth and at the same time separating two compartments allowing transport studies *in vitro*. Additionally, we implemented flow conditions to provide *in vivo*-like mechanical stimuli to the cells and prove for influences on the model characteristics. Taken together, this advanced intestinal test system should provide more reliable data in basic and preclinical research.

3 Materials

3.1 Biological materials

Table 2: Biological materials

Tissue/Cells	Source
Porcine jejunum	Pig (6 weeks, female) (Niedermeyer, Dettelbach)
Human cell line Caco-2	DMSZ ACC 169
Human PBMCs	Institute for Clinical Transfusion medicine and Hemotherapy of the University Hospital Würzburg
Human jejunum	University Hospital Würzburg, Institutional Ethics Committee approval number 182/10 (Surgery Unit, PD Dr. med. C. Jurowich)

3.2 Equipment

Table 3: Equipment

Equipment/Device	Producer
Analytical Balance	Kern, Balingen-Frommern (GER)
Aspiration Device: VacuBoy	Integra Biosciences, Fernwald (GER)
Autoclave: „Tecnoclav"	Biomedis, Giessen (GER)
Table-top Autoclave	Systec, Wettenberg (GER)
„Varioklav"	H+P, Hackermoos (GER)
Blocking Station	Leica, Wetzlar (GER)
Cell Incubator: 37°C, 5 % CO_2	Heraeus, Hanau (GER)
Centrifuges: Multifuge X3R	Thermo Fisher Scientific, Dreieich (GER)
Centrifuge 5417R	Eppendorf, Hamburg (GER)
Centrifuge 5424	Eppendorf, Hamburg (GER)
Cold-Storage Room, 4°C	Genheimer, Höchberg
Cooling Plate	Leica, Wetzlar (GER)
Digital Camera	Canon, Krefeld (GER)
Digital Hand Counter	NeoLab, Heidelberg (GER)
Dish Washer	Miele, Gütersloh (GER)
Drying oven	Memmert, Schwabach (GER)
Embedding Station	Thermo Fisher Scientific, Dreieich (GER)
Flow cytometer: FACS Calibur	BD, Heidelberg (GER)

Equipment/Device	Producer
Freezer:	
-80°C	Thermo Scientific, Waltham (USA)
-20°C	Liebherr, Biberach a.d. Riss (GER)
Freezing Container: Mr. Frosty	VWR, Darmstadt (GER)
Fume Hood	Prutscher Laboratory Systems, Neudörfl (AUT)
Hot Air Sterilizer	Memmert, Schwabach (GER)
Ice Maker: „AF-80"	Scotsman, Mailand (ITA)
Immersion Thermostat for Water Bath	Lauda, Lauda-Königshofen (GER)
Incubator	Medite, Burgdorf (GER)
Laminar air flow cabinet Safe 2020	Thermo Fisher Scientific, Dreieich (GER)
Liquid Nitrogen Storage Tank: MVE 815 P-190 (-180 °C)	German-cryo, Jüchen (GER)
Magnetic Stirrer with Integrated Heater: Type 720-HPS	VWR, Darmstadt (GER)
Millicell ERS-2	Millipore, Billerica, MA (USA)
Microplate Reader: Tecan Sunrise	Tecan, Crailsheim (GER)
Microscopes: Axiovert 40C , AxioVision Observer.D1	Zeiss, Göttingen (GER)
Biorevo BZ-9000	Keyence, Neu-Isenburg (GER)
LeicaTCS SP8	Leica, Wetzlar (GER)
Multi-Channel Pipette Plus	Eppendorf, Hamburg (GER)
Multistep Pipette	Brand, Wertheim (GER)
Neubauer Cell Counting Chamber	Hartenstein, Würzburg (GER)
Paraffinized Tissue Floating Bath: Type 1052	Medax, Kiel (GER)
pH Meter	Mettler Toledo, Giessen (GER)
Pipette Tamping Machine	BellCo Glass Dunn, Asbach (GER)
Pipettes: 0.5-10 μL, 10-100 μL, 100-1000 μL	Eppendorf, Hamburg (GER)
Pipetting Aid: Pipet Boy	Brand, Wertheim (GER)
Power Supplies: EV202, EV243	PeqLab Biotechnology, Erlangen (GER)
Pump	Ismatec, Wertheim-Mondfeld (GER)
Pump tubing cassette	Ismatec, Wertheim-Mondfeld (GER)
Rocking Platform Shaker	NeoLab, Heidelberg (GER)
Roller Mixer	Hartenstein, Würzburg (GER)
Safety Cabinet: Safe 2020	Thermo Fisher Scientific, Dreieich (GER)
Septophag	Hesse, Emmerich (GER)
Sliding Microtome RM 2255	Leica, Wetzlar (GER)
Steam Cooker: „MultiGourmet"	Braun, Kronberg/Taunus (GER)
C1000 Thermal Cycler	Bio-Rad, CA, (USA)
Timer	Carl Roth GmbH, Karlsruhe
TissueLyser LT	Qiagen, Hilden (GER)

Equipment/Device	Producer
Ultrapure Water System	Millipore, Schwalbach (GER)
Vortexer	Carl Roth GmBH, Karlsruhe (GER)
Water Bath	Julabo Labortechnik, Seelbach (GER)

3.3 Disposable materials

Table 4: Disposable materials

Disposable material	Producer
Aluminum Foil	Carl Roth GmBH, Karlsruhe (GER)
Cell Culture Flasks: 75 cm², 150 cm²	TPP, Trasadingen (GER)
Cell Culture Multiwell Plates: 6 well, 12 well, 24 well, 96 well	TPP, Trasadingen (GER)
Cell scraper	Sarstedt, Nümbrecht (GER)
Cell sieve	BD Biosciences, Heidelberg (GER)
Centrifuge Tubes: 15 ml, 50 ml	Greiner Bio-One, Frickenhausen (GER)
Cling Film	Toppits, Minden (GER)
Combitips Plus: 0.5 ml, 1 ml, 2.5 ml, 5 ml	Eppendorf, Hamburg (GER)
Cover Slips for Object Slides: 24 x 60 mm	Menzel-Gläser, Braunschweig (GER)
Cryo Tubes: 1.8 ml	Nunc, Wiesbaden (GER)
Disposable Pipettes: 5 ml, 10 ml, 25 ml, 50 ml	Greiner Bio-One, Frickenhausen (GER)
Disposal Bags	Hartenstein, Würzburg (GER)
Embedding Cassettes	Klinipath, Duiven (NED)
Embedding Filter Paper	Labonord, Mönchengladbach (GER)
Gloves: Latex Nitrile	Cardinal Health, Kleve (GER) Kimberly-Clark, Koblenz (GER)
Grease Pencil	Dako, Hamburg (GER)
Microtome Disposable Blades: Type A35	pfm Medical, Köln (GER)
Object Slides: uncoated (26 x76 x1 mm) Polysine™ (25 x75 x1 mm)	Menzel, Braunschweig (GER) Langenbrinck, Emmendingen (GER)
Parafilm®, M	Carl Roth, Karlsruhe (GER)
Pasteur Pipettes	Brand, Wertheim (GER)
Petri Dishes: 145 x20 mm	Greiner Bio-One, Frickenhausen (GER)

Disposable material	Producer
Pipette Tips: 0.5-10 µL, 10-100 µL, 100-1000 µL	Eppendorf, Hamburg (GER)
Pump tubing	Ismatec, Wertheim-Mondfeld (GER)
Reaction Tubes: 1.5 ml, 2.0 ml	Sarstedt, Nümbrecht (GER)
Scalpel Blades, rounded	Bayha, Tuttlingen (GER)
Septophag Disposable Bags: white/transparent	Porod, Frauenhofen (AUT)
Silicone tube	Carl Roth GmbH, Karlsruhe (GER)
Sterile Filter (Attachement for Disposable Syringes): Diameter 50 mm, Pore Size 0.2 µm	Sartorius Stedium Biotech, Göttingen (GER)
Syringes: 5 ml, 10 ml, 20 ml	BD Biosciences, Heidelberg (GER)
Transparent Sterilized Pack	Melag, Berlin (GER)
Weighing Dish	Hartenstein, Würzburg (GER)

3.4   Laboratory materials

Table 5: Laboratory materials

Laboratory material	Producer
Beakers: 1 l, 250 ml	Schott, Mainz (GER)
Cell Crowns for static 3D Culture	Chair of Tissue Engineering and Regenerative Medicine, Würzburg (GER)
Centrifuge Tubes Rack	NeoLab, Heidelberg (GER)
Cold Protection Gloves	VWR, Darmstadt (GER)
Funnel	Hartenstein, Würzburg (GER)
Glass Pipettes: 5 ml, 10 ml, 25 ml	Brand, Wertheim (GER)
Humidity Chamber	Chair of Tissue Engineering and Regenerative Medicine, Würzburg (GER)
Laboratory Bottle: 1 l, 250 ml, 100 ml, 50 ml	Schott, Mainz (GER)
Magnetic Stirring Bar	Hartenstein, Würzburg (GER)
Magnetic Stirring Bar Retriever	Hartenstein, Würzburg (GER)

Laboratory material	Producer
Object Slide Racks: Glass, Stainless Steel	Mercateo, Münch (GER)
Protective Goggles	NeoLab, Heidelberg (GER)
Reaction Tubes Rack	NeoLab, Heidelberg (GER)
Scalpel	Bayha, Tuttlingen (GER)
Spatula	VWR, Darmstadt (GER)
Spoon Spatula	Hartenstein, Würzburg (GER)
Spray Flask (Ethanol, 70 %)	Hartenstein, Würzburg (GER)
Stainless Steel Casting Moulds for Embedding Tissue: 24 x37 x9 mm	Labonord, Mönchenglattbach (GER)
Sterile Filter (Attachement for Laboratory Bottles)	Hartenstein, Würzburg (GER)
Tweezers	Assistent, Sondheim (GER)
Volumetric Flasks with Plug: 1 l, 2 l	Schott, Mainz (GER)

3.5 Chemicals and solutions

Table 6: Chemicals and solutions

Chemical/Solution	Producer	Catalog No
A83-01 (3-(6-Methyl-2-pyridinyl)-N-phenyl-4-(4-quinolinyl)-1H-pyrazole-1-carbothioamide)	Tocris Bioscience, R&D Systems, Minneapolis, Minnesota (USA)	2939
Acetone ($\geq$ 99,5 %)	Carl Roth, Karlsruhe (GER)	5025.5
Advanced Dulbecco's Modified Eagle Medium F12 (DMEM)	Invitrogen, Carlsbad, CA (USA)	12634-028
Albumine Fraction V (BSA)	Carl Roth, Karlsruhe (GER)	T844.2
Ammonium Persulfate (APS)	Carl Roth, Karlsruhe (GER)	9592.1
Ammonium persulfate (APS) $(NH_4)_2S_2O_8$	Carl Roth, Karlsruhe (GER)	9592.1

Materials

Chemical/Solution	Producer	Catalog No
Anti-Anti	Invitrogen, Carlsbad, CA (USA)	15240-062
B 27 Supplement	Invitrogen, Carlsbad, CA (USA)	12587-010
Bromophenol Blue (Sodium Salt)	Carl Roth, Karlsruhe (GER)	A512.1
Calcium Chloride ($CaCl_2$)	VWR, Darmstadt (GER)	1.02391.1000
Cell recovery solution	Corning, Hickory, NC (USA)	354253
Chloral hydrate ($C_2H_3Cl_3O_2$)	VWR, Darmstadt (GER)	22682265
Citric Acid	VWR, Darmstadt (GER)	1.00244.1000
Collagenase Type XI	Sigma-Aldrich, St. Louis, MO, (USA)	C7657-25MG
1,4-diazabicyclo[2.2.2]octane (DABCO)	Carl Roth, Karlsruhe (GER)	0718.1
DAPI Fluoromout-G™	SouthernBiotech, Birmingham (USA)	SBA-0100-20
DAPT (N-[N-(3,5-Difluorophenacetyl)-l-alanyl]-S-phenylglycine t-butyl ester	Sigma-Aldrich, St. Louis MO (USA)	04-0041-5mg
Demineralized Water	University Clinic, Würzburg (GER)	-
Dimethyl sulfoxide (DMSO)	Sigma-Aldrich, St. Louis, MO (USA)	D2438-50ML
Dispase II	Invitrogen, Carlsbad, CA (USA)	17105-041
DNeasy Blood & Tissue Kit	Qiagen, Hilden, Germany	69506
Donkey Serum	Sigma-Aldrich, St. Louis, MO (USA)	D9663-10ML
Dulbecco's Modified Eagle Medium (DMEM)	Invitrogen, Carlsbad, CA (USA)	41965-039
Dulbecco's Phosphate Buffered Saline (PBS⁻)	Sigma-Aldrich, St. Louis, MO (USA)	D8537-6X500ML
Eosin	Sigma-Aldrich, St. Louis, MO (USA)	861006-25G

Chemical/Solution	Producer	Catalog No
Ethanol, absolute	Carl Roth, Karlsruhe (GER)	9065.2
Ethanol, denatured (96 %)	Carl Roth, Karlsruhe (GER)	T171.2
Ethylenediaminetetraacetic acid (EDTA - Na_2 *2 H_2O)	Sigma-Aldrich, St. Louis, MO (USA)	E5134-1KG
Fetal Calf Serum	Lonza, Cologne (GER)	8SBO16
Ficoll-Paque™ premium (density 1.077±0.001 g/ml at +20°C)	GE Healthcare, Uppsala (SWE)	17-5442-03
FibroLife® Fibroblast Serum Free Medium Complete Kit	Lifeline® Cell Technology, Frederick, MD (USA)	LL-0001
FITC-Dextran	Sigma-Aldrich, St. Louis, MO (USA)	G2838
Gastrin ([Leu15]-Gastrin I)	Sigma-Aldrich, St. Louis, MO (USA)	G9145-.5MG
Gentamycin	Sigma-Aldrich, Munich (GER)	G1397
Glycerol (86 %)	Carl Roth, Karlsruhe (GER)	4043.1
Glycine	AppliChem, Darmstadt (GER)	A1067,1000
GlutaMAX	Invitrogen, Carlsbad, CA (USA)	350500-87
Haematoxylin	Carl Roth, Karlsruhe (GER)	3861.1
Hank's Balanced Salt Solution (HBSS$^-$)	Sigma-Aldrich, St. Louis, MO (USA)	H9394
Hepes	Sigma-Aldrich, St. Louis, MO (USA)	H0887-20ML
Hydrochloric acid (HCl; 37 %, 1M)	VWR, Darmstadt (GER)	1.09057.1000
Recombinant Human IL-4	Preprotech, Rocky Hill, NY (USA)	200-04
iScriptTM Reverse Transcription Supermix	Bio-Rad, CA (USA)	1708840
Isopropanol	Carl Roth, Karlsruhe (GER)	2316.5

Chemical/Solution	Producer	Catalog No
JAG-1	Anaspec, Fremont, CA (USA)	61298
LY2157299	Axon MedChem, Groningen (NL)	1491
Magnesium Chlorite Hexahydrate (MgCl2 *6 H2O)	Carl Roth, Karlsruhe (GER)	HN03.3
Matrigel-Matrix Growth Factor Reduced (GFR) phenol red-free	Corning, Hickory, NC (USA)	356231
Minimum Essential Medium (MEM)	Life Technologies, Carlsbad, CA (USA)	41090-028
MEM Non-Essential Amino Acids (NEAA, 100x)	Life Technologies, Carlsbad, CA (USA)	11140-035
Mounting Medium: Entellan	Merck, Darmstadt (GER)	1079600500
Mounting Medium: Mowiol	Carl Roth, Karlsruhe (GER)	0713
N2-Supplement	Invitrogen, Carlsbad, CA (USA)	17502-048
N-Acetylcysteine	Sigma-Aldrich, St. Louis, MO (USA)	A9165-5G
Nicotinamide	Sigma-Aldrich, St. Louis, MO (USA)	N1630-100MG
N,N,N',N'-Tetramethylethylendiamin (TEMED)	Carl Roth, Karlsruhe (GER)	2367.2
Paraffin	Carl Roth, Karlsruhe (GER)	6642.6
Paraformaldehyde (PFA)	AppliChem, Darmstadt (GER)	A3813,1000
Penicillin / Streptomycin (100x concentrated)	PAA, Cölbe (GER)	P11-010
Phosphate-Buffered Saline (PBS-)	Invitrogen, Carlsbad, CA (USA)	10010-015
Phosphate-Buffered Saline (PBS) Tablets	Invitrogen, Carlsbad, CA (USA)	18912-014
Potassium alum	VWR, Darmstadt (GER)	1.01047.1000
Potassium Chloride (KCl)	Merck, Darmstadt (GER)	1049361000

Chemical/Solution	Producer	Catalog No
Quant-iT™ PicoGreen® dsDNA Assay Kit	Invitrogen, Carlsbad, CA, (USA)	P7589
Recombinant Human Granulocyte-macrophage colony-stimulating factor (GM-SCF)	Preprotech, Rocky Hill, NY (USA)	300-03
Recombinant Human R-Spondin 1	Preprotech, Rocky Hill, NY (USA)	120-38
Recombinant Human Epidermal Growth Factor (EGF)	Preprotech, Rocky Hill, NY (USA)	100-15
Recombinant Murine Noggin	R&D, Rocky Hill, NY (USA)	6057-NG-025
RNA Ladder, 20 µL	BioRad, Munich (GER)	700-7255
RNeasy Micro Kit plus	Qiagen, Hilden, Germany	
RLT plus lysis buffer	Qiagen, Hilden (GER)	
Roswell Park Memorial Institute Medium (RPMI 1640)	Gibco, Thermo fisher scientific (USA)	61879-010
SB202190	Sigma-Aldrich, St. Louis, MO (USA)	S7067-5MG
Sodium Chloride NaCl	Carl Roth, Karlsruhe (GER)	HN00.3
Sodium Deoxycholic Acid	Carl Roth, Karlsruhe (GER)	3484.7
Sodium Pyruvate (100x)	Life Technologies, Carlsbad, CA (USA)	11360-039
Sso-Fast Eva Green Supermix	Bio-Rad, CA (USA)	1725200
Tris	Carl Roth, Karlsruhe (GER)	4855.1
Triton-X 100	Carl Roth, Karlsruhe (GER)	3051.2
Trizma Hydrochloride	Sigma-Aldrich, St. Louis, MO (USA)	T5941-1KG
Trypan Blue, 0.4 %	Sigma-Aldrich, St. Louis, MO (USA)	T8154-100ML
TrypLE Express	Invitrogen, Carlsbad, CA (USA)	12605-010
Tween-20	VWR, Darmstadt (GER)	8.22184.0500

Chemical/Solution	Producer	Catalog No
Ultrapure Water	Millipore, Schwalbach (GER)	
Wnt3A	Preprotech, Hamburg (GER)	315-20
Xylene	Carl Roth, Karlsruhe (GER)	9713.3
Y-27632 (ROCK inhibitor)	Tocris Bioscience, R&D Systems, Minneapolis, Minnesota (USA)	1254/10
β-Mercaptoethanol	Carl Roth, Karlsruhe (GER)	4227.1

3.6 General buffers and solutions for cell culture

Table 7: General buffers and solutions for cell culture

Buffer/Solution	Composition	
Flow cytometer (FC) Buffer	0.5 %	BSA
	2 mM	EDTA
		in PBS⁻-solution

3.7 Cell culture medium

Table 8: Cell culture medium

Medium/Solution	Composition	
Basal Medium	500 ml	DMEM-F12 Advanced supplemented with
	1x	N2
	1x	B27 w/o vitamin A
	1x	Anti-Anti
	10mM	HEPES
	2 mM	GlutaMAX
	1 mM	N-acetylcysteine

Medium/Solution	Composition	
Crypt Culture Medium	50 %	Basel Medium
	50 %	Wnt3A-conditioned medium
	500 ng/ml	hR-Spondin 1
	100 ng/ml	rec Noggin
	50 ng/ml	mEGF
	10 mM	Gastrin
	10 mM	Nicotinamide
	500 nM	A83-01
	10 µM	SB202190
	500 mM	LY2157299
	10 µM	Y-27632 (added the first two days)
	10 µM	JAG-1(added for single cells the first two days)
	10 µM	DAPT (added for differentiation)
Caco-2 Culture Medium	500 ml	MEM
	20 % (v/v)	FCS
	1 % (v/v)	Non-essential Amino Acids (NEAA)
	1 %(w/v)	Sodium Pyruvate
Collagenase Working Solution (500 U /ml)	1000 mg	Collagenase
	436 ml	Cell-specific Medium
Dispase Solution (2 U/ml)	2 U/ml	Dispase Powder
		Dissolved in PBS$^-$
FibroLife® medium	480 ml	FibroLife® Basal Medium
	+	HLL Supplement
	+	LifeFactors® Kit
Human dendritic cell Medium	500 ml	RPMI
	10 %	FCS
	50 ng/ml	rh GM-SCF
	50 ng/ml	rh IL-4
PBS$^-$ Solution	1	PBS Tablet (5 g)
	500 ml	Ultrapure Water
		pH 7.2
		Stored at 4°C
PBS$^-$/EDTA Solution	5 l	PBS- Solution
	1 g	EDTA - Na$_2$ x 2 H$_2$O
		pH 7.2
		Stored at 4°C
PBS$^+$ Solution	5 l	PBS- Solution
	0.5 g	MgCl$_2$ x 6 H$_2$O
	0.5 g	CaCl$_2$
		pH 7.2
		Stored at 4°C

Medium/Solution	Composition

3.8 Materials and solutions for histology

Table 9: Materials and solutions for histology

Chemical/Solution		Composition
Antibody Diluent	5 % (w/v)	BSA
	5 %	Donkey Serum
	0.3 %	Triton
		in PBS⁻-solution
Citrate Buffer Stock Solution (10 x concentrated)	42 g/l	Citric acid
	17.6 g/l	NaOH pellets
		in demineralized water
		pH 6.0
Citrate Buffer Working Solution	10 % (v/v)	Citrate buffer stock solution
		in demineralized water
Eosin	10 mg/ml	Eosin
		in demineralized water
		Stored at RT
Haemalaun	1.2 g/l	Haematoxylin
	0.2 g/l	$NaIO_3$
	20 g/l	Potassium alum
	20 g/l	Chloral hydrate
	1 g/l	Citric acid in demineralized water
		Used after 4 weeks of maturation.
		Stored at RT
HCl /EtOH (H&E Staining)	6.85 % (v/v)	HCl, 1M
		in Ethanol (50 % v/v)
PFA 4 %	40 g/l	Paraformaldehyde
		in PBS⁻ solution (solved at 60°C)
		pH 7.4
TBST, 0.05 M	100 ml	TBS Stock 0.5 M
	5 ml	Tween-20 (0.5 % v/v)
	900 ml	Demineralized Water
		Stored at 4 °C.

Chemical/Solution	Composition	
Tris Buffered Solution (TBS) Stock, 0.5 M (10x concentrated)	78.8 g 87.66 g ad 1 l	Trizma hydrochloride NaCl with Ultrapure Water pH 7.6 Autoclaved before Use Stored at 4 °C.
Triton-X Permeabilizing Solution	0.2 % (v/v) in 0.05 M	Triton-X 100 TBS Buffer Stored at RT

3.9 Enzymes

Table 10: Enzymes

Buffer/Solution	Composition	
0.05 % Trypsine/EDTA Working Solution	10 ml 90 ml	Trypsine /EDTA Stock Solution (10x) PBS⁻

3.10 Antibodies

Table 11: List of antibodies for immunofluorescence staining and flow cytometry

Antibody	Producer	Catalog No.
Mouse anti-E-Cadherin	Becton Dickinson,	610181
Rabbit anti-Cytokeratin	Dako,	Z0622
Mouse anti-Cytokeratin 18	Dako,	M7010
Mouse anti-Villin	DCS,	V616C01
Mouse anti-EMA (Mucin 1)	Imgenex,	IMG-80045
Rabbit anti-Mucin 2	Santa Cruz,	SC-15334
Rabbit anti-Chromogranin A	Santa Cruz,	SC-13090
Mouse anti-Lysozym	Santa Cruz,	SC-27958
Rabbit anti-Vimentin	Abcam,	ab8069
Anti-mouse-Alexa 555	Invitrogen, Carlsbad, CA, USA	A-31570

Antibody	Producer	Catalog No.
Anti-rabbit-Alexa 555	Invitrogen, Carlsbad, CA, USA	A-31572
Anti-mouse-Alexa 647	Invitrogen, Carlsbad, CA, USA	A-31571
Anti-rabbit-Alexa 647	Invitrogen, Carlsbad, CA, USA	A-31573
CellMask™ Deep Red	ThermoFisher Scientific, Waltham, MA, USA	C10046

3.11 qPCR

Table 12: List of primers for gene expression analysis

Primer	NCBI	Sequence	Product
Mucin 2	NM_002457.3	AGGATCTGAAGAAGTGTGTCACTG TAATGGAACAGATGTTGAAGTGCT	249 bp
Claudin 4	NM_001305.4	CATCGGCAGCAACATTGTCA CGAGTCGTACACCTTGCACT	103 bp
CYP3A4	NM_017460.5	TGTCCTACCATAAGGGCTTTTGTAT TTCACTAGCACTGTTTTGATCATGTC	136 bp
Mdr1	NM_000927.4	CTGGTGTTTGGAGAAATGACAGATA TGGTCATGTCTTCCTCCAGATTC	130 bp
HPRT1	NM_000194.2	TGACCTTGATTTATTTTGCATACC CGAGCAAGACGTTCAGTCCT	102 bp

3.12 Software

Table 13: Software

Software	Company
CellQuest	Becton Dickinson (USA)
Endnote X7	Thomson Reuters, Philadelphia, PA (USA)
FlowJo	FlowJo, LLC (USA)

Graphpad Prism 5	GraphPad Software Inc. (USA)
ImageJ	NIH (USA)
Keyence BZ-II Viewer Keyence BZ-II Analyzer	KEYENCE Deutschland GmbH, Neu-Isenburg (GER)
Office Excel 2013 Office PowerPoint 2013 Office Visio 2013 Office Word 2013	Microsoft Deutschland GmbH, Unterschleißheim (GER)
Tecan-i-control TM 1.7	Tecan, Crailsheim (GER)

4 Methods

4.1 Cell culture

Cell culture was performed using a laminar airflow safety cabinet to ensure sterile conditions. All materials in direct or indirect contact with cells were either sterile disposable materials or sterilized by autoclaving (121°C, 1.5 h), baking (180°C, 8 h) or gamma sterilization (25 kGy). Cells were cultured in physiological medium in an incubator at 37°C in a humidified atmosphere of 95 % with 5 % CO_2. The cells were routinely monitored for morphology, growth and possible contaminations.

4.1.1 Preparation of porcine decellularized scaffolds

Starting material for the so called "Biological Vascularized Matrix (BioVaSc)" was jejunal porcine gut tissue from 6-8 weeks old pigs. The pigs were obtained from veterinary controlled breeding of a local pig farmer (Niedermaye, Dettelbach). Pigs were sedated with 5-7 mg/kg body weight (BW) Azaperon (Stresnil®) by intramuscular injection, anesthetized with 20-25 mg/kg BW Ketamin (Ursotamin®) by intramuscular injection, heparinized with 500–600 i.U./kg BW by intravenous injection and euthanised with 0.3-0.4 ml/kg BW (T61®) by intravenous injection. After opening the abdomen, different segments of the jejunum were extracted, either with or without supplying vessel system. The following study were based on matrix without the vessel system. Decellularization was performed according to a standardized protocol published previously [106, 114]. The SIS-muc (small intestine submucosa with mucosa) was prepared by washing the gut lumen several times with cold PBS⁻-buffer to remove faeces and the vessel system to remove rest of blood. Gentamycin, an antibiotic was used to prevent bacterial contamination and release of endotoxins. The next day the decellularization process was started by perfusion of lumen and vessel system with cold sodium desoxycholate solution (45 g/2 l ddH$_2$O). The vessels were perfused with a pump via a tubing system, which was pressure controlled (max. 80 mmHg). After perfusion with a total volume of 4 l cold sodium desoxycholate solution, lumen and vessels were washed with about 7 l PBS⁻-buffer. The successful removing of the cells resulted in a more and more white tissue. The gut tissue was stored at 4°C overnight. After washing with 3-4 l PBS⁻-buffer the vascular

system was removed and the remaining gut lumen cut into pieces of about 10 cm with a scissor. The matrix tube imposed on a 15 ml centrifuge-tube and the serosa was removed by rip down the outer membrane with a forceps. Matrix pieces were washed 3 times and incubated in DNase solution (100 mg/300 ml PBS$^+$+1 % PenStrep) over night at 4°C. The next day the DNase was removed by washing with PBS$^-$-buffer. To determine the sodium desoxycholate concentration at different time points of the decellularization process, samples of 1 ml were taken and analysed with the gallic acid test. After transfering the matrix to fresh PBS$^-$ without antibiotics, the matrix was send to gamma sterilization (25 kGy, BBF Sterilisationsservice GmbH, Rommelshausen, Germany). After sterilisation, the now sterile SIS-muc was transferred to sterile PBS under sterile conditions and stored at 4°C.

Unlike the SIS-muc, for the standard SIS the mesentery was already removed from the gut before the decellularization. For generation of the SIS the gut lumen was washed first by flushing the lumen with running tap water. Afterwards, the gut was cut into pieces of 10-15 cm length and the intestine pieces get turned inside out by everting them with tweezers. The intestine pieces were pulled onto 15 ml centrifuge-tube and the mucosa scraped off by using the handle of a tweezer. The pieces were stored over night at 4°C in PBS$^-$ + 1 % PenStrep on a rocking shaker. The desoxycholate solution (34 g/l) at RT was filled into the lumen of the gut pieces by closing the ends with clamps. After incubation of 1.5 h in a filled Erlenmeyer flask on a shaker at 4°C the tubes were emptied and filled with PBS$^-$-buffer instead for rinsing and incubated for another 1 h at 4°C on the shaker. For further washings steps, the tubes were cut open by cut off the clamps at both ends and transferred into fresh PBS$^-$-buffer with PenStrep which was replaced 4-5 times. For gamma sterilization the matrix was transferred into buffer without antibiotics. The complete process was control by the gallic acid assay and the sterilization carried out like described for SIS-muc.

4.1.2 Caco-2 cell line

The Caco-2 cell line was obtained from the DSMZ (Leibniz Institute DSMZ-German Collection of Microorganisms and Cell Cultures, Braunschweig, Germany). Cells were defrosted and expanded from frozen stocks and used for experimental studies between

passage 20 to 40. Cells culture was performed using Minimum Essential Medium (MEM) supplemented with 20 % fetal calf serum (FCS), 1 % sodium-pyruvate and 1 % non-essential amino acids (NEAA). To keep the confluence under 90 % cells had to be passaged every 2-3 days. Intestinal mucosa models were prepared by seeding 0.3×10^6 Caco-2 cells on decellularized porcine gut scaffolds (SIS-muc), fixed between two plastic cylinders. Models were cultured for at least 21 days under static conditions. Cell culture medium was changed 3 times a week. Before starting experiments with NPs, the integrity of the models was tested with FITC-dextran permeability (4 kDa). Only models with relative transport rate of less than 0.5 % after 30 minutes (min) were used. For confirmation, all model tissues were fixed after each experiment with 4 % paraformaldehyde (PFA), paraffin-embedded and analyzed for monolayer integrity after HE-staining by microscopy (Keyence BZ-9000, Japan).

4.1.3 Dendritic cells

For the co-culture model combining the intestinal barrier represented by Caco-2 monolayer with components of the adaptive immune system, dendritic cells (DCs) were introduced into the system. Peripheral blood mononuclear cells (PBMCs) were isolated from buffy coats obtained from the Institute for Clincal Transfusion Medicine and Hemotherapy of the University Hospital Würzburg by Ficoll-Paque™ premium. Blood was transferred into 50 ml tube and mixed 1:1 with PBS$^-$. A 50 ml tube containing 12 ml ficoll was prepared and the blood carefully added on top to avoid mixing. The blood plus ficoll suspension was centrifuged at 2000 rpm for 20 min without breaks. The leukocyte fraction (white high dense layer) between the yellowish plasma on top and whitish ficoll beneath was collected with a Pasteur pipette and transferred to a new tube containing 10 ml PBS$^-$. After resuspension the cell suspension was centrifuged at 1800 rpm for 10 min and the supernatant discarded. The washing step was repeated 2 more times decreasing centrifugation of 1200 rpm and finally 800 rpm to remove remaining ficoll. For differentiation of monocytes towards DCs 1×10^7 PBMCs were resuspended in RPMI with 10 % FCS and transferred to a 150 cm^2 cell culture flask to let the cells adhere to the flask surface for 2 h at 37°C. Afterwards the cells were washed several times until all non-adherent lymphocytes were removed. For differentiation cells were cultured for 5 days in RPMI medium with 10 % FCS

supplemented with Granulocyte-macrophage colony-stimulating factor (GM-CSF; 50 ng/ml) and interleukin 4 (IL-4; 50 ng/ml). On day 5 cells were counted and $0.5x10^6$ DCs in 1.5 ml medium added to the basolateral compartment of the Caco-2 model (day 18).

4.1.4 Primary cells from human intestinal tissue - isolation and expansion

Biopsy tissue was obtained from obese adults during routine stomach bypass operation at the University Hospital Würzburg in collaboration with the surgery unit (study approval number 182/10). For isolation of intestinal epithelial cells and subepithelial myofibroblasts, a biopsy in size of about 4-6 cm of the complete jejunal gut tube was removed by the surgeon, sealed with a surgical stapler and transported on ice. Tissue was washed serval times with cold HBSS to removed intestinal contents and blood. Muscle layers and mucosa were separated with a scissor. Muscle layer was disposed and the mucosa washed again for several times with HBSS. For isolation of the cells, pieces of 10 cm² or smaller were used for isolation. Villi were scraped of using a glass slide. Tissue was transferred into 50 ml falcon tube with 20 ml cold HBSS, vortexed for 5 sec and supernatant discarded. This washing step was repeated until supernatant was cleared of cell debris. Afterwards, tissue was incubated in cold 2 mM EDTA/HBSS⁻ solution for 30 min at 4°C with gentle rotation. After the tissue was washed once in 20 ml HBSS by inverting the tube 5 times. The mucosa was transferred in a tube with 10 ml HBSS and shaked 5 times. This process was repeated 3-4 times. Each cell fraction was checked for amount and size of crypts in drops under the microscope. The best supernatants, containing the most intact crypts and the least single cells and cell debris were pooled and spinned at 300 g for 5 min. Pellet was resuspended in 10 ml basal medium and crypts were counted. Desired amount of crypts were centrifuged in a non-stick 1.5 ml tube at 300 g for 5 min and supernatant removed. Tube with pellet was placed on ice. Pellet was re-suspended in cold Matrigel. Drops of 50 µl per well were seeded in 24-well-plate and incubated for 5-10 min until the Matrigel was well solidified. Medium was prepared according to the protocol published by Sato *et al.* 2011 [85]. Fresh prepared Crypt Culture Medium (Tab. 7) was added (500µl/well) using Wnt3A-condition medium and basal medium supplemented with growth factors [115]. For cell expansion organoids were passaged by digestion

with TrypLE Express and seeded again in Matrigel. To enrich the stem cell population organoids were passaged every 3-5 days [88].

Subepithelial myofibroblasts were isolated after IECs by digestion of the remaining connective tissue. Connective tissue was cut into small pieces and transferred to a tube with 0.3 mg/ml Dispase II/ 0.25 mg/ml Collagenase Type XI solution. After digestion of 30 min at 37°C cells were centrifuged and pellet was resuspended in FibroLife® medium supplemented with 2 % FCS and Anti-Anti (1x). Cells were cultured for up to 5 passages.

4.1.5   Wnt3A-conditioned medium

Wnt3A conditioned medium was produced using the L-Wnt3A cell line (ATCC® CRL-2647™), which secretes biological Wnt3A protein in the medium. Conditioned medium was produced according to the protocol provided by ATCC. Cells were splitted 1:10 in 10 ml culture medium (without G418) and added to a T75 flask. The cells were cultured for 4 days which is when they get confluent. Medium was taken off and sterile filtrated (first batch). Cells are cultured for 3 more days with new medium (second batch) and discarded afterwards. The two batches were mixed and frozen at -20 °C. Wnt3A activity of the conditioned medium was determined by Wnt Reporter Activity Assay [116].

4.1.6   Primary intestinal tissue model - different culture conditions

The primary models of the intestinal mucosa were prepared by seeding $8x10^5/cm^2$ single IECs with or without $4x10^5/cm^2$ fibroblasts on decellularized porcine gut scaffolds (SIS) fixed between two plastic cylinders, so called cell crowns and cultured in 24-well-plates at 37°C in the incubator. Seeded area of the 24-well format was $0.54\,cm^2$ per model. For SIS preparation, porcine jejunal segments were explanted from 6-8 weeks old domestic pigs (Niedermayer, Dettelbach) and decellularized according to a standardized protocol published previously (4.1.1). Models were cultured for 7 days either under static conditions in a standard well-plate, under dynamic conditions on an orbital shaker (OS, 77 rpm) or in a perfusion bioreactor (BR, flow rate: 3.8 ml/min). All models were initially kept in proliferation medium for 48 h under static conditions allowing cells to adhere. Afterwards, medium was changed

to differentiation medium, *i.e.* reduction of Wnt3A-conditioned-medium to 25 % and no addition of nicotinamide and SB202190. Additionally, 10 μM DAPTl, a γ-secretase inhibitor to block Notch-signalling, was added to drive differentiation towards secretory lineage. Models were furthermore cultured till day 7, either under static or dynamic conditions. The barrier integrity of the models was tested by measuring the TEER using a hand-electrode before the experiments. Complementary, FITC-dextran permeability assay (4 kDa) was performed after the experiments. Only models with an *in vivo*-like TEER-value higher than 40 Ωxcm^2 (above cell-free scaffold) and FITC-dextran transport of <2 % after 30 min were considered for analysis as the primary models showed a lower tightness compared to the Caco-2 models. For further analysis all tissue models were either fixed with 4 % PFA or stored at -80 °C in RLT plus lysis buffer.

4.2 Histology

4.2.1 Fixation and embedding of tissues

For histological characterization of the *in vitro* models the models were fixated after the experiments. Before the fixation the tissue was washed once with PBS⁻, which was then replaced by 4 % paraformaldehyde (PFA). Models were incubated with PFA for at least 1 h at 4°C. Afterwards, the fixed tissue was prepared for embedding in paraffin or Tissue-Tek.

For Cryo-embedding in Tissue-Tek and section preparation, fixated samples were embedded in Tissue-Tek within a plastic form, frozen on dry ice and stored at -80°C. Frozen sections were made at 10 μm, dried at RT for 30 min and stored at -80°C.

For Paraffin embedding and section preparation, fixated samples were wrapped in a paper and enclosed in labeled embedding cassettes. To remove remaining PFA, the embedding cassettes were placed in tap water. For starting the embedding the cassettes they were placed into the embedding station, which was started with program in Table 14.

Table 14: Standard program of automatic embedding machine

Step	Solution	Time
Washing out PFA	Tap H_2O	1 h
Dehydration	Ethanol 50 %	1 h
	Ethanol 70 %	1 h
	Ethanol 80 %	1 h
	Ethanol 96 %	1 h
	Isopropanol I	1 h
	Isopropanol II	1 h
Removing alcohol from tissue	Xylene I	1 h
	Xylene II	1 h
Infiltrating tissue with paraffin	Paraffin I	1.5 h
	Paraffin II	1.5 h

After paraffin embedding, the samples were kept at 60°C in liquid paraffin and removed from the embedding cassettes. Tissues were cut into equal pieces and blocked inside a stainless steel casting mold with paraffin.

Paraffin sections were made at 5 µm with a sliding microtome (Leica) and dried at 37°C overnight. Poly-L-lysine coated slides were used to ensure attachment of the samples during heat induced antigen unmasking.

4.2.2 Deparaffinization and rehydration of tissue sections

Before histological stainings, paraffinized tissue sections had to be deparaffinized and rehydrated so aqueous staining solutions and antibodies can penetrate the tissue. The tissue slices in paraffin were incubated for 1 h at 60°C to melt the paraffin. Afterwards, deparaffinization and rehydration protocol was started (Tab. 15).

Table 15: Deparaffinization and rehydration protocol

Step	Solution	Time
Deparaffinization	Xylene I	10 min
	Xylene II	10 min
Rehydration	Ethanol 96 % I	Dipped 3 times
	Ethanol 96 % II	Dipped 3 times
	Ethanol 70 %	Dipped 3 times
	Ethanol 50 %	Dipped 3 times
	Deionized H_2O	Immerged until disturbances cleared

4.2.3 Haematoxylin & Eosin (H&E) staining

As initial control of the tissue integrity haematoxylin-eosin staining was performed to estimate cell survival and morphology. After deparaffinization and rehydration H&E staining was performed according to standard protocol:

Table 16: H&E staining protocol

Step	Solution	Time
Staining Basophilic Structures	Hemalaun	8 min
Rinsing off Hemalum	Deionized H_2O	Until solution clears
Differentiating Hemalum	HCL / Ethanol	Dipped 2 times
Rinsing	Deionized H_2O	Dipped once
Blueing	Tap H_2O	5 min
Staining Acidophilic Structures	Eosin	1 min
Dehydration*	Ethanol 70 %	Dipped 3 times
	Ethanol 96 %	2 min
	Isopropanol I	5 min
	Isopropanol II	5 min
	Xylene I	5 min
	Xylene II	5 min

After the dehydration slides were mounted with Entellan®.

4.2.4 Feulgen staining

Feulgen staining was performed on deparaffinized and rehydrated tissue sections to look for DNA leftover in the decellularized scaffolds. The purine-bases adenine and guanine of the DNA were removed by acid hydrolysis with 5 M HCl resulting in free aldehyde groups. Basic fuchsine and sulfurous acid of the Schiff`s reagent bind to these free aldehyde groups resulting in a purple staining of the DNA containing cell nuclei. Surplus dye was removed by rinsing with sodium metabisulfite solution.

Table 17: Feulgen staining protocol

Step	Solution	Time
Hydrolysis of DNA	Hydrogen chloride (HCL) 5 M	50 min
Rinsing	Deionized H_2O	2 min
Rinsing	Deionized H_2O	2 min
Staining of DNA	Schiff`s reagent	60 min
Rinsing	Sodium metabisulfite solution	3 min
Rinsing	Sodium metabisulfite solution	3 min
Rinsing	Deionized H_2O	2 min
Dehydration*	Ethanol 70 %	Dipped 3 times
	Ethanol 96 %	2 min
	Isopropanol I	5 min
	Isopropanol II	5 min
	Xylene I	5 min
	Xylene II	5 min

After the dehydration slides were mounted with Entellan®.

4.2.5 Masson's trichrome staining

After deparaffinization and rehydration of tissue sections trichrome staining performed. The positively-charged basic dye hematein, which is the oxidized form of the used iron hematoxylin, colors cell nuclei black while acid fuchsin and ponceau de xylidene causes a red staining of the cytoplasm. Furthermore, erythrocytes are stained

orange by 2 % phosphorous molybdenum acid-Orange G. Light green is used, in order to stain the connective tissue and acidic mucous substances.

Table 18: Trichrome staining protocol

Step	Solution	Time
Staining of cell nuclei	Haematoxylin after Weigert	1-2 min
Rinsing	Deionized H_2O	
Blueing	Tab H_2O	10 min
Staining of muscle and cytplasm	Acid fuchsin with ponceau de xylidene	5 min
Rinsing	CH_3COOH 1%	Dipped 3 times
Staining of erythrocytes	Phosphorous molybdenum 2% acid Orange G	1 min
Rinsing	CH_3COOH 1%	Dipped 3 times
Light green	Light green	5 min
Rinsing	CH_3COOH 1%	5 min
	Ethanol 96 %	5 min
	Isopropanol	5 min
	Xylene	5 min

After the dehydration slides were mounted with Entellan®.

4.2.6 Immunofluorescence

Immunofluorescence staining was performed to characterize the tissue samples for specific cell markers. Prior to staining, protocols to deparaffinize the tissue and unmask the epitopes from fixation were performed. Slides were treated with heat in citrate buffer pH 6 for 20 min or in EDTA buffer pH 8 for 20 min at 100°C. Subsequently, the sections were washed in PBS. Frozen sections were not pre-treated. Afterwards, sections were incubated for at least 30 min with host serum of the secondary antibody species, to prevent unspecific binding of the secondary antibody. The primary antibody was diluted 1:100 and the secondary antibody was diluted 1:400 if not indicated otherwise. For double staining, primary antibodies raised in different species were combined in one solution. Therefore, the according secondary antibodies were applied.

Primary antibodies were incubated overnight at 4°C. After 3 times washing with PBS for 10 min, secondary antibodies were added and incubated at RT for 1 h. After final washing with PBS 3 times for 5 min, the sections were mounted in ready to use Mowiol with DAPI.

4.2.7 SEM and TEM imaging

For ultrastructural analysis of tissue models by transmission (TEM) and scanning electron microscopy (SEM), samples were washed with 0.1 M PBS and fixed in 2.5 % glutaraldehyde (50 mM sodium cacoylic acid pH 7.2, 50 mM KCl, 2.5 mM MgCl2) at 4°C until for 12-18 h.

For TEM specimens were then washed 3 times with 50 mM sodium cacodylic acid (pH 7.2), fixed at 4°C in 2 % osmium tetroxide (50 mM sodium cacodylic acid pH 7.2) for 2 h, washed with deionized water, and stained overnight at 4°C with 0.5 % aqueous uranyl acetate. A dehydration process, embedding in Epon812 (Serva) and ultrathin sectioning of the samples was applied [117] followed by analysis and image recording with a JEOL JEM-2100 microscope (JEOL, Freising, Germany) at 200 kV equipped with a F416 4kx4k camera (TVIPS, Gauting, Germany).

For SEM, samples were fixed with 2.5 % glutaraldehyde (see above), washed 3 times with 50 mM cacodylic acid (pH 7.2) and then stepwise dehydrated with acetone, critical point dried (critical point dryer: BAL-TEC CPD 030) and metal coated (sputter coater BAL-TEC SCD 005) with gold-palladium. Specimens were inspected with a field emission SEM (JEOL JSM-7500F) using the detectors for secondary electrons (LEI and SEI detectors) at 5kV.

For analysis of the nanoparticles, the particles were centrifuged and washed 3 times deionised water (Millipore). Supernatant was discarded and particles resuspended in 20 μl of deionised water. Particles were dried on a glass cover slide at RT and coated with gold or platinum for SEM analysis.

4.3 Flow cytometry

Flow cytometry provides a tool for characterization of single cells in a quantitative manner. Flow cytometry was used to characterize subepithelial fibroblasts,

differentiation and activation status of DCs as well as to quantify proliferation of IECs. Cells were detached enzymatically or non-adherent suspension cells taken and counted. organoids had to be digested with accutase for ~5 min at 37°C to get single cells. Desired cell number ($1\text{-}5\text{x}10^5$) was transferred to a tube and centrifuged with 250 g for 5 min. The cell pellet was resuspended and washed in FC buffer 3 times (250 g, 5 min). For staining of surface proteins the cells were resuspended in 100 µL FC buffer, the antibodies added and incubated for 30 min at RT in the dark. After a washing step with 1 ml Fc-buffer, the cells were resuspended in 100 µL FC buffer and analysed with the flow cytometer (FACSCalibur). For intracellular protein staining cells were fixed and permeabilized using the commercial kit BD Cytofix/Cytoperm™ Fixation/Permeabilization Solution Kit (BD Bioscience, Chicago, IL, USA) according to manufacturer´s instructions. The data were processed with the CellQuest software and analysed with the FlowJo.

4.4 Gene expression analysis by qPCR

DNA was either extracted from native porcine gut tissue or the respective decellularized SIS using the DNeasy Blood & Tissue Kit. DNA amount was determined using Quant-iT™ PicoGreen® dsDNA Assay Kit and normalized to the dry weight. Qualitative control was done by gel electrophoresis with 2 % agarose gel. RNA was extracted from tissue samples using the RNeasy Micro Kit plus with a TissueLyser LT and following the manufacturer´s protocol. iScriptTM Reverse Transcription Supermix for RT-qPCR was used to generate cDNA. RT-qPCR was carried out using a CFX 96 Real time system with a C1000 Thermal Cycler and the Sso-Fast Eva Green Supermix. The following reaction condition was chosen: 40 cycles of 95 °C 10 sec, 60 °C 10 sec, 72 °C 30 sec. Exon-spanning primer pairs were either selected from previous literature [85, 88, 118, 119]or self-designed using NCBI-Primer designing tool and manufactured by a supplier (Eurofins Genomics, Ebersberg, Germany) (Table 11).

4.5 FITC-dextran assay

FITC-dextran is a substrate available in different sizes of the sugar chain and covalent coupled with a Fluorescein isothiocyanate (FITC) which makes it easy to detect and quantify. FITC-dextran 4 kD was solved in the basal cell culture to get a final

concentration of 0.25mg/ml. The FITC-dextran solution was sterile filtrated with a 0.2 μm filter. Before the assay, medium of the *in vitro* models was exchanged and incubated at 37°C for minimum 30 min. For the 24-well-format a volume of 300 μl apical (donor) and 900 μl basolateral (acceptor) was chosen, for the 12-well-format 500 μl and 1500 μl. First basal culture medium was added basolaterally before FITC-dextran solution was added apical. Models were incubated for 30 min on an orbital shaker at 37°C in an incubator. After incubation, probes of 100 μl were taken from the basolateral compartment and pipetted to a black 96-well-plate. Absorption was measured at Excitation of 490 nm and Emission of 525 nm with an ELISA-reader (Tecan infinite 200, Switzerland). Donor solution was measured and defined as 100 percentage. Permeability for FITC-dextran was calculated in percentage of the donor considering dilution by the basolateral volume.

4.6 TEER-measurement

To ensure barrier integrity TEER measurement is a widely used method where the electric resistance of the barrier is measured. A barrier models requires two by the barrier separated compartments in this case the intestinal epithelium. The tightness of the epithelial layer is influences by the confluency of the monolayer and the expression of the tight-junction proteins which seal the paracellular gap. We used the commercially available hand-electrode. Before every testing, a standard resistor was used to calibrate the device. Medium of the *in vitro* models was exchanged and incubated at 37°C for minimum 30 min. The hand-electrode was sterilized by incubation in 70 % Ethanol for 10 min, drying under the sterile hood in a petri dish and incubation in the used cell culture medium for another 15 min. For the measurement the longer electrode was put in the medium of the outer compartment (basolateral) while the shorter electrode was used for die inner compartment of the cell crown (apical). The measurement was carried out until the values showed to be stable. For normalization cell crowns with no cell seeded on the matrix were measured and the values subtracted from the ones with cells.

4.7 Transport studies

For validation of the human primary intestinal model, substances with different transport properties were chosen and tested in a transport assays. Propranolol as a high permeable substance, sodium-fluorescein as a substance with low permeable properties and Rhodamin123 as a substrate for the efflux transporter Mdr1. Test substances were solved in basal cell culture medium for preparation of a stock solution and further diluted afterwards.

Reference substances were added in a volume of 300μl of basal medium to the apical compartment using following concentrations: 400 μg/ml fluorescein, propranolol and 5μg/ml rhodamin123. Samples (100μl) of the basolateral lumen (900μl) were taken at 0, 15, 30, 45, 60, 75, 90 min. Quantitative Analyses of fluorescein and rhodamin123 was done by measurement of the fluorescence intensity with a Tecan microplate Reader Infinite M200 (Tecan; Männedorf, Switzerland). Sample concentration was calculated by linear correlation of concentration and fluorescence intensity. Propranolol concentration was analyzed by HPLC-MS/MS. The apparent permeability coefficient (Papp-value) was calculated for every substance by following formular [77]:

$$P_{app} = \frac{dQ}{dt} \times \frac{1}{A \times C_0} \left[\frac{cm}{s}\right]$$

dQ/dt = permeability rate, C_0 = initial concentration, A = surface of the monolayer

4.8 Nanoparticles

Poly(lactic-"co"-glycolic acid) (PLGA) based nanoparticles (NPs) with a size of 214 nm were solved in a volume of 300 μl basal medium and added at a concentration of 1.0 mg/ml to the apical donor compartment of an intestinal mucosa Transwell® system with 900 μl medium in the basolateral acceptor compartment. Samples of 100 μl were collected at 30, 60, 120, 180, 240, 300 and 360 min of culture. To determine qualitative transport, the fluorescence intensity of coumarin 6-loaded NPs was measured with a Tecan microplate Reader. Serial dilutions of the starting concentration of the NPs were used as standards to estimate the NP concentrations of the samples. For analysis by SEM (Supra 25, Carl Zeiss AG, Germany), basolateral solutions were centrifuged, washed twice with distilled H_2O, dried on a glass slide and sputtered with platinum.

Uptake of NPs in IECs was confirmed by confocal microscopy with Leica TCS SP8 (Leica, Wetzlar, Germany).

5 Results

5.1 Functional tests on an improved Caco-2 model

For investigation of the uptake and effects of encapsulated antigens for peroral vaccination, a co-culture model of Caco-2 cells with dendritic cells was setup and characterized. In this study, we initially started to use an improved intestinal model based of the decellularized SIS-muc derived from porcine gut tissue previously published by Pusch *et al.* 2011 [75].

5.1.1 Adaption of the Caco-2 model

After completing the decellularization process (4.1.1) the permeable matrix still showed the characteristic crypt-villus structure of the small intestine (Fig. 4 A, C). The surface of this collagen based matrix was covered by the basal lamina of the former epithelium (Fig. 4 B). In comparison, the standard Caco-2 barrier model is based on the Transwell® system with two compartments separated by a porous PET-membrane (Fig. 4 D-F). The membrane shows randomly distributed pores with a size of 1 μm.
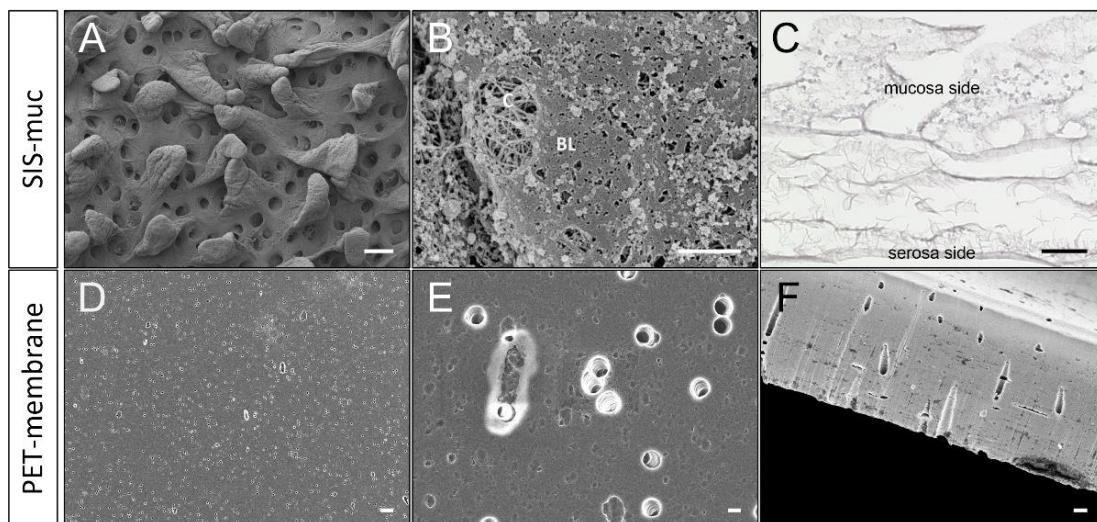
Figure 4: Ultrastructure of decellularized scaffold (SIS-muc) and PET-membrane. Scaffold shows characteristic topography of the small intestine with its crypt-villus structure on the mucosa side (A, C). On the mucosa side the network of collagen fibrils is covered by a thin layer, the basal lamina (B; CF: collagen fibrils, BL: basal lamina).

The standard porous PET-membrane of a Transwell® with randomly distributed 1 μm pores (D-F). Scale bar in A, D: 100 μm; B, E: 1 μm; C, F: 50 μm.

To create a similar approach as the Transwell® system with two separated compartments we fixed the decellularized scaffold between two cylinders in so called cell crowns with an area of 1 cm^2 (Fig. 5 A). Due to the crypt-villus topography the SIS-muc had an enlarged surface with an increased number of cells covering the surface compared to the PET-membrane insert (Fig. 5 B).
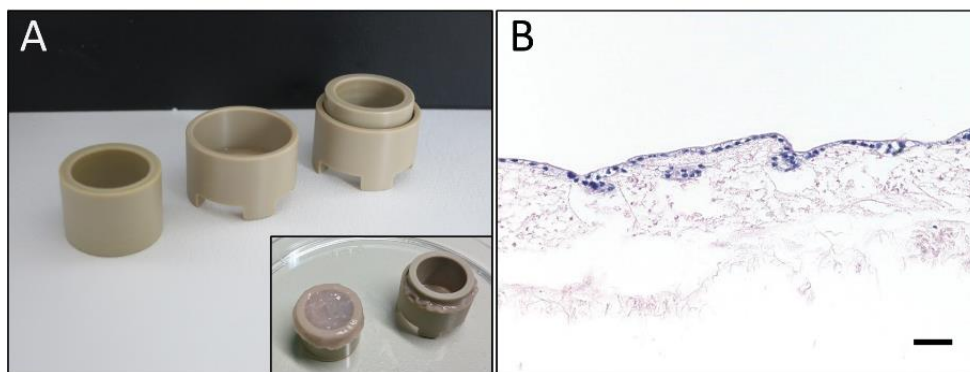
Figure 5: Caco-2 model based on SIS-muc. Two plastic cylinders, so called cell crowns, to fix the decellularized matrix in between (A). Confluent monolayer of Caco-2 cells grown on decellularized matrix (SIS-muc) shown by hematoxylin and eosin staining (B). Scale bar in B: 50 μm.

5.1.2 Immune cell differentiation

Due to their role in antigen processing and presentation, DCs were previously identified as main delivery target for vaccination antigens. The dendritic cells were obtained and differentiated from PBMCs according to protocols kindly provided by Prof. Walden´s group, Charite Berlin. After isolation of the cellular components from the blood by a density gradient and selection of cells by plastic adhesion, cells were differentiated by supplementation of IL-4 and GM-CSF for 3 days (Fig. 6).
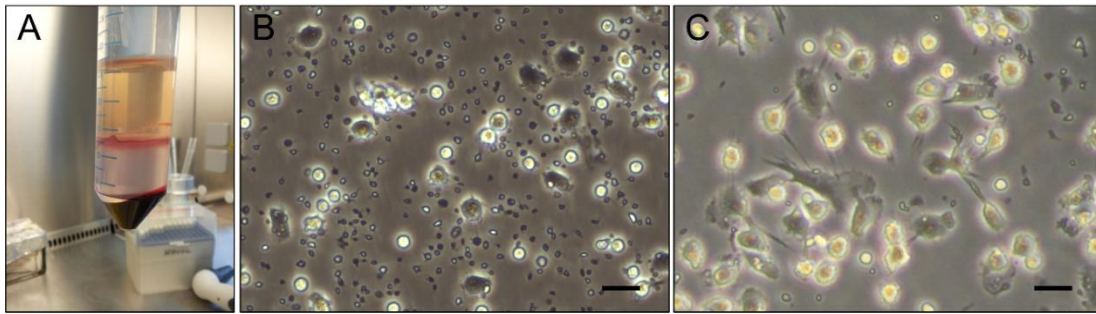
Figure 6: Preparation of PBMCs. Isolation of monocytes by Ficoll density gradient (A), adherent monocytes after 2 h (B) and DCs after completing differentiation protocol (C).

After completing the differentiation process the cells were stained for CD11c and HLA-DR (major histocompatibility complex II; MHC-II), both characteristic markers for DCs. To proof the functionality of these cells we furthermore tested the capability for immune cell activation. Thus, after incubation of the cells with bacteria-derived lipopolysaccharide (LPS) the cells showed an upregulation of the mature DC markers CD80 and CD86 (Fig. 7).
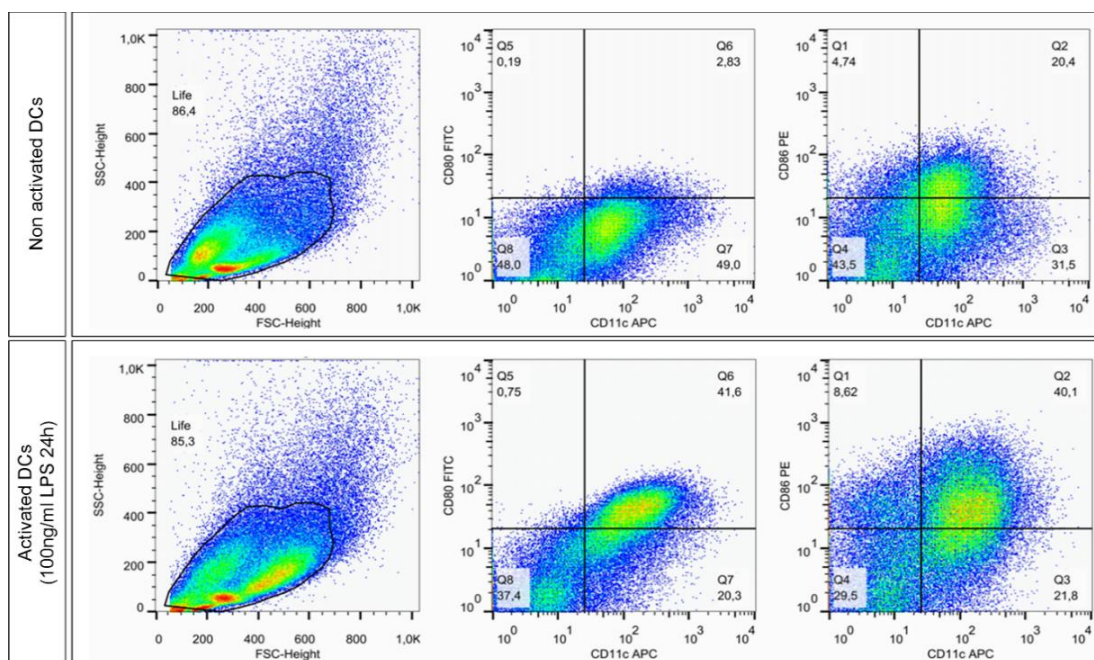
Figure 7: Activation of dendritic cells. Differentiated DCs derived from monocytes show expression of CD11c, CD80 and CD86. Activation of the DCs by LPS stimulation led to increase of activation markers CD80 and CD86.

Differentiated immature DCs were applied to the basolateral compartment of our test system as described earlier (4.1.3). Such set up allowed easy access to the DCs for the described analyses.

5.1.3 Caco-2 transport assay performance

For peroral antigen delivery two different particle types were developed and modified during this project. One system based on the synthetic polymer PLGA and modifications with PEG-PAGE and Mannose was developed at the University of Saarland, AG Prof. Lehr. The other system was based on the naturally occurring polymer Chitosan and developed at the University of Kiel, AG Prof. Scherließ.

Considering the size of the particles with about 200 nm an uptake by endocytosis was expected. To investigate how fast the particles are taken up, the Caco-2 cells were incubated with the particles for up to 1 h. Confocal microscopy of Caco-2 cells after incubation with fluorescence-labelled PLGA and Chitosan NPs confirmed intracellular uptake at various time points (Fig. 8). PLGA NPs showed a very fast accumulation in

the cytosol of the cells starting at 15 min reaching a maximum after 30 min and slowly decreasing afterwards. In contrast, the amount of Chitosan NPs in the cells increased slower compared to the PLGA NPs. A notable number of particles could firstly be detected after 30 min, while the maximum was reached after 45 min.
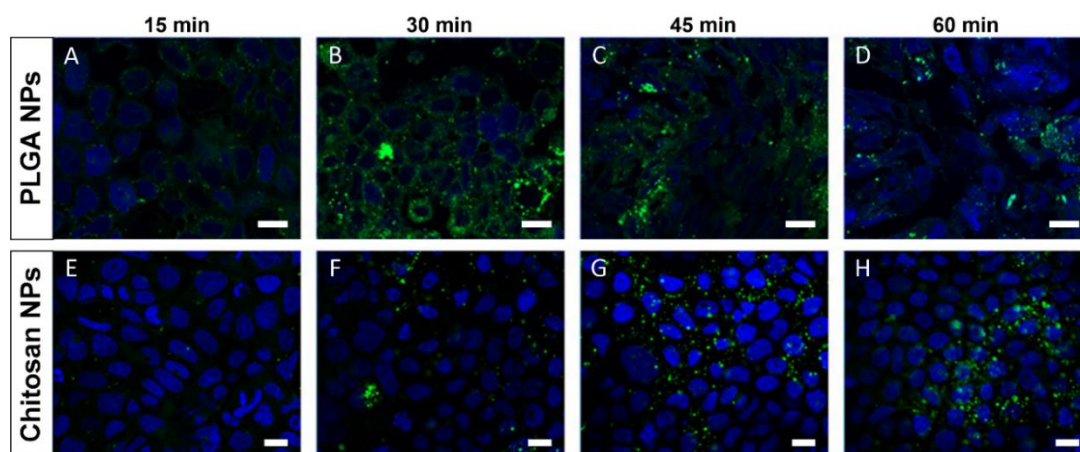

Figure 8: Cellular uptake of nanoparticles. Caco-2 cells incubated for up to 1 h with fluorescence-labelled PLGA- and Chitosan-NPs at a concentration of 1mg/ml. Particle uptake was detected by fluorescence microscopy. Scale bars: 20 μm.

Differentiated DCs were incubated with PLGA NPs and Chitosan NPs to investigate their ability to phagocytose the particles. Confocal imaging revealed the characteristic dendrites growing out of the cells (Fig. 9 A). After incubation with the particles both PLGA and Chitosan NPs could be localized within the cytosol of the DCs (Fig. 9 B, C).
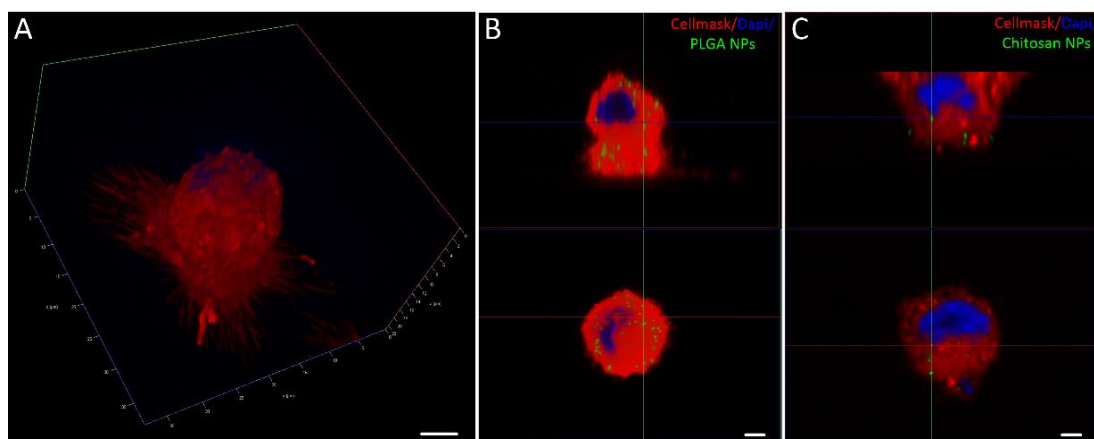
Figure 9: Confocal imaging of dendritic cells. Adherent dendritic cells differentiated from monocytes showed characteristic dendrites (A). After incubation with PLGA NPs (B) and Chitosan NPs (C) cells showed uptake of the particles. Scale bars: 5 µm.

In order to quantify the uptake of the particles into cells over a longer timespan we performed flow cytometry analysis. To estimate the amount of particles taken up, the fluorescence intensity per cell was directly correlated to the amount of NPs within the cytosol of the cells. Epithelial cells were enzymatically detached from the matrix, digested to singles cells and analysed at five different time points, at 0, 0.5, 1, 2, 4, 6 h. In addition, phagocytosis of NPs by DCs added to the basolateral compartment was quantified at the same time points (Fig. 10). As expected by the fluorescence imaging (Fig. 8) PLGA and modified PLGA NPs showed strong uptake in epithelial cells within the first 30 min while Chitosan NPs had a delayed uptake. After 4 h, the DCs in the basolateral compartment showed an increased fluorescence intensity for PLGA-, PP-PLGA- and ManPP-PLGA-NPs (Mannose-PEG-PAGE-PLGA). In contrast, within the timeframe of 6 h no significant increase in fluorescence signal could be detected for the Chitosan-NPs indicating that transport is much slower as for all the other tested NPs (Fig. 10).
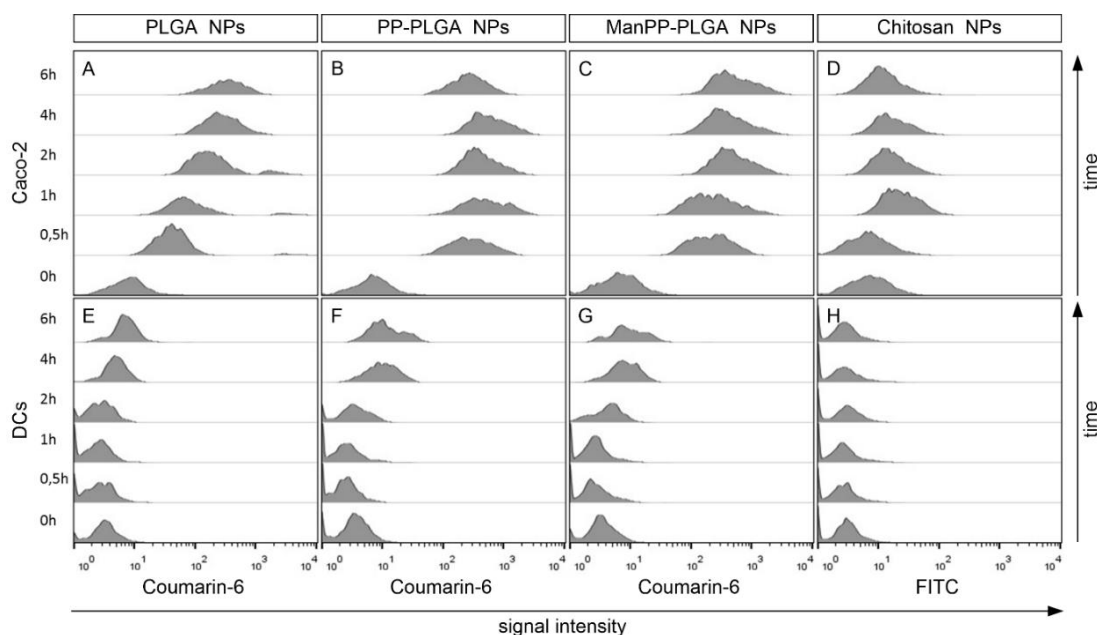
Figure 10: Quantitative analysis of cellular particle uptake by flow cytometry. Uptake of fluorescence-labelled nanoparticles by apical Caco-2 cells and basolateral cultured dendritic cells was investigated over a timeframe of 6 h by flow cytometry. All PLGA based particles were Coumarin-6 labelled, encapsulated within the particles while the Chitosan-NPs were FITC labelled. Fluorochromes were both excited at 488 nm and detected at 530 nm by BD FACSCalibur [113].

Finally, we determined the concentration-dependent transport across the epithelial layer. Therefore, three different concentrations were apically applied and incubated for 6 h. All particles showed a direct correlation between concentration and amount of transported particles (Fig. 11). Thus, a higher applied concentration also resulted in an increased transport of particles towards the basolateral compartment for all formulations. When comparing the different particle types at the same concentration with each other no significant difference could be found (Fig. 11 E).
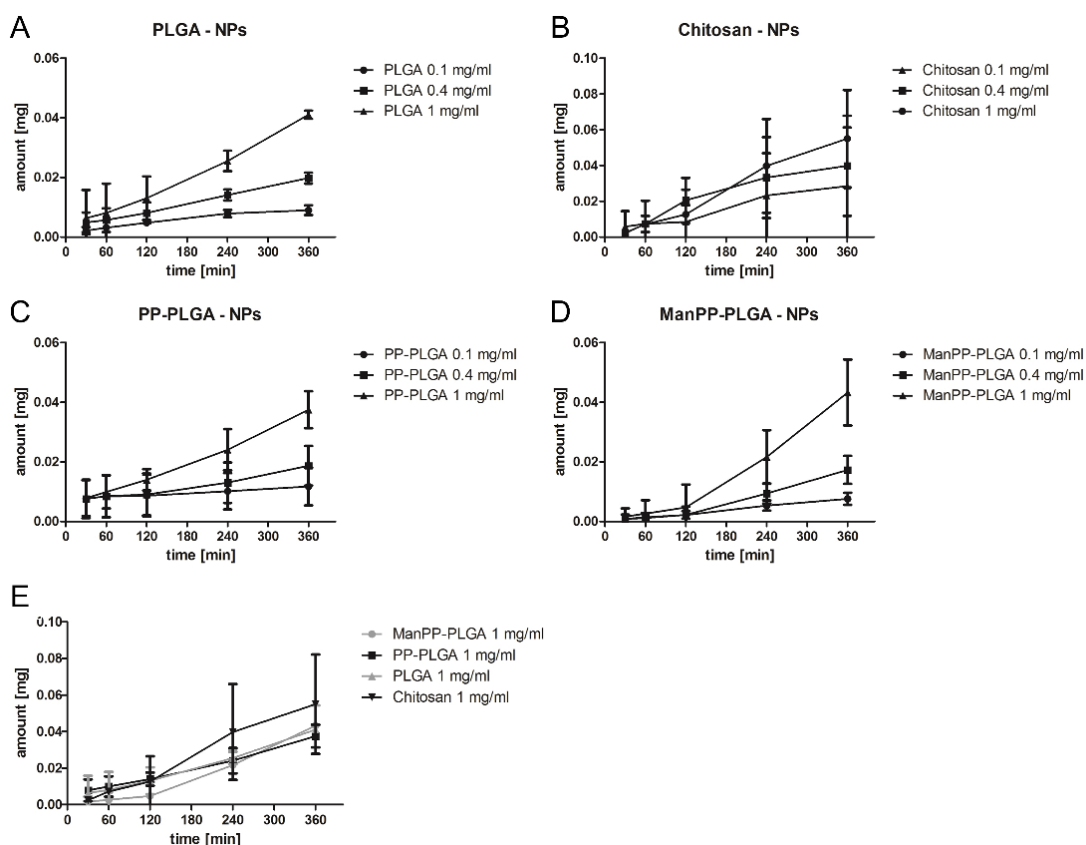
Figure 11: Penetration of a Caco-2 epithelial barrier by nanoparticles. All types of particle show increasing transport across the epithelial barrier correlating with applied amount of particles and time. Concentration of 0.1 mg/ml, 0.4 mg/ml and 1 mg/ml of PLGA (A), Chitosan (B), PP-PLGA (C) and ManPP-PLGA particles (D) was tested. The four tested particle types showed no significant differences in overall transport effectivity at a concentration of 1mg/ml (E) [100].

To proof that the measured fluorescence intensity is caused by loaded particles and not by free fluorochrome the basolateral lumen was checked for particles. The centrifuged and washed medium showed nanoparticles by SEM qualitative analysis for PLGA, PP-PLGA, ManPP-PLGA and Chitosan particles (Fig. 15).
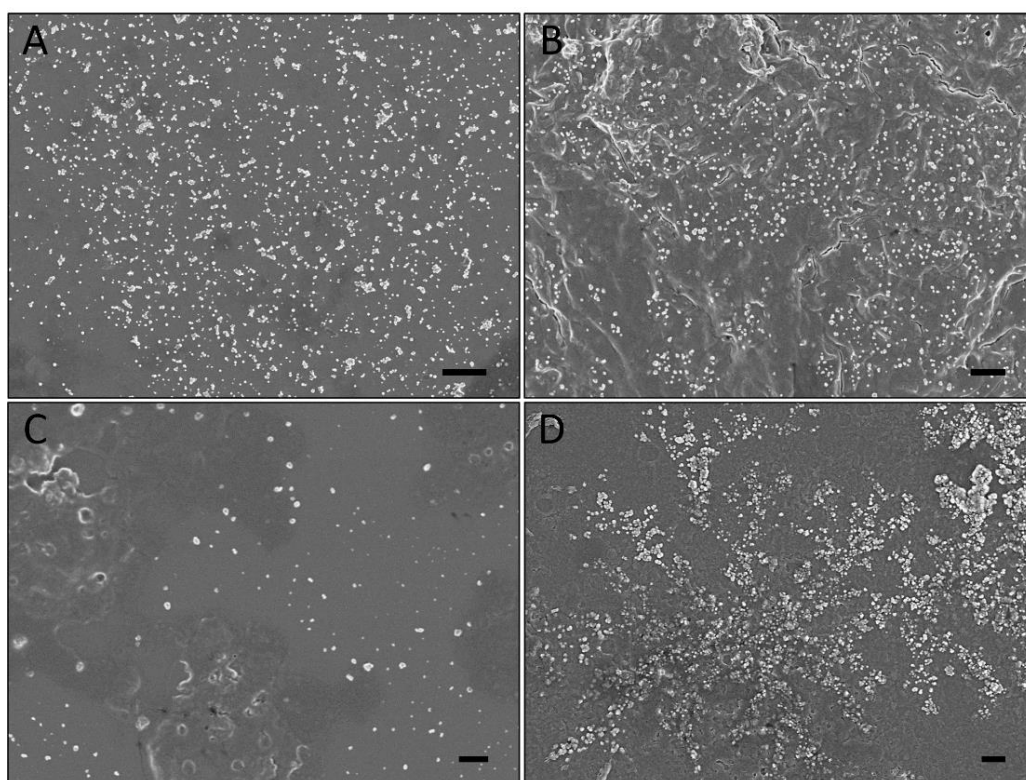
Figure 12: Qualitative proof of particle transport by SEM analysis. After crossing the epithelial barrier (A) PLGA, (B) PP-PLGA, (C) ManPP-PLGA and (D) Chitosan NPs can be found basolaterally at the bottom of the cell culture well as detected qualitatively by SEM imaging after 6 h incubation with the particles. Scale bar in A: 3 µm and in B-C: 1 µm.

The formulation provided by our project partners were all in the same size range between 179 nm and 267 nm in average (Tab. 19). The calculated permeability coefficient (P_{app}-value *i.e.* average speed of NP transport across the barrier) was between 2.3 to 4.1×10^{-6} cm/s (Tab. 19). Only Chitosan showed a slight but not significant higher P_{app}-value. The relative transport was about 7.7 % for the PLGA-NPs, 5.9 % for the PP-PLGA-NPs, 7.5 % for the ManPP-PLGA-NPs and 9.5 % for the Chitosan NPs of the applied amount (Tab. 19). The recovery rate for the particles within the test system based on the measured fluorescence after the 6 h of incubation revealed a recovery rates of less than 50 % for the PLGA-based particles while the Chitosan particles showed rates of over 90 % (Tab. 19).

Table 19: Summary of the transport studies

Formulation	Average particle size [nm]	Permeability coefficient (P_{app}) [cm/s]	Total transport [%]	Recovery rate [%]
PLGA	267	2,7E-06	7.7± 0.27	47.6
PP-PLGA	191	2,5E-06	5.9± 1.27	46.3
ManPP-PLGA	179	2,3E-06	7.5± 1.99	47.6
Chitosan	249	4,1E-06	9.5± 4.39	92.8

In summary, we could show that the co-culture models based on a decellularized scaffold proved to be suitable to test particulate formulations. Epithelial cells as well as DCs demonstrated an intracellular uptake of particles. All PLGA based particles showed a comparable transepithelial transport rate. Only the transport of Chitosan particles was a slightly increased.
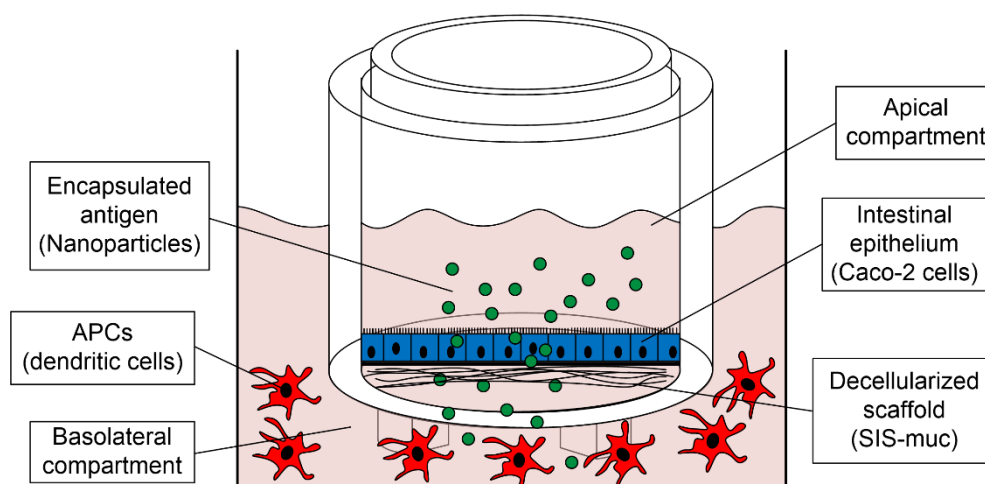

Figure 13: Co-culture model for peroral drug delivery testing. Models based on decellularized scaffold covered with a Caco-2 monolayer representing the intestinal barrier. Dendritic cells in the lower basolateral volume can be included to investigate immune response due to antigen processing.

5.2 Establishment of a primary small intestinal tissue model

To further improve the intestinal tissue model the Caco-2 cells were replaced by freshly isolated, human primary cells. This should lead to an even more physiological model, reflecting very closely the properties of the small intestine. Thus, based on the well-established organoid technology, primary intestinal epithelial cells from human small intestinal donor tissue were isolated, expanded and seeded on a decellularized scaffold spanned into a cell crown system.

5.2.1 Pilot studies for model establishment

As for the improved Caco-2 model, the primary intestinal model developed in this study was based on a decellularized biological scaffold generated from porcine jejunum of the small intestine. However, to increase standardisation, only the small intestinal submucosa (SIS) part was used for the primary culture, exhibiting a more plane surface and reduced barrier properties compared to the SIS-muc (data not shown).

5.2.1.1 Matrix preparation - SIS

The mucosa was removed mechanically, followed by the decellularization process and finally the gamma-sterilization, as described (4.1.1). After this process the obtained scaffold appears macroscopically completely white (Fig. 14 B). To verify the preservation of ECM components, Masson trichrome staining was used to visualize collagen fibers of the former subepithelial connective tissue (Fig. 14 C, D; green). Furthermore, Feulgen staining and gel-electrophoresis after DNA isolation confirmed no significant amount of DNA leftovers after the decellularization (Fig. 14 F, G). More sensitive quantitative analysis by PicoGreen® assay confirmed a small remaining amount of DNA within the scaffold (mean 219 ± 168 ng DNA per mg dry weight, n=3). SEM imaging confirmed a relative plane surface covered with collagen fibers (Fig. 14 H).
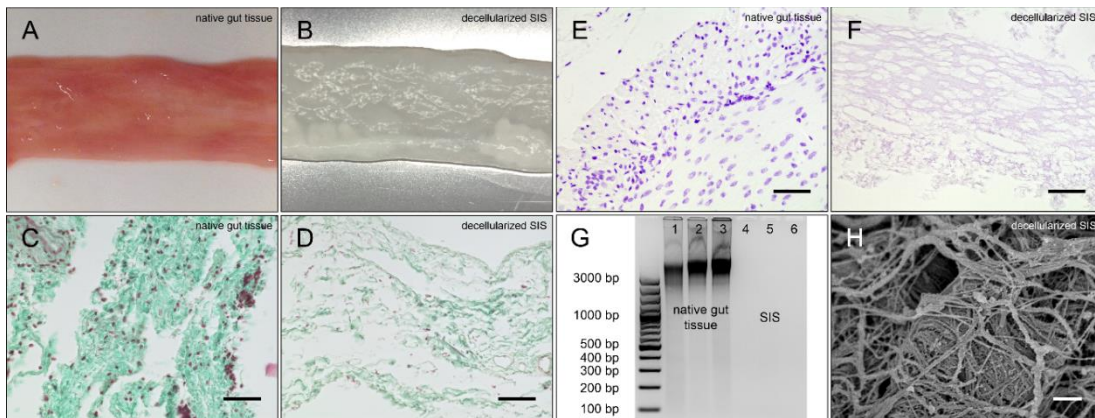
Figure 14: Decellularized biological matrix (SIS) used for intestinal model. Visual control of porcine tissue before and after the decellularization process (A, B). Trichrome staining revealed a matrix of green stained collagen fibers, which were preserved during the process (C, D). Feulgen staining demonstrated that DNA of the porcine cells was completely removed (E, F). Qualitative agarose gel electrophoresis verified that there was no detectable DNA after the decellularization process of the SIS (G, lane 4-6). SEM analysis of the SIS revealed dense collagen fibers (H). Scale bar in A-F: 20 µm, in H: 1 µm [120].

5.2.1.2 Cell expansion - organoid culture and myofibroblasts

The isolated intestinal crypts were embedded in Matrigel, where they formed organoid structures. To keep the population of proliferating cells high during the expansion, the organoids had to be kept very small (size ~150-200 µm) and therefore were splitted very frequently, every 3-5 days (Fig. 15 A). During expansion the organoids showed markers for all the differentiated intestinal cell types as well as undifferentiated stem and progenitor cells indicated by Ki67 positive cells (Fig. 15 B). Quantification by flow cytometry after EdU-labelling, which is incorporated into DNA during cell division revealed a high number of EdU-positive, proliferating cells of ~29.5 $\pm$ 4.8 % (n=4) (Fig. 15 C). During the project we established a human organoid cell bank of 37 different donors, which are listed in Table 21 (Supplement).
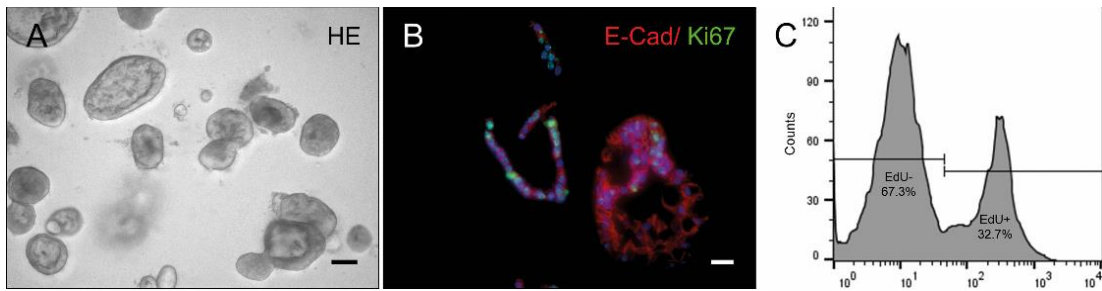
Figure 15: Propagation of intestinal organoids. Intestinal epithelial cells growing as organoids embedded in Matrigel (A). Immunostaining of organoids showed accumulation of proliferating cells positively-stained for Ki67 (green nuclei; B). Quantification of proliferating cell population by flow cytometry revealed a population of 32.7 % dividing cells (C). Scale bar in A: 100μm, in B: 20 μm.

In order to implement the mucosal niche we integrated a mesenchymal component in our model. Therefore, myofibroblasts from the subepithelial tissue were isolated and expanded. Characterization by flow cytometry demonstrated cells positively for α-Smooth-Muscle-Actin (αSMA) and mesenchymal marker Vimentin and negative for muscle marker Desmin and endothelial marker CD31 (Fig. 16 A). Transmitted light microscopy of subepithelial myofibroblasts (Fig. 16 B) and immunofluorescence microscopy demonstrated very heterogenous population of cells positive for αSMA, Vimentin and Desmin (Fig. 16 B, C, D).
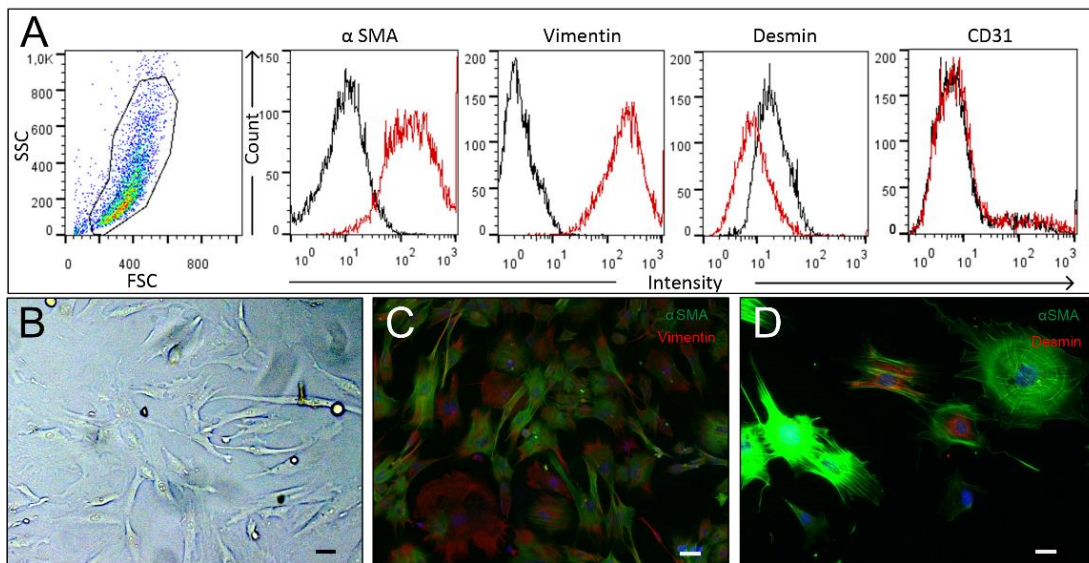
Figure 16: Characterization of human intestinal subepithelial myofibroblasts. Isolated myofibroblasts were analysed by flow cytometry showing to be positive for SMA and Vimentin and negative for Desmin and CD31 (A). Microscopic analysis revealed a population with very heterogenous morphology (B). Immunofluorescence staining showed cells positive for α-Smooth-Muscle-Actin (αSMA, green) and/or Vimentin (red) (C) as well as αSMA (green) and/or Desmin (red) (D). Scale bar in B, C: 50 μm, in D: 20 μm.

5.2.1.3 Cell density

Transwell-like models were based on the cell crown system with an area of 0.54 cm^2 of seeded surface. Different cell concentrations were tested to determine the optimal cell number necessary. organoids were enzymatically digested to single cells and seeded on the scaffold. After 7 days, HE-staining revealed a confluent monolayer for all three cell concentrations 2x10^5, 4x10^5 and 6x10^5 cells per 0.54 cm^2 (Fig. 17, A-C). The cell density of 4x10^5 cells turned out to be the best regarding barrier functions with the lowest FITC-dextran permeability of 2.3% and the highest average TEER-value of 35 Ωxcm^2 and was chosen for the following experiments.
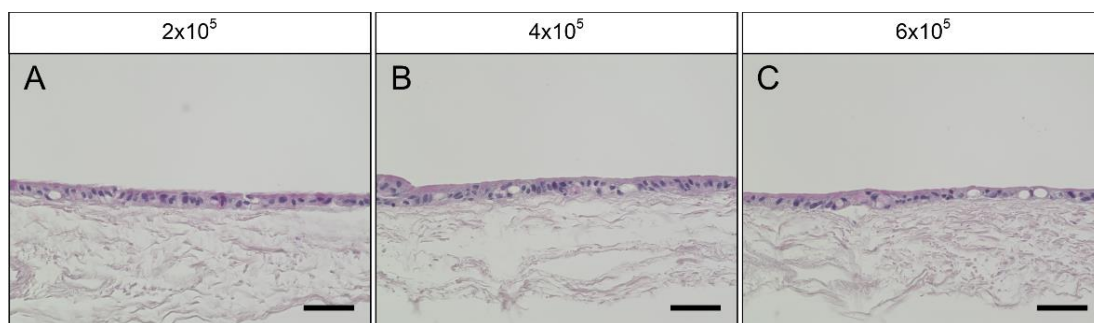
Figure 17: Determination of the optimal cell density. Different amount of cells were seeded on SIS to look for the capability to build a confluent monolayer. All three cell concentrations $2x10^5$, $4x10^5$ and $6x10^5$ cells per 0.54 cm^2 showed a confluent cell layer after 7 days in the HE-staining (A-C). Scale bars: 50 µm.

5.2.1.4 Wnt3A concentration and co-culture

The Wnt-signalling presents the main pathway responsible for cell proliferation in the intestinal epithelium. The main signal-protein Wnt3A with the highest activity is produced by the neighbouring subepithelial myofibroblasts. Wnt3A can also be supplemented to the medium by using recombinant Wnt3A or Wnt3A-conditioned medium. The recombinant Wnt3A alone was tested and showed no sufficient activity leading to cell death after a few days of culture. However, Wnt3A-conditioned medium, which obviously contained important co-factors showed a very good activity and was exclusively used to propagate the cells. Different concentrations of Wnt3A-conditioned medium in combination with co-culture were tested (Fig. 18). Aim was to generate cells, which have sufficient proliferation potential at the beginning of the monolayer culture to provide a confluent monolayer of epithelial cells, essential for a tight barrier model. After 2 day with proliferation medium, medium was changes to induce differentiation (4.1.6). Supplementation between 25-50 % Wnt3A-conditioned medium resulted in a confluent cell layer on the SIS after 5 more days in culture (Fig. 18 A, C). Additional co-culture with myofibroblasts did not hinder the formation of a confluent layer and resulted in some inclusions within the epithelium (Fig. 18 B, D).
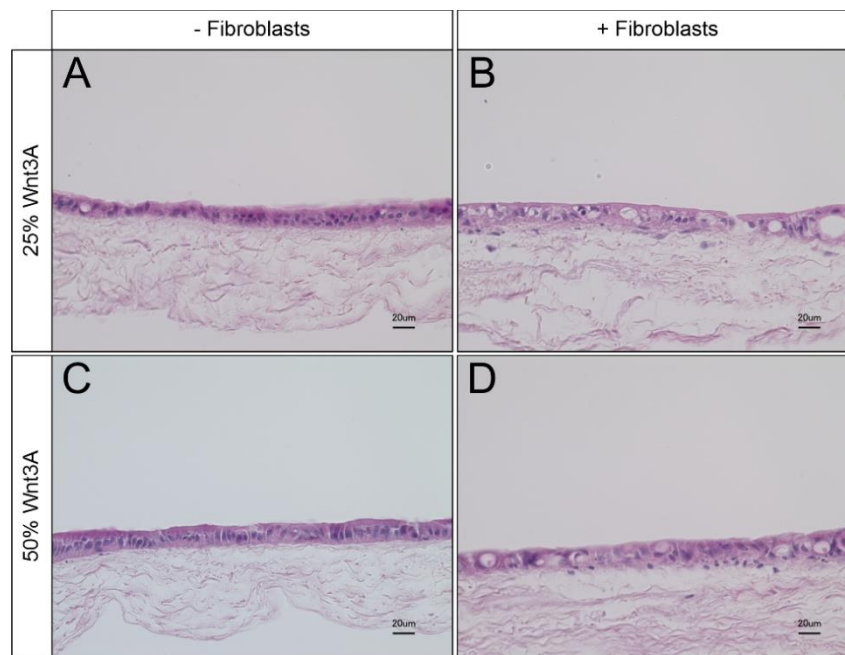
Figure 18: Co-culture with myofibroblasts and different Wnt3A concentration. Wnt-signalling which is essential for growth of the intestinal epithelial cell can be provided by medium supplementation or by co-culture with myofibroblasts. Both, 25 % (A) and 50 % (C) of added Wnt3A-conditioned medium resulted in a confluent monolayer. Additional co-culture with intestinal myofibroblasts also showed a confluent layer with inclusions in the epithelium at 25 % Wnt3A-conditioned medium (B) as well as 50 % (D) (n=3).

The barrier integrity was the most crucial factor to validate the primary Transwell-like model and to ensure reliable testing. Measuring the TEER-value with the chopstick electrodes showed to be an easy way to determine the barrier function of the models and non-invasive. Comparing 25 % and 50 % Wnt3A-conditioned medium with or without myofibroblasts revealed no clear differences (Fig. 19 A). FITC-dextran permeability instead showed a very robust barrier for 25% Wnt3A-conditioned medium in co-culture with myofibroblasts (Fig. 19 B). For this reason, following experiments were carried out under this conditions.
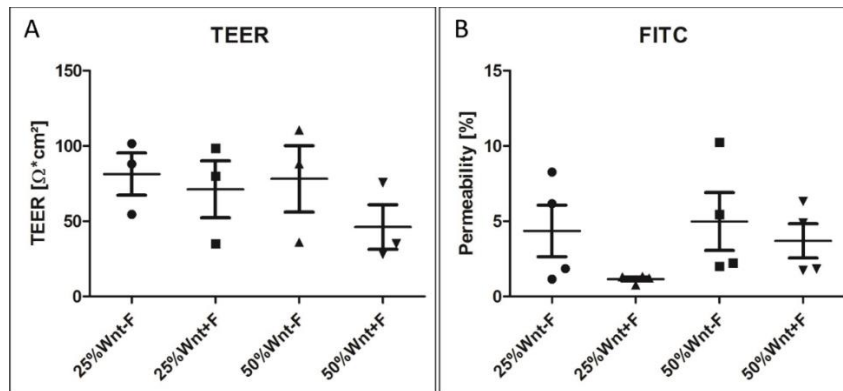
Figure 19: Barrier integrity - different culture conditions. The models with 25% and 50% Wnt3A-conditioned medium were compared regarding their barrier integrity, measuring TEER (A) and the FITC-dextran permeability (B). In addition the influence of co-culture with myofibroblasts was investigated (n=3).

5.2.1.5 Culture time

To investigate the influence of culture time we looked for the FITC-dextran permeability of the primary barrier model at 7, 10, 14 days and compared the values with native human jejunum mucosa tissue and the standard Caco-2 model after 14 days on SIS (Fig. 20). The permeability of the primary models was increased after 10 days (~1.5 %) and 14 days (~1.8 %) compared to 7 days (~1 %). The native human mucosa tissue showed a permeability of 0.1 % and the Caco-2 model <0.1 % (Fig. 20).
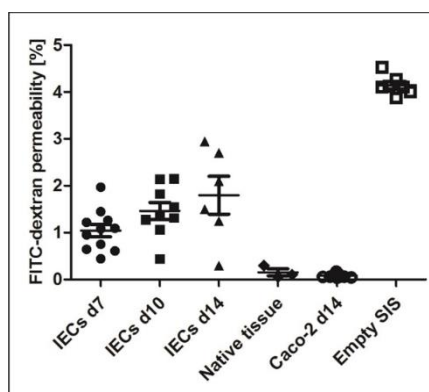
Figure 20: Barrier integrity - culture duration. The FITC-dextran permeability of the primary Transwell-like models based on SIS at different time points was compared with native mucosa form human jejunum tissue and Caco-2 cells after 14 days of culture.

With respect to these preliminary studies, the Transwell-like models were cultured for 7 days with a cell density of 0.8×10^5 cells/cm^2 in co-culture with myofibroblasts using 25% Wnt3A-conditioned medium. These conditions were chosen to ensure a reliable setup of the models.

5.2.2 Adaption and detailed characterization of the primary model

Based on the pilot experiments described above, intestinal epithelial cells (IECs), expanded as organoid culture, were digested to single cells and seeded on the decellularized SIS matrix for 7 days under static culture conditions. For a more detailed characterization, firstly biological effects of co-culture with subepithelial myofibroblasts were investigated regarding the morphology, barrier integrity and gene-expression. HE staining of monoculture model after 7 days revealed the formation of a confluent monolayer covering the surface of the scaffold (Fig. 21 A). In comparison to the monoculture the monolayer morphology of the co-culture model appeared to be more heterogenic with cystic inclusions in the epithelium (Fig. 21 B, black star). The myofibroblasts were located directly under the epithelium (Fig. 21 B, C; arrows) and stained positive for Vimentin (Fig. 21 C). However, the measured TEER-values were very low compared to the Caco-2 model and revealed no significant differences between mono- and co-culture, both in a range of about 20-60 $\Omega \times$cm^2. Interestingly, the permeability values for 4 kDa FITC-dextran transport turned

out to be more robust *i.e.* ~1.2 ± 0.3 % vs. 4.4 ± 3.4 % after 30 min. Statistics confirmed by significant differences between the variances of the two groups (Fig. 21 E). Gene-expression analysis for Mucin 2 characteristic for goblet cells, and Claudin 4 indicating tight junctions revealed no significant differences between mono- and co-culture (Fig. 21 F). In contrast to the organoids, the monolayer cultures showed a 4-fold downregulation of Muc2 expression and 15-fold up-regulation of Claudin 4 expression.
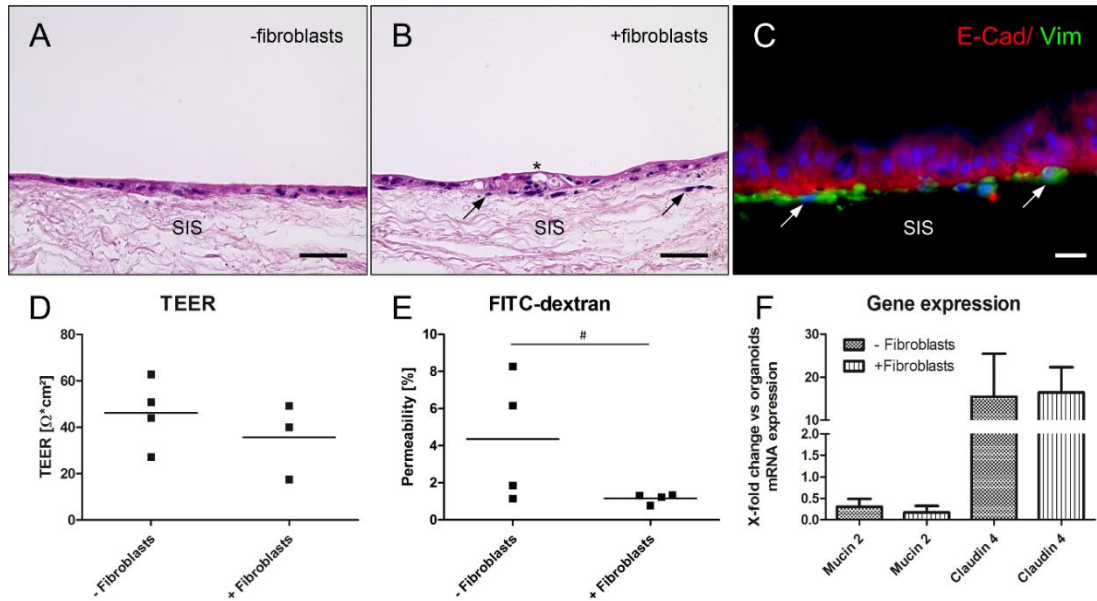

Figure 21: Establishment of intestinal co-culture on decellularized SIS. HE-staining of mono-and co-culture showed a tight epithelial layer on top of the biological matrix (A, B, arrow: fibroblasts, star: inclusions). Immunostaining of epithelial cells (C; red: E-Cadherin) and fibroblasts (C; arrow; green: Vimentin). Transepithelial resistance is comparable between mono- and co-culture (D; TEER) but FITC-dextran permeability was more robust in co-culture (E). Statistical analysis revealed only statistical trends for biological relevance in the mean value comparison (#P < 0.11), however showed statistical significance in the comparisons of the variances of the two groups (P < 0.0016). The co-culture revealed no differences in gene expression of Mucin 2 and Claudin 4, but differences of the monolayer culture compared to organoids could be detected for both genes (F). Scale bar in A, B: 40 μm, in C: 20 μm (n≥3) [120].

5.2.3 Influence of controlled dynamic culture conditions

The intestinal epithelium *in vivo* is exposed to constant mechanical stimuli caused by the peristaltic transport of chyme through the gastrointestinal tract. To simulate these shear forces and to investigate the influence of mechanical stress on our model we compared static, dynamic-shaker (OS) and dynamic-bioreactor (BR) conditions.

5.2.3.1 Theoretical determination of sheer-stress in the OS and BR system

To analyze the influence of dynamic culture engineers designed custom made devices to culture models under the different conditions and to separate the apical from the basolateral compartment, necessary for transport assays. For static culture in well-plates the already for Caco-2 described plastic cylinders so called cell crowns were used (Fig. 5, Fig. 22 A). This system shows similar features like the well-known Transwell® system. To provide mechanical forces to the cells perfusion bioreactors were used. The bioreactor also consists of two separated chambers, where medium was pumped through above and below the scaffold (Fig. 22 B). As alternative dynamic set up the cell crowns were simply placed on an orbital shaker (Fig. 22 A). To apply comparable mechanical stress to the models, the forces induced by medium movement were simulated by a dynamic computer modulation demonstrating $7.1x10^{-3} \pm 7.3x10^{-4}$ dyne/cm^2 for the shaker (Fig. 22 C) and $6.2x10^{-3} \pm 1.0x10^{-3}$ dyne/cm^2 for the bioreactor (Fig. 22 C, D) across the scaffold surface. Medium flow of 3.8 ml/min was considered to produce optimal mechanical forces and set as starting point. Cell crowns were used in 24-well-format, which have a surface of 0.54 cm^2 and can be cultured in standard well-plates, static in an incubator or on a shaker (Fig. 22 E). For generation of a constant medium flow through the bioreactor, a medium reservoir was connected to a peristaltic pump via tubing (Fig. 22 F).
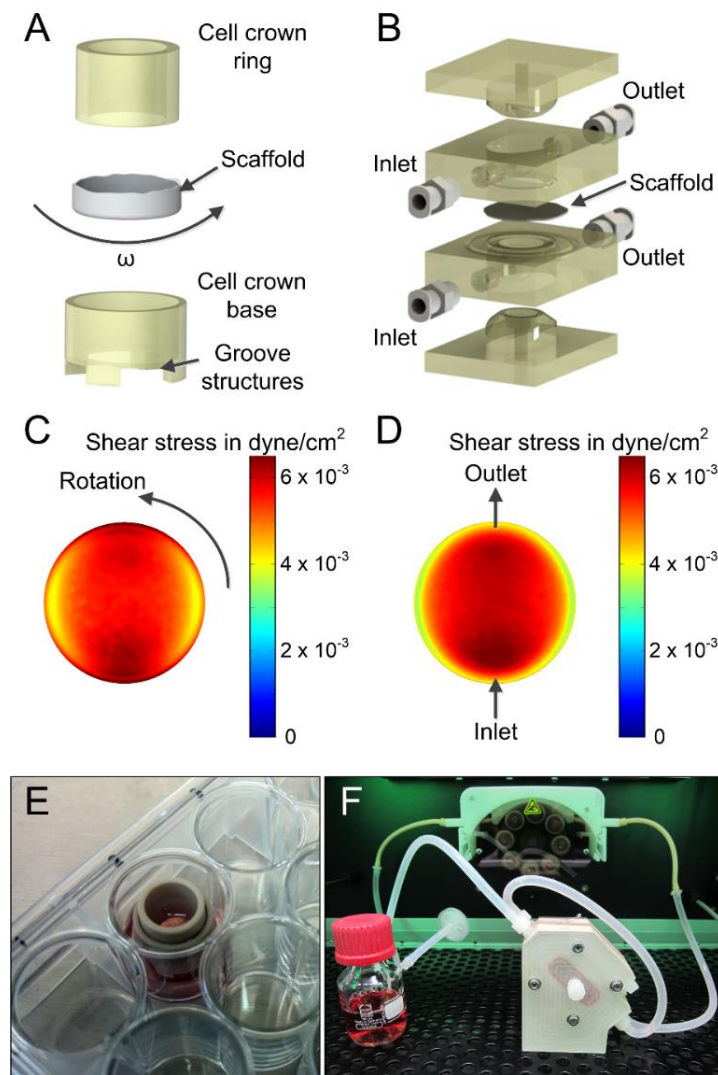
Figure 22: Culture devices and fluid dynamic characterization. The cell crown system supported usage of a biological scaffold in a 24-well. The scaffold was clamped between the cell crown ring and the cell crown base. A fit ensured separation of inner and outer fluid domain. Convective flow was induced by a continuous rotational motion of constant frequency ω (1/s). Groove structures underneath the scaffold facilitated increased mass transport (A). A bioreactor system allowed dynamic culture conditions at the interface between two fluidic domains. Cell culture medium was pumped through each domain from the respective inlet to the outlet (B). Fluid dynamic simulations revealed an almost homogenous mechanical shear stress distribution on the scaffold surface in the cell crown system on the shaker (C). The bioreactor design ensured reproducible mechanical stimulation. Except from a small ring, shear stress was distributed homogeneously across the scaffold surface (D). Images showing a cell crown in 24-well-plate format (E) and the flow-through bioreactor in a custom-designed incubator (F).

5.2.3.2 Comparison of static, OS and BR conditions

Histological analysis of the primary epithelium showed a high prismatic, more physiological morphology of the cells in the bioreactor (Fig. 23 C) in contrast to the static and OS conditions (Fig. 23 A, B). Under the dynamic conditions (Fig. 23 B, C) the myofibroblasts migrated into the matrix, while in the static culture they stayed directly under the epithelium (Fig. 23 A).
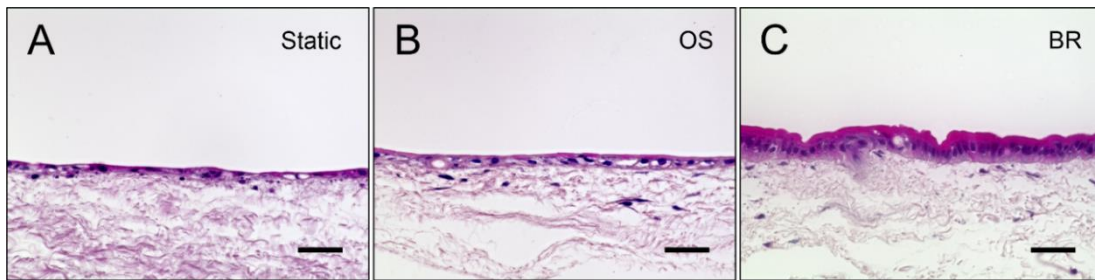
Figure 23: Histological analysis of static compared to dynamic culture conditions. H&E-staining of static culture (A), dynamic culture on a shaker (B) and in the bioreactor (C) showed differences in cell morphology and migratory potential of feeder cells into the matrix. Scale bar: 20 μm (n≥3).

On a transcriptomic level, applied culture conditions induced a 5-fold downregulation Mucin 2 compared to the organoids, while Claudin 4 expression was 6-15-fold higher, respectively (Fig. 24 A). However, the expression level of the metabolic enzyme Cytochrome P450 (CYP3A4) and the efflux transporter Multidrug-resistance-protein 1 (Mdr1) were only significant higher in the bioreactor (Fig. 24 B, C).

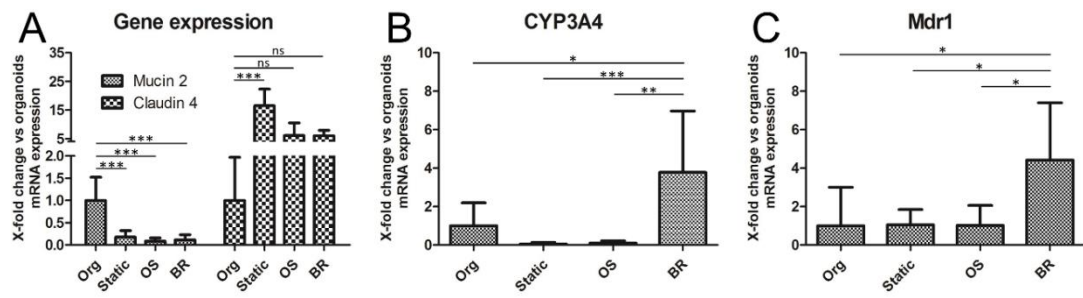**Figure 24: Influence of different culture conditions on gene expression.** Gene expression in monolayer cultures was reduced for Mucin 2 and induced for Claudin 4 compared to the organoids (A). Changes in gene expression between different culture conditions are particularly evident for CYP3A4 and Mdr1 under bioreactor conditions (B, C).

For functional assessment of the barrier properties typical reference substances with known transport activities were tested. Fluorescein, known as low permeable substance showed 3×10^{-6} cm/s higher P_{app}-values in models under static and OS conditions compared to the bioreactor with less than 1×10^{-7} cm/s, which is even lower than the Caco-2 model (dotted line) (Fig. 25 A). Similar effects were shown for the high permeable propranolol which showed P_{app}-values of 6.5×10^{-6} cm/s, which is about 2×10^{-6} lower compared to the other conditions and 5 times lower than observed in the Caco-2 model (Fig. 25 B). Rhodamin123 a known substrate of the Mdr1 efflux transporter. The ratio between basolateral-apical (b/a) and apical-basolateral (a/b) transport revealed a strong increased efflux activity in the bioreactor model, which was 10-fold higher and comparable to the Caco-2 model (Fig. 25 C).
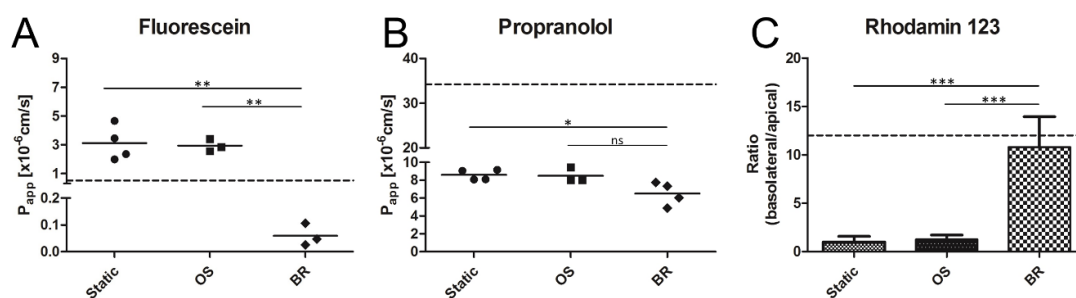
Figure 25: Impact of different culture conditions on the barrier function. Transport activity in was tested by low-permeable Fluorescein (A), high-permeable Propranolol (B) and Rhodamin123 as a substrate for the efflux transporter P-glycoprotein (C). In the bioreactor culture, Fluorescein and Propranolol showed notable slower transport, in contrast the efflux transporter activity was significantly higher as compared to the static and shaker culture. Dotted line shows Papp values for Caco-2 standard model according to Bock *et al.* 2004 [103].

5.2.4   Molecular characterization

Standard cell line-based models only consist of one cell type, whereas the here presented primary model showed all the characteristic cell types of the small intestine, better reflecting the *in vivo* situation. Histological analysis of the epithelial monolayer not only showed cells positive for general epithelial markers like Cytokeratin 18 (CK 18), pan-Cytokeratin (pCK) and E-Cadherin (E-Cad) (Fig. 26 A-F), but also for Mucin 1 and Mucin 2 (Fig. 26 C, F; mucus producing goblet cells) and Villin marking the microvilli (Fig. 26 B; absorptive enterocytes), which all together represent the majority of cells to be found in the intestine. In addition, we detected other, rare cell types of the secreting lineage, the hormone-producing enteroendocrine cells, which were positive for Chromogranin A (Fig. 26 D) and Paneth cells secreting lysozyme (Fig. 26 E).
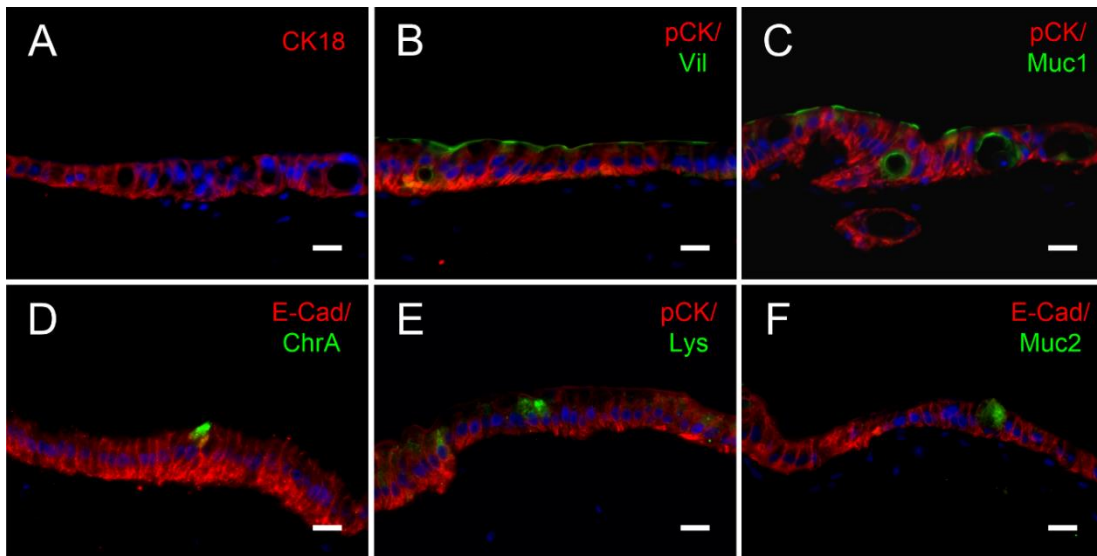
Figure 26: Histological characterization of the model under bioreactor conditions. Immunohistological stainings of CK18 (Cytokeratin 18), pan CK and E-Cad (E-Cadherin) showed IECs (A-F) in combination with characteristic differentiation markers: Enterocytes (B; Villin), enteroendocrine cells (D; Chromogranin A), paneth cells (E; Lysozyme) and goblet cells (C, F; Muc1/2). Scale bar: 20 μm.

Electron microscopy with SEM and TEM revealed a cell surface densely covered with microvilli (Fig. 27 A, B). Analysis on ultrastructure level further more confirmed tight-junction complexes sealing the epithelium and desmosomes as cell-cell connections (Fig. 27 C).
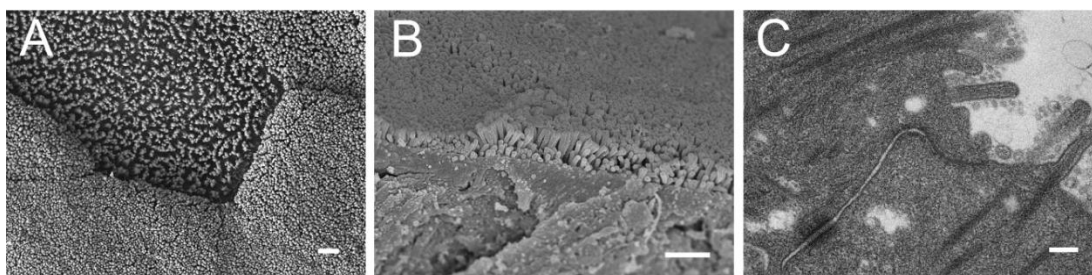
Figure 27: Histological characterization on ultrastructure level. SEM (G) and TEM (H) image of epithelial cells indicate ultrastructural features such as microvilli, desmosomes (star) and tight junctions (arrow). Scale bar in A, B: 1 µm, in C: 200 nm.

5.2.5 Particle studies on the primary model

In order to test the particulate formulations which have been applied on the Caco-2 model before (see 5.1.3) in the primary system we firstly applied PLGA NPs (1 mg/ml) with an average size of 214 nm for up to 6 h. First transport was detectable after 1-2 h, which increased linear over time (Fig. 28 A). A relative transport of about 5.5 % of the apically applied amount could be detected after 6 h, which is similar to the Caco-2 model. Visual control by confocal imaging confirmed the uptake of the fluorescence-labelled NPs (green) into the cytosol of the IECs. The apical cell membrane was visualized with CellMask™ Deep Red (Fig. 28 B; red) and the cell nucleus with DAPI (blue). To proof that indeed particles were transported across the intestinal barrier model and membrane, SEM imaging was performed on representative samples taken from the basolateral compartment after 6 h (Fig. 28 C).
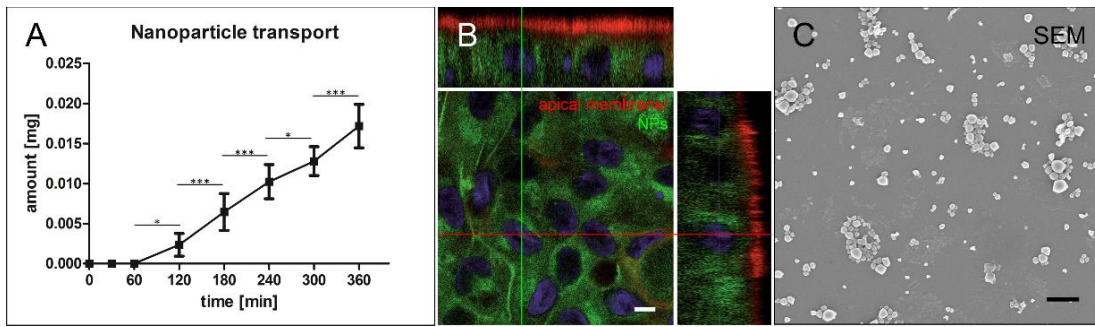
Figure 28: Functional NP uptake studies. Linear transport of PLGA-NPs (1 mg/ml) was observed over a time period of 6 h (A, n=3). Confocal image showing NPs (green) in the cytosol and red labelled apical cell membrane (B). SEM image of particles from the basolateral compartment after transport confirmed particles crossing the epithelial barrier (C). Scale bar in C: 1 µm [120].

In pilot experiments, ManPP-PLGA-NPs and Chitosan-NPs were selected for further investigation within the primary system. In this preliminary studies the ManPP-PLGA-NPs (Fig. 29 A) showed linear transport starting after 30 min with an efficiency comparable to standard PLGA-NPs (Fig. 29 A).
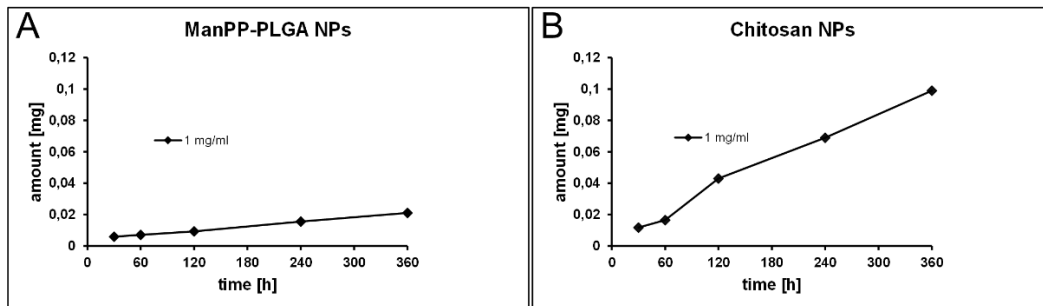
Figure 29: Preliminary study of selected particles on a primary intestinal model. Permeability of ManPP-PLGA-NPs (A) and Chitosan-NPs (B) was tested on a primary model at a concentration of 1 mg/ml for 6 h.

The relative transport in percentage of the basolaterally added amount of ManPP-PLGA-NPs was about 8.1 % in the primary model, which was also comparable to the Caco-2 model with 7.5 % (Tab. 19). In contrast, compared to the PLGA-NPs the Chitosan-NPs showed a higher transport rate in the primary system with about 21.5 %, whereas in the Caco-2 model only 9.5 % of the applied amount were found basolaterally (Tab. 20).

Table 20: Comparing particle transport in Caco-2 and primary tissue model

Formulation	Average particle size [nm]	Primary Total transport [%]	Caco-2 Total transport [%]
ManPP-PLGA	179	8.1± 3.77	7.5± 1.99
Chitosan	249	21.5± 5.23	9.5± 4.39

To verify the intracellular uptake of the ManPP-PLGA-NPs and Chitosan-NPs into primary IECs, fluorescence labelled particles were identified by confocal microscopy. NPs (green) were found within the cells on the level of the cell nuclei (Dapi, blue) underneath the cell membrane (Cellmask, red) (Fig. 30).
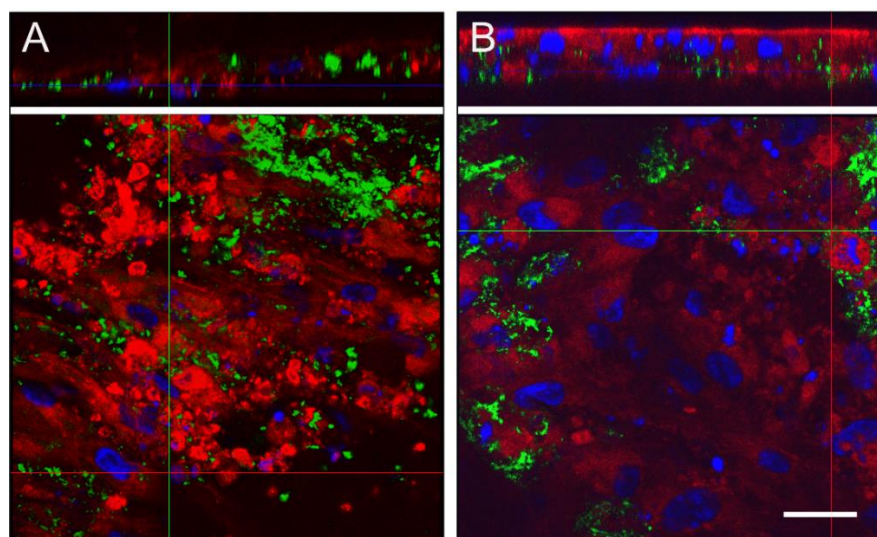
Figure 30: Visual confirmation of particle uptake. Confocal images showing uptake of fluorochrome labelled ManPP-PLGA (A) and Chitosan NPs (B) (green) into primary intestinal epithelial cell after incubation of 2 h (cellmembrane: red). Scale bars: 50 µm.

In summary, the established of a primary small intestinal *in vitro* model showed barrier properties characteristic for the human small intestine (Fig. 31). Histological characterization demonstrated all epithelial cell types which typically occurs in the native gut tissue. In addition this model showed to be suitable to test particulate formulations used in bioavailability or vaccination studies.
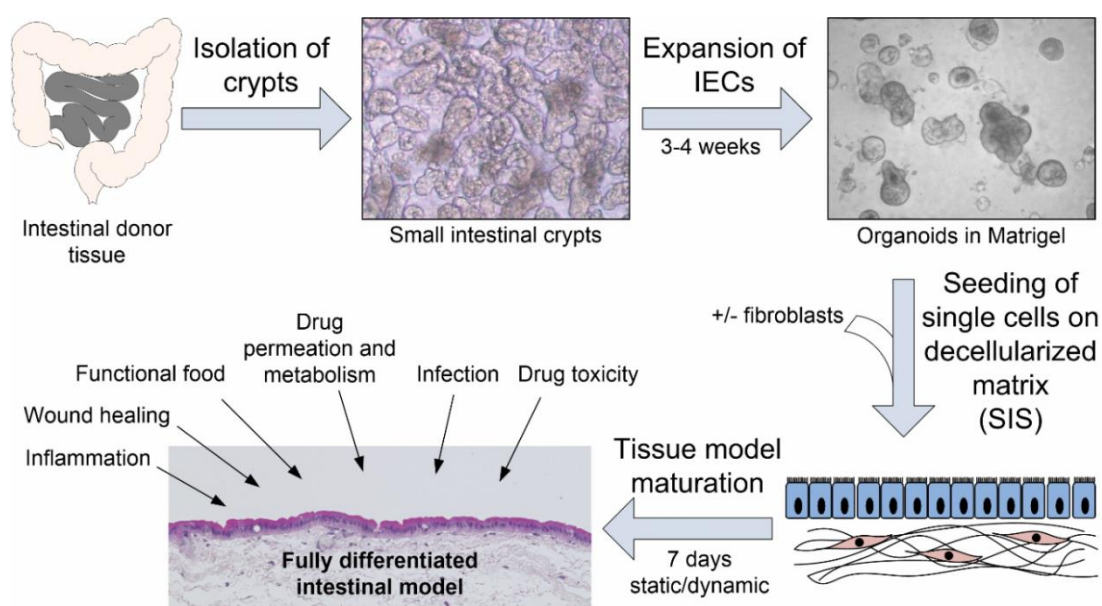
Figure 31: Schematic of primary intestinal tissue model established in this study. Intestinal epithelial cells (IECs) were isolated from human small intestinal tissue and expanded as organoid culture for 3-4 weeks. After enzymatic digestion single cells were seeded on a decellularized biological scaffold (SIS) with or without intestinal fibroblasts. Tissue models were cultured for 7 days under static or dynamic conditions and can be used for various research applications (Illustration gut: Copyright © motifolio.com) [120].

6 Discussion

The small intestine in the human body represents one of the most important contact surfaces to our environment. It's main physiological function is the absorption of essential nutrients, water and vitamins while at the same time protecting us from toxic xenobiotics and pathogens [121].

The bioavailability of orally administered drugs is dependent on transport efficiency from the gut towards the blood and finally the concentration at the targeted location. Besides the transport mechanisms, the potential metabolisation in the lumen of the gastrointestinal tract and other tissues which drugs have to pass to reach the location of interest can have great impact on the bioavailability [122].

Determination of the bioavailability is often only based on the blood drug concentration as concrete indication, requiring animal testing without directly investigating any transport or metabolism mechanism. Besides, animal studies are related with high costs and time consuming analysis, interpretation and correlation of data. Studies showed that *in vivo* data based on animals often lack a complete correlation due to species differences between human and mice or rats [123]. By the 3R-principles, under ethical point of view, a further reduction of animal testing is mandatory and leads logically to increased importance of new alternative test systems [108, 124].

First of all, newly developed *in vitro* models have to fulfil different biological requirements for testing to allow accurate *in vivo* prediction. For screening purposes the models should be suitable for high-throughput testing and have to generate reproducible data [80]. Current cell line based models like the Caco-2 Transwell® model constructed on a porous PET-membrane are used to screen substances for solubility, permeability, toxicity and release [125]. To allow a preselection of potential drug molecules, substances are classified by their properties in the biopharmaceutical classification system (BCS) [111].

Easy setup and use of these established models allows the testing of high numbers of substances but also comes with limitations. The artificial membrane and cells from

cancerogenic origin lead to limited correlation with the physiological conditions and therefore low predictive power [126]. For this reason new, more physiological models which still fulfil the current requirements have to be developed. The complexity has to be adjustable and is given by the scientific questions [73]. Such advanced tissue models might help to increase the correlation and reduce animal testing [86].

In this study, we used techniques of tissue engineering to improve the existing standard Caco-2 model for screening purposes with the ultimate goal to replace the rather artificial cell line model with primary human cells of the small intestine. Models were set up in variable complexity and under different culture conditions and compared regarding functionality and physiological aspects.

6.1 Improvement of the Caco-2 model

In drug development many promising candidates fail in the late phase of clinical trials which means great loss of time and money. This issue is linked to the low predictive power of preclinical tools like cell line based *in vitro* models or non-correlating animal testing [127, 128]. This problem together with ethical doubts about *in vivo* studies and European law initiatives to reduce animal testing promote the development of more physiological and more predictive tissue models [129].

The "Bundesministerium für Bildung und Forschung (BMBF)" funded the project „Platform for efficient epithelial transport for pharmaceutical applications by innovative particular carrier systems" (PeTrA, Förderkennzeichen: 13N11454) as part of the funding program "Efficient drug transport in biological systems - BioMatVital: Biotransporter". One part of the project was the development of particle delivery systems for antigens aiming on peroral vaccination. For prescreening purposes we developed an intestinal barrier model combining the intestinal epithelium and components of the immune system i.e. dendritic cells [113]. We initially used Caco-2 cells, a colorectal cancer cell line, which is used as the standard model to investigate toxicity and uptake of orally delivered drugs *in vitro*. To investigate the uptake and effects of encapsulated antigens for peroral vaccination, dendritic cells were added to the basolateral compartment of a Caco-2 model allowing investigation of antigen processing and immune response (Fig. 31).

6.1.1 Development of a co-culture model

The Caco-2 cell line has been used for many years as the standard test system for the small intestine to study interactions of oral administered pharmaceutical formulations with the intestinal epithelium in respect of toxicity and bioavailability [77, 79]. For these assays PET membranes with 0.4 - 3.0 µm pores are coated with rattail collagen type I, which supports standardization and high throughput drug testing [130]. However, on the PET membrane the Caco-2 cells build an unphysiologically tight epithelial barrier compared to the native small intestine demonstrating the need for alternatives [131, 132].

The crypts and villi of the gut represent the natural niche of the intestinal epithelial cells, which consists of two main components, the neighbouring cells and the extracellular matrix [49]. This characteristic environment can have great influence on status and function of the cells [133]. Cells like intestinal myofibroblasts or intraepithelial immune cells can secrete paracrine factors that are responsible for the homeostasis within the intestinal epithelium [72]. The ECM builds a 3D supportive structure mainly consisting of collagen-, laminin-, and elastin-fibers, which give the tissue characteristic stiffness and molecules like fibronectin for specific cell-matrix bonds [134].

Here, we used a modified Caco-2 model based on a decellularized scaffold derived from porcine gut (small intestinal submucosa with mucosa; SIS-muc) which was already demonstrated to be suitable to build up intestinal tissue models [75]. Compared to cells cultured on an artificial porous PET-membrane, intestinal epithelial cells seeded on biological scaffolds showed a more physiological behaviour in turn of morphology and functionality [75]. Through its 3D structure and molecular composition the matrix controls cellular functions, such as polarization [135-137]. In addition, the SIS-muc exhibited the conserved crypt-villus structure and the basal membrane covering the surface, characteristic for the small intestine providing the optimal environment for the intestinal cells [4]. However, the calculation of the surface of the SIS-muc is rather challenging since the size of villus structures can vary within the gut and also from pig to pig. A known, defined and reproducible area of absorptive epithelium, is very

important with respect to the dependency of predictive readouts for permeation, such as the permeability coefficient (P_{app} [cm/s]) on the surface area [77].

For investigation of particle formulations for peroral tumor-vaccination we integrated immune cells in our system. For an effective vaccination against cancer, the vaccines should trigger a strong cell-mediated immune response due to the activation of both CD4-positive helper cells and CD8-positive cytotoxic T lymphocytes [138]. DCs are part of the adaptive immune system, which can trigger an immunity and link the innate and adaptive immune response [139]. They belong to the group of antigen presenting cells (APCs) like macrophages which are able to phagocytose proteins or pathogens, present them to other immune cells [138]. Therefore, monocytes were isolated from PBMCs and differentiated towards DCs according to standard protocol [113]. Buffy coats provide a reliable source of human monocytes for separation and purification by Ficoll gradient [140]. High purification can be achieved by additional magnetic-activated cell sorting (MACS) or fluorescence-activated cell sorting (FACS). Monocytes were selected from the PBMCs by adherence to the cell culture dish which allows a separation from other non-adherent cell like lymphocytes. After the differentiation, non-adherent cell were identified as CD14-negative, CD11c-positive immature dendritic cells. DCs differentiated from monocytes demonstrated some heterogeneity with different subsets [140, 141]. Cells did not show the characteristic CD103 positive phenotype of lamina propria DCs which were shown to have classical DC functions and initiate the adaptive immune response [142]. Stimulation of the immature DCs by LPS resulted in an upregulation of the activation co-stimulators CD80 and CD86, which are important for the T cell activation and demonstrated the immune competence of the cells [143]. Adding the DCs basolateral in the well-plate proofed to be suitable for this approach but prevents a direct contact to the epithelium. Studies have shown that DCs *in vivo* can penetrate the epithelium with their dendrites to directly take up antigens from the gut lumen [144]. Compared to another co-culture model where the immune cells got embedded in a collagen-gel, our models allow easy access to the cells with no additional stress to the immune cells induced by digestion of the gel [73]. The co-culture with immune competent cells demonstrated strong influence on the barrier function and cytokine response in case of an inflammation or contact with bacteria [145, 146].

The here used more artificial standard model was built up with Caco-2 cells due to feasibility for screening purposes. The use of primary IECs would allow to build up an autologous models by using either blood from the patient or isolated intraepithelial immune cells from the donor tissue [147]. From the immunological point of view the isolated intraepithelial DCs are the best choice as they show a specific priming, however, low cell numbers make this approach suboptimal and not feasible for upscaling [148]. More recently, studies could show that M cells located in the gut are a specialized site for antigen uptake, sampling the gut lumen for antigens [47]. Studies in mice and human tissue models demonstrated the importance of these cells triggering an immune response caused by *S. Typhimurium* infections [48, 149]. Previously published data showed that differentiation towards functional M cell can be achieved by RANKL-induced differentiation of human Lgr5 positive ISCs [149]. Therefore, an integration of M cells seems to be important to further investigate the antigen uptake in infection or vaccination studies. Furthermore, developing drug delivery systems directly targeting these cells could help to increase the efficiency of the uptake.

This new tissue model combines the advantages of the biological scaffold not posing as an additional physical barrier and the co-culture with immune competent cells which demonstrated to have major impact on the intestinal barrier properties.

6.1.2   Tested formulations

To deliver proteins orally, various challenges have to be overcome to succeed [132]. First, for formulations to pass the stomach they need to be protected from the aggressive acidic milieu and the peptidases. To achieve this goal, coatings with polymers like Eudragit® have been developed that allow pH-dependent drug release, *e.g.* only in neutral pH environment like the small intestine while being stable in an acidic environment like in the stomach [150]. Even if the proteins have reached the location of resorption, the small intestine, peptidases produced by the pancreas can digest the proteins and destroy them before bringing about any effect [71, 122]. Additionally, the epithelium is covered by a loose mucus layer which has to be penetrated by the formulation before the active agent can be taken up by the epithelial cells [35]. Beside the free pancreatic digestion enzymes in the lumen, the brush border,

which covers the apical cell membrane of the IECs, also features membrane-bound peptidases and carboxylases.

One potential strategy for the treatment of cancer is the tumor-vaccination to turn the cytotoxic T cells against the tumor. For this strategy, small peptide sequences, representing parts of tumor-specific-proteins, are used to induce a immune reaction to prime the T cells to kill the tumor cells [151]. To protect these proteins from digestive enzymes or denaturation, one approach is to encapsulate the proteins in nanoparticles [152].

In this project, nanoparticles based on the synthetic polymer PLGA and natural polymer Chitosan were developed by our partners with the aim of delivering antigens for peroral vaccination [113]. Chitosan has been demonstrated to be suitable for delivery of DNA and antigens into cells [153]. PLGA is one of the best known and described polymers, attractive for its properties *e.g.* biodegradability and biocompatibility, FDA approval in drug delivery systems was well as possible modifications of surface properties [154]. Additionally to the basic PLGA two modifications, PEG-PAGE-PLGA (PP-PLGA) and Mannose-PEG-PAGE-PLGA (ManPP-PLGA) were tested on our model. Basic PLGA shows a limited loading capacity for hydrophilic drugs due to its hydrophobic properties [113]. To overcome this major limitation and make the drug carrier more effective, modifications with polyethylene glycol (PEG) were developed and investigated. These modifications with PEG increased the loading capacity for proteins, led to faster release kinetics and additionally increase the mucus permeability. Because direct functionalization of PEG is difficult, Poly(allyl glycidyl ether) (PAGE) was added allowing additional modifications, in this case mannose [113]. Targeting mannose-receptors on the surface of DCs has been reported to promote cross-presentation of antigens by MHC-I complex, which is necessary to activate CD8-positive cytotoxic T cells [155]. The size of the particles was determined by the optimal size for phagocytosis by DCs which is important to get an immune response. As size for the particles about 200 nm was chosen which is about the size of a virus and thus expected to be taken up by endocytosis and phagocytosis [113, 156]. For visualization the particles were labeled with encapsulated Coumarin-6 for the PLGA particles and covalent coupled FITC for

the Chitosan particles. Incubation of Caco-2 cells in a simple 2D well-plate culture with basic PLGA-NPs and Chitosan NPs confirmed a visual uptake of both particle types with PLGA-NPs showing a slightly faster uptake. To get a kinetic for the intracellular uptake by the Caco-2 cells and the basolateral DCs we measured the fluorescence intensity of the cells by flow cytometry which should correlate with the amount of labelled particles taken up. Like in the histological control, the PLGA based particles showed a slightly faster uptake by the Caco-2 cells compared to the Chitosan based particles. Quantification by the fluorescence signal remained difficult due to the different encapsulation efficiency in the different modified PLGA-NPs. Directly comparing the PLGA based NPs with the Chitosan NPs is also not possible due to the different labeling. After 4 h a first signal for the PLGA based NPs was detected in the DCs while the Chitosan NPs showed no signal after 6 h. The missing signal might be due to the delay in the Chitosan particle uptake resulting from a too small time frame of the experiment [113]. The kinetics for the four different particles transported across the intestinal barrier were investigated over a time span of 6 h using the Caco-2 model on SIS-muc scaffold. Concentration was determined from applied weight of polymer, measuring the fluorescence intensity of the samples. From literature it is known that only 0.4 % to 0.6 % of the encapsulated coumarin-6 is released over 5 to 48 h [157, 158]. SEM detection demonstrated particles to be found basolaterally after transport. The apically applied amount of particles was correlated with the amount found basolaterally for all four types of particles. No significant differences in transport efficiency could be found. All PLGA based particles showed a recovery rate of about 50 % which could be caused by the non-covalent labelling or adherence to the biological scaffold. For Chitosan the recovery rate was almost 100 %. The ManPP-PLGA-NPs were chosen from the set of the PLGA based particles together with the Chitosan-NPs for further studies with the primary model.

This data shows two different types of particulate carrier systems, suitable to deliver encapsulated antigens across the intestinal barrier. Together with the immunological data showing antigen processing and presentation by DCs, followed by activation of CD4- and CD8-positve T cells, these carrier systems have great potential for new peroral vaccination strategies. Also, these carrier systems could serve as new tool for

various drug formulations to increase the bioavailability and allow targeted transport to a specific location.

6.2 Primary small intestinal tissue model

For testing of toxicity and oral drug delivery, cell line based tissue models like the Caco-2 model are routinely used, standardized, reproducible and easy to handle tool [159]. Besides these striking arguments for such models, they also come with some disadvantages as these models lack essential characteristics of the gut like mucus production and specific transporter activity [80, 82]. The mucus layer covers the whole mucosa, representing the first part of the intestinal barrier everything passing the gut gets in contact with. Depending on surface charge and size anything *e.g.* drug formulations or bacteria can stick to it and get flushed away without even getting in contact with the epithelium underneath [160]. Also, the characteristic expression of efflux transporters and metabolic enzymes from IECs can have major impact on the outcome and thereby the predictive power of performed transport studies [161]. For this reason, research has been more and more focusing on the development of primary cell based models, better reflecting the physiology of the small intestine.

6.2.1 Establishment of a primary intestinal monolayer model

As already mentioned, biological scaffolds consisting of various ECM molecules have many advantages compared to the very artificial PET-membrane, providing a perfect surface for cell attachment and growth with no need of additional coating (6.1.1). Despite the SIS-muc scaffold exhibiting the typical 3D structure of villi and crypts and being covered by a basal membrane which offers a perfect *in vivo* like environment to the cells, this scaffold also comes with some disadvantages. The uneven topography with the high villi structure of the jejunum tends to collapse in static culture due to the loss of stability caused by the decellularization process, resulting in unstructured and undefined surfaces. This fact makes it difficult to estimate the surface covered by the epithelium. To perform reproducible drug delivery studies, it is essential have a defined, known surface on a models to calculate the permeability coefficient value (P_{app}) for a substance and compare data sets with each other [79]. To ensure such a more defined surface and a confluent monolayer covering the scaffold, we decided to

use the SIS instead. Additionally with this, the amount of cells needed to seed one model decreases due to the lower surface which is advantageous as the expansion of the primary cells is costly and labour intensive.

The decellularization process for the SIS is similar to the SIS-muc but without DNAse digestion. Histology by Feulgen staining proved no cell fragments to be left in the scaffold. Qualitative detection of DNA by gel-electrophoresis showed no band while quantification by PicoGreen® assay showed mean DNA leftovers of 219 ng DNA per mg dry weight. For research and development this is acceptable as the much stricter good manufacture process (GMP) standards values are less than 50 ng per mg dry weight and no DNA fragments bigger than 200 bp [162]. Further characterization of the scaffold by Masson trichrome staining and SEM revealed a planar (ultra)structure of collagen fibers.

Long term culture of primary intestinal epithelial cells became possible the first time 2009 with the protocol published by Sato *et al.* [17]. Isolated crypts get embedded in Matrigel, a hydrogel consisting of basal membrane components providing a 3D environment for the cells [163]. Culture of the cells in small Matrigel droplets comes with a high effort as the gel has to be dissolved for every passaging, with high costs and limitations in expansion. The crypts isolated from the gut tissue contain the ISCs and progenitor cells. To keep these cells in their undifferentiated and proliferating condition, cells were provided with growth factors mimicking the intestinal stem cell niche, the crypt. The Wnt-signaling represents the most important factor driving the proliferation in the intestinal stem cell niche [164]. While recombinant Wnt3A demonstrated to be more or less inactive, the use of Wnt3A-conditioned medium proved to be effective and essential for the culture of human IECs [165]. This observation is probably attributable to the serum requirement to the lipid modification of Wnt-molecules. In the absence of serum, the proteins tend to precipitate due to their hydrophobic nature [165, 166]. Cells cultured within Matrigel form so called organoids, which possess crypts-like structures growing out where the stem cells are located and a lumen surrounded by a polarized, differentiated epithelium [17]. However, standardized drug transport or infection studies are not feasible with organoid models. The organoids embedded in Matrigel allow only limited access to the cells either by

diffusion or by microneedle injections [167, 168]. The unknown surface area of the organoids and access only from the basolateral side make drug delivery studies very difficult [169]. Additionally, dead cells accumulating in the organoid lumen tend to attract and bind molecules or bacteria. To transform organoids into a confluent monolayer, cells had to be kept in a proliferating state. To enrich the population during expansion, organoids had to be kept small and passaged every 3 days [88]. Under these conditions the proliferation rate reached about 30 % which was crucial to get a confluent monolayer.

The IECs are surrounded by mesenchymal cells, specifically myofibroblasts, which modulate the signaling and therefore are key players within the niche [170]. These subepithelial myofibroblasts are a heterogenous population expressing characteristics of smooth muscle cells and fibroblasts and are closely located to the crypts [171]. Studies showed that they interact with the epithelium trough Wnt-, BMP- and Notch signaling [172-174]. Previous co-culture studies demonstrated a supportive effect on IECs growth [49, 72]. To investigate the influence of the co-culture on the functionality of our model, myofibroblasts were isolated from human gut tissue. Characterization of the cells showed a heterogenic population immunostained positive for α-smooth muscle actin, the mesenchymal marker vimentin and some slightly positive for Desmin, a marker for muscle cells [49].

To guarantee a confluent monolayer for the barrier model different conditions were tested. Looking for the ideal cell number organoids were digested to single cells and seeded them on the SIS scaffold. organoids themself did not attach to the scaffold and were floating in the medium while dissociated cells were shown to promote monolayer growth [175]. A cell number of 4×10^5 cells per model turned out to be the optimal choice when considering the barrier properties by TEER measurement and FITC-dextran permeability. Different Wnt3A-conditioned medium concentrations were tested either in monoculture or in co-culture with the myofibroblasts to see whether it makes a difference in growth and integrity of the monolayer. All four conditions resulted in a confluent monolayer. While histologically there was no obvious difference between the 25 % and the 50 % Wnt3A-conditioned medium, the co-culture showed inclusions within the epithelium compared to the monoculture. TEER measurement

revealed a high variation within the different groups, whereas FITC-dextran permeability showed the most robust barrier for 25 % Wnt3A-concentration in combination with the co-culture. The inclusions may be caused by dysregulation in the Wnt-pathway.

Tissue models were cultured up to 14 days and compared with native tissue and Caco-2 models. The primary models showed an increased permeability at day 10 and day 14 compared to day 7 for FITC-dextran. This fits to data of the native gut showing a lifecycle for intestinal epithelial cells of 5-6 days [12]. This short time culture is a big advantage, as it allows more flexible experiments compared to the Caco-2 model with a maturation time of 2 to 3 weeks.

6.2.2 Characterisation of the barrier properties

Only a few primary intestinal barrier models with two separated compartments have been developed using various cell sources from ileum, rectum [88], or other parts of small intestine [87], fetal [89], post-mortem tissue (MatTek) or unknown donor origin. In this study, primary intestinal IECs were isolated from human jejunum donor tissue from obese patients. The different origin of the cells makes it difficult to directly compare the models. Like standard Caco-2 assays the other primary models are all based on the Transwell® system with a porous PET membrane as scaffold [86-89], which contains unequally distributed pores leading to impermeable areas and thus a significant artificial barrier for specific test formulations. This has been tested in a direct comparison of paracellular and transcellular drug transport after application on empty and Caco-2-seeded PET membranes and decellularized SIS-muc [75]. In this study, primary intestinal IECs were isolated from human jejunum donor tissue, expanded for about 4 weeks and seeded on the decellularized SIS scaffold, either in monoculture or in co-culture with subepithelial myofibroblasts. The influence of the co-culture on the tissue model was investigated by looking at the barrier integrity and differentiation towards mucus producing goblet cells. Confluent monolayer was demonstrated after 7 days of static culture in both approaches. Myofibroblasts were located in direct contact with of the IECs beneath the epithelium, nicely reflecting the

in vivo situation [84]. To investigate the barrier integrity, two different analytical methods were applied to the models.

First used was the TEER measurement, where the electrical resistance of the model's barrier was determined [176]. This standard method is non-invasive and allows to draw conclusions regarding the barrier integrity without disruption of the model. The TEER-values of our tissue model were in average about 40 Ωxcm^2, which is far lower than the values described for the Caco-2 model [130]. However, experiments with the Ussing chamber using native tissue and recently published primary models demonstrated comparable TEER values [87, 89, 131]. Other studies with primary cells however showed much higher values between 130 and 900 Ωxcm^2, which could be explained by different cell sources and cell culture protocols [86, 88]. Manual TEER measurement shows a high liability for discrepancies caused by multiple factors like temperature fluctuation and medium compositions [177]. As an alternative method, the barrier's permeability for FITC-dextran was determined using a dextran with a size of 4 kDa. This method is also used to investigate endothelial leakage during inflammation processes [178]. The transport rates measured for the monoculture fluctuate strongly and measure in average about 4 % whereas the co-culture models showed very robust values of about 1 %. This effect might be caused by modulation of the signalling by factors secreted from the myofibroblasts [49]. Tightness of the epithelial barrier is mainly determined by the cell-cell connections which seal the paracellular gap between the cells [179]. When looking at the gene expression level of the tight junction protein Claudin 4, we detected an upregulation within the monolayer culture compared to the organoids indicating a tighter barrier [180]. The tight junctions are a complex of many protein, building a very dynamic, finely regulated barrier [179]. Taken this complex regulation into account, functional assays like mannitol or FITC-dextran transport provide a more reliable method to investigate the paracellular permeability.

As mentioned before, the mucus layer covering the cells is an important part of the intestinal barrier. Most models like the Caco-2 model lack this component of the barrier due to the missing goblet cells. The mucus-producing goblet cells are a unique feature of the primary model, building the mucus layer which represents an physical barrier

and also the first line of defence against pathogens [33]. Gene-expression analysis revealed a Mucin 2 expression in the primary monolayer models, indicating the presence of goblet cells in this model. Differences in the expression compared to the organoids may be caused by an insufficient differentiation protocol.

6.2.3 Influence of controlled dynamic culture conditions

The field of tissue engineering connects cell biology with technical engineering. Bioreactors developed for specific tissues were demonstrated to be useful tools to mimic mechanical stress (in tissue) with great impact on the phenotype of the cultured tissue models [74, 75, 107, 181, 182]. The intestine is no static organ, coordinated contractions of longitudinal and ring muscles move the chyme in peristaltic waves through the intestine, while the villi simultaneously contract and relax [183]. These movements together with the flow of the chyme apply a natural mechanical stress to the cells. Many studies showed a strong influence of these forces on cell differentiation and functionality [74, 75]. To investigate the influence of mechanical stress on our tissue models and to compare them with a static culture we tested two dynamic approaches regarding their barrier functionality. The first and very simple dynamic culture system was based on an orbital shaker on which we cultured our models. The medium on the epithelium was moved around in the cell crowns by the shaking and provided sheer stress to the cells. This approach, if working, would allow an easy scale up of dynamic models. The second dynamic culture was based on a flow-through bioreactor connected over tubes with a pump to generate a medium flow. This type of bioreactor custom-designed for this purpose, allows a very defined mechanical stimulation of the cells. Additionally, two separate flow through chambers allow individual conditions for both tissue sides and can be used for instance for co-culture models with epithelium on one side and endothelium on the other side.

However, the dynamic culture on the shaker did not result in significant differences compared to the static culture. A reason could be unequal movement and waves on the shaker which interfere with the system [120]. Unlike the shaker, the perfusion bioreactor applies controllable and defined conditions to the cells. The used bioreactor culture conditions induced an average shear stress of 0.005 dyne/cm² on the cell's

surface forces which are comparable to physiological relevant values of about 0.002-0.08 dyne/cm^2 within the human intestine [74]. This was the first time we could demonstrate biologically relevant effects of the dynamic approach. Only the bioreactor conditions resulted in a more physiological tissue model showing IECs with high-prismatic morphology, increased expression of CYP3A4, an important metabolic enzyme and high efflux transporter activity [32]. Additionally, barrier properties investigated by transport for low-permeable Fluorescein and high-permeable Propranolol proved to be comparable to the Caco-2 model [184]. Further functional assays with FDA approved reference substances will help to determine the functionality and characteristics of this model more precisely [185]. Taken together, the bioreactor approach demonstrated to have relevant biological impact on the morphology, gene-expression and functionality of the primary IECs based tissue models cultured under such dynamic conditions.

6.2.4 Molecular characterization

Cell line models do not reflect the cellular complexity as they lack the various characteristic cell types present in the native small intestine [76]. Especially the Caco-2 model shows only enterocytes and no mucus producing goblet cells responsible for the mucus layer covering the mucosa, which is an important part of the barrier [132]. This is in particular of interest for infection and drug studies as pathogens or formulations could stick to the mucus and get flushed away without any contact to the epithelium [7, 160]. To investigate drug formulations and microorganisms regarding their interactions with the mucus or their mucus permeability, models with mucus layer are needed. Gene-expression and immunostaining demonstrated mucus producing cells within the primary model described here. The goblet cells account for about 8 % of the total epithelial cells in the native epithelium, so far goblet cells were not quantified in this model [88]. The study by VanDussen *et al.* with primary IECs from the ileum showed similar numbers of goblet cells to the native tissue with 8.4 and 8.7 % of the total cell number. Also they could show a mucus layer covering the epithelium by using fluorescence labelled beads to make the layer visible [88]. Next to mucus producing goblet cells, chromogranin-producing enteroendocrine cell and lysozyme-secreting Paneth cells were also identified within this model. Enteroendocine cells

secrete hormones and other signalling molecules controlling many parameters connected to the metabolism *e.g.* satiety, hunger, motility of the gut and mucus secretion [45]. These cells which account for only 0.5 % of the total cell number, were shown to be present in the model of VanDussen *et al.* in comparable number [88]. Paneth cells are located next to the stem cells at the base, responsible for maintenance of the stem cells and secreting antimicrobial peptides and proteins [36, 40]. Also the SEM and TEM imaging revealed an epithelium nicely covered apically by microvilli, the brush boarder which contains important enzymes and transporters for digestion and absorption [121]. TEM imaging also showed tight junctions between the cells that are the key components of the barrier function but also indicate a polarization of the cells which is important for directed transport mechanisms [10]. *In vivo*, the crypts contain the proliferative and regenerative potential given by the stem cells whereas the villi are the differentiated, functional compartment. This complex homeostasis is controlled by opposite gradients proliferation and differentiation signals [84]. As the differentiation in our model was induced overall by medium supplementation, all cells of the tissue model lost their proliferation potential and the model thereby its regenerative potential. Having a model with regenerative potential would be interesting to investigate wound healing after injuries, infections or inflammatory conditions [186]. Further studies are necessary to improve the differentiation process without hindering the proliferative/regenerative potential.

6.2.5   Particle studies on the primary model

The most promising formulations selected by the prescreening studies with the Caco-2 model were tested on the new primary model. As standard particles, PLGA was tested first for comparison. The primary model showed a transport comparable to the Caco-2 model with about 6 % for the PLGA-NPs [120]. Confocal imaging demonstrated intracellular particles. ManPP-PLGA-NPs also showed a comparable transport rate of about 8 % in the primary and Caco-2 model, while the Chitosan NPs transport rates were 2 times higher in the primary model. These difference can either be explained by the different surface charge of the particle or the differences in the model setup. Loaded chitosan particles showed a positive zeta potential, while loaded PLGA particles had an almost neutral charge [113]. Therefore, Chitosan NPs show more hydrophilic

properties and stick more easily stick to proteins. In contrast, the PLGA-NPs exhibited almost no surface charge and show more hydrophobic properties. While the primary model was based on the thinner, plane SIS scaffold, the SIS-muc with preserved crypt-villus structure and a basal lamina was used for the Caco-2 model [75]. The thicker scaffold, together with the dense basal lamina covering the surface could pose a stronger physically barrier for the particles. The basal membrane has been shown to present a physical barrier for nanoparticles which were even smaller [187]. Differences probably also occur from variances in endocytose transport between these two different cell types from different gut regions. The primary cells originate from the small intestine, the part of the gut specialized on substance uptake of any type, whereas the Caco-2 cells come from the colorectal region, where only water is transported with any significance through the epithelial layer. The size of the particles suggest the uptake mechanism to be endocytosis (1.2.4) [157].

The in this thesis newly introduced primary small intestinal model provides a more physiological test system, suitable to study the uptake of particle formulations as carrier system for novel orally delivered drugs. By using a biological decellularized matrix in combination with myofibroblasts migrating into the scaffold, this model also allows to investigate the influence of the ECM and subepithelial connective tissue on such processes. Additionally, with the goblet cells present in this model and producing mucus, it will also be possible to study the interaction of pharmaceutical formulations with the characteristic mucus-layer covering the intestinal epithelium.

7 Conclusions and future perspectives

In conclusion, the Caco-2 co-culture model with dendritic cells based on a decellularized biological scaffold proved to be suitable to screen particular formulations *in vitro*. The first time, different particulate formulations for oral vaccine delivery were tested for cellular uptake and transport kinetics on such a tissue model. The selected PLGA, ManPP-PLGA-NPs and Chitosan NPs were finally tested on the newly developed primary tissue model to compare both models. While the transport of PLGA based particles was comparable in both models, the Chitosan particles showed significant higher transport in the primary model. These divergent results, together with limitations of the commonly used models show the need for new, more physiological tissue models.

The ultimate goal of this work was the development of a human primary *in vitro* model of the small intestine that reflects the main physiological characteristics found in the native gut. The here presented primary model is the first of its kind based on a biological scaffold. The model contains all essential cell types and characteristic barrier properties of the small intestine. The co-culture with myofibroblasts as mesenchymal component of the gut demonstrated a modulation of the epithelial cells growth. Furthermore, dynamic culture conditions demonstrated the first time an improvement of the transporter functions and barrier integrity for a primary cell based model. Additionally, with mucus-producing cells present in the model it provides even more physiological test conditions. Such advanced tissue models might be a potential tool for more predictive preclinical studies, useful to investigate *e.g.* pharmaceuticals, human pathogens, probiotic organisms or diseases. Furthermore, primary models could be interesting for personalized medicine, testing for optimal patient treatment. Eventually it could help to reduce animal testing.

The in this thesis presented primary model has to be further characterized in its properties and functionality to determine parameters for the new model. The differentiation protocol has to be further optimized to guarantee constant quality and distribution of the cell types. The integration of gradients for pathways responsible for growth and differentiation mimicking regulating structure of the cell niche of the gut

would allow to study the regeneration of the mucosa, *e.g.* after wounding or infections. Especially a defined and characterized mucus layer would be of great interest to study the protection and barrier function associated with drug absorption and pathogens within the gut.

Depending on the scientific question to address, co-culture with different cell types are possible, *e.g.* endothelial cells or immune cells could be of interest. As an organ with contact to our environment, the immune system is strongly embedded within the gut, deciding between protection and tolerance. The enteric nervous system as brain of the gut and its function is not totally understood yet. Furthermore, integration of the microbiome will be of interest to study the interaction of the gut with its billions of inhabitants. If the fine balance between all these players somehow gets disturbed, pathological events like inflammatory bowel disease occur. *In vitro* co-culture experiments would help to better understand the complex interactions of the various cells and microorganisms present in the gut.

8 References

[1] Lucius, R., and Schwegler, J.S. Der Mensch - Anatomie und Physiologie: Thieme; 2011.

[2] Lüllmann-Rauch, R., and Paulsen, F. Taschenlehrbuch Histologie: Thieme; 2012.

[3] Schünke, M., Schulte, E., and Schumacher, U. Prometheus : LernAtlas der Anatomie. [2]. Innere Organe : 121 Tabellen: Thieme; 2012.

[4] Nowitzki-Grimm, S., Kügel, J.W., Biesalski, H.K., and Grimm, P. Taschenatlas Ernährung: Thieme; 2015.

[5] Helander, H.F., and Fändriks, L. Surface area of the digestive tract – revisited. Scandinavian Journal of Gastroenterology 49, 681-689, 2014.

[6] Niess, J.H., and Reinecker, H.-C. Dendritic cells in the recognition of intestinal microbiota. Cellular Microbiology 8, 558-564, 2006.

[7] Johansson, M.E., and Hansson, G.C. Microbiology. Keeping bacteria at a distance. Science (New York, NY) 334, 182-183, 2011.

[8] Birchenough, G.M.H., Johansson, M.E., Gustafsson, J.K., Bergstrom, J.H., and Hansson, G.C. New developments in goblet cell mucus secretion and function. Mucosal Immunol 8, 712-719, 2015.

[9] Barker, N. Adult intestinal stem cells: critical drivers of epithelial homeostasis and regeneration. Nat Rev Mol Cell Biol 15, 19-33, 2014.

[10] Watson, A.J.M., and Hughes, K.R. TNF-α–induced intestinal epithelial cell shedding: implications for intestinal barrier function. Annals of the New York Academy of Sciences 1258, 1-8, 2012.

[11] Leblond, C.P., and Walker, B.E. Renewal of Cell Populations. Physiological Reviews 36, 255-276, 1956.

[12] Messmann, H. Klinische Gastroenterologie: Thieme; 2011.

[13] Barker, N., van Es, J.H., Kuipers, J., Kujala, P., van den Born, M., Cozijnsen, M., Haegebarth, A., Korving, J., Begthel, H., Peters, P.J., and Clevers, H. Identification of stem cells in small intestine and colon by marker gene Lgr5. Nature 449, 1003-1007, 2007.

[14] de Lau, W., Barker, N., Low, T.Y., Koo, B.-K., Li, V.S.W., Teunissen, H., Kujala, P., Haegebarth, A., Peters, P.J., van de Wetering, M., Stange, D.E., van Es, J., Guardavaccaro, D., Schasfoort, R.B.M., Mohri, Y., Nishimori, K., Mohammed, S., Heck, A.J.R., and Clevers, H. Lgr5 homologues associate with Wnt receptors and mediate R-spondin signalling. Nature 476, 293-297, 2011.

[15] Carmon, K.S., Lin, Q., Gong, X., Thomas, A., and Liu, Q. LGR5 Interacts and Cointernalizes with Wnt Receptors To Modulate Wnt/β-Catenin Signaling. Molecular and Cellular Biology 32, 2054-2064, 2012.

[16] Blanpain, C., and Simons, B.D. Unravelling stem cell dynamics by lineage tracing. Nat Rev Mol Cell Biol 14, 489-502, 2013.

[17] Sato, T., Vries, R.G., Snippert, H.J., van de Wetering, M., Barker, N., Stange, D.E., van Es, J.H., Abo, A., Kujala, P., Peters, P.J., and Clevers, H. Single Lgr5 stem cells build crypt-villus structures in vitro without a mesenchymal niche. Nature 459, 262-265, 2009.

[18] Snippert, H.J., van der Flier, L.G., Sato, T., van Es, J.H., van den Born, M., Kroon-Veenboer, C., Barker, N., Klein, A.M., van Rheenen, J., Simons, B.D., and Clevers, H. Intestinal Crypt Homeostasis Results from Neutral Competition between Symmetrically Dividing Lgr5 Stem Cells. Cell 143, 134-144, 2010.

[19] van der Flier, L.G., Haegebarth, A., Stange, D.E., van de Wetering, M., and Clevers, H. OLFM4 Is a Robust Marker for Stem Cells in Human Intestine and Marks a Subset of Colorectal Cancer Cells. Gastroenterology 137, 15-17, 2009.

[20] van der Flier, L.G., van Gijn, M.E., Hatzis, P., Kujala, P., Haegebarth, A., Stange, D.E., Begthel, H., van den Born, M., Guryev, V., Oving, I., van Es, J.H., Barker, N., Peters, P.J., van de Wetering, M., and Clevers, H. Transcription Factor Achaete Scute-Like 2 Controls Intestinal Stem Cell Fate. Cell 136, 903-912, 2009.

[21] Potten, C.S., Booth, C., Tudor, G.L., Booth, D., Brady, G., Hurley, P., Ashton, G., Clarke, R., Sakakibara, S., and Okano, H. Identification of a putative intestinal stem cell and early lineage marker; musashi-1. Differentiation; research in biological diversity 71, 28-41, 2003.

[22] Muñoz, J., Stange, D.E., Schepers, A.G., van de Wetering, M., Koo, B.-K., Itzkovitz, S., Volckmann, R., Kung, K.S., Koster, J., Radulescu, S., Myant, K., Versteeg, R., Sansom, O.J., van Es, J.H., Barker, N., van Oudenaarden, A., Mohammed, S., Heck, A.J.R., and Clevers, H. The Lgr5 intestinal stem cell signature: robust expression of proposed quiescent '+4' cell markers. The EMBO Journal 31, 3079-3091, 2012.

[23] Potten, C.S., Gandara, R., Mahida, Y.R., Loeffler, M., and Wright, N.A. The stem cells of small intestinal crypts: where are they? Cell Proliferation 42, 731-750, 2009.

[24] Sangiorgi, E., and Capecchi, M.R. Bmi1 is expressed in vivo in intestinal stem cells. Nat Genet 40, 915-920, 2008.

[25] Takeda, N., Jain, R., LeBoeuf, M.R., Wang, Q., Lu, M.M., and Epstein, J.A. Inter-conversion between intestinal stem cell populations in distinct niches. Science (New York, NY) 334, 1420-1424, 2011.

[26] Jensen, K.B., Collins, C.A., Nascimento, E., Tan, D.W., Frye, M., Itami, S., and Watt, F.M. Lrig1 Expression Defines a Distinct Multipotent Stem Cell Population in Mammalian Epidermis. Cell Stem Cell 4, 427-439, 2009.

[27] Breault, D.T., Min, I.M., Carlone, D.L., Farilla, L.G., Ambruzs, D.M., Henderson, D.E., Algra, S., Montgomery, R.K., Wagers, A.J., and Hole, N. Generation of mTert-GFP mice as a model to identify and study tissue progenitor cells. Proceedings of the National Academy of Sciences of the United States of America 105, 10420-10425, 2008.

[28] Li, L., and Clevers, H. Coexistence of quiescent and active adult stem cells in mammals. Science (New York, NY) 327, 542-545, 2010.

[29] Li, N., Yousefi, M., Nakauka-Ddamba, A., Jain, R., Tobias, J., Epstein, Jonathan A., Jensen, Shane T., and Lengner, Christopher J. Single-Cell Analysis of Proxy Reporter

Allele-Marked Epithelial Cells Establishes Intestinal Stem Cell Hierarchy. Stem Cell Reports 3, 876-891, 2014.

[30] Casali, A., and Batlle, E. Intestinal Stem Cells in Mammals and Drosophila. Cell Stem Cell 4, 124-127, 2009.

[31] Gropper, S.S., and Smith, J.L. Advanced Nutrition and Human Metabolism: Cengage Learning; 2012.

[32] Paine, M.F., Hart, H.L., Ludington, S.S., Haining, R.L., Rettie, A.E., and Zeldin, D.C. THE HUMAN INTESTINAL CYTOCHROME P450 "PIE". Drug Metabolism and Disposition 34, 880-886, 2006.

[33] McGuckin, M.A., Lindén, S.K., Sutton, P., and Florin, T.H. Mucin dynamics and enteric pathogens. Nat Rev Micro 9, 265-278, 2011.

[34] Gustafsson, J.K., Ermund, A., Ambort, D., Johansson, M.E.V., Nilsson, H.E., Thorell, K., Hebert, H., Sjövall, H., and Hansson, G.C. Bicarbonate and functional CFTR channel are required for proper mucin secretion and link cystic fibrosis with its mucus phenotype. The Journal of Experimental Medicine 209, 1263-1272, 2012.

[35] Johansson, M.E.V., Sjövall, H., and Hansson, G.C. The gastrointestinal mucus system in health and disease. Nature reviews Gastroenterology & hepatology 10, 352-361, 2013.

[36] Clevers, H.C., and Bevins, C.L. Paneth Cells: Maestros of the Small Intestinal Crypts. Annual Review of Physiology 75, 289-311, 2013.

[37] Paneth, J. Ueber die secernirenden Zellen des Dünndarm-Epithels. Archiv f mikrosk Anatomie 31, 113-191, 1887.

[38] Lehrer, R.I., and Lu, W. α-Defensins in human innate immunity. Immunological Reviews 245, 84-112, 2012.

[39] Wanniarachchi, Y.A., Kaczmarek, P., Wan, A., and Nolan, E.M. Human Defensin 5 Disulfide Array Mutants: Disulfide Bond Deletion Attenuates Antibacterial Activity Against Staphylococcus aureus. Biochemistry 50, 8005-8017, 2011.

[40] Salzman, N.H., Ghosh, D., Huttner, K.M., Paterson, Y., and Bevins, C.L. Protection against enteric salmonellosis in transgenic mice expressing a human intestinal defensin. Nature 422, 522-526, 2003.

[41] Salzman, N.H., Hung, K., Haribhai, D., Chu, H., Karlsson-Sjoberg, J., Amir, E., Teggatz, P., Barman, M., Hayward, M., Eastwood, D., Stoel, M., Zhou, Y., Sodergren, E., Weinstock, G.M., Bevins, C.L., Williams, C.B., and Bos, N.A. Enteric defensins are essential regulators of intestinal microbial ecology. Nat Immunol 11, 76-82, 2010.

[42] Parry, L., Young, M., El Marjou, F., and Clarke, A.R. Evidence for a Crucial Role of Paneth Cells in Mediating the Intestinal Response to Injury. STEM CELLS 31, 776-785, 2013.

[43] Sato, T., van Es, J.H., Snippert, H.J., Stange, D.E., Vries, R.G., van den Born, M., Barker, N., Shroyer, N.F., van de Wetering, M., and Clevers, H. Paneth cells constitute the niche for Lgr5 stem cells in intestinal crypts. Nature 469, 415-418, 2011.

[44] Yilmaz, O.H., Katajisto, P., Lamming, D.W., Gultekin, Y., Bauer-Rowe, K.E., Sengupta, S., Birsoy, K., Dursun, A., Yilmaz, V.O., Selig, M., Nielsen, G.P., Mino-Kenudson, M., Zukerberg, L.R., Bhan, A.K., Deshpande, V., and Sabatini, D.M. mTORC1 in the Paneth cell niche couples intestinal stem-cell function to calorie intake. Nature 486, 490-495, 2012.

[45] Engelstoft, M.S., Egerod, K.L., Lund, M.L., and Schwartz, T.W. Enteroendocrine cell types revisited. Current Opinion in Pharmacology 13, 912-921, 2013.

[46] Khorrami, M.-H., Salehi, P., Nouri-Mahdavi, K., Ghalamkari, A., and Tadayyon, F. Dramatic Effect of a Somatostatin Analogue in Decreasing Mucus Production by the Intestinal Segment After Enterocystoplasty. The Journal of Urology 180, 2501-2503.

[47] Wang, M., Gao, Z., Zhang, Z., Pan, L., and Zhang, Y. Roles of M cells in infection and mucosal vaccines. Human Vaccines & Immunotherapeutics 10, 3544-3551, 2014.

[48] Kanaya, T., and Ohno, H. The Mechanisms of M-cell Differentiation. Bioscience of Microbiota, Food and Health 33, 91-97, 2014.

[49] Lei, N.Y., Jabaji, Z., Wang, J., Joshi, V.S., Brinkley, G.J., Khalil, H., Wang, F., Jaroszewicz, A., Pellegrini, M., Li, L., Lewis, M., Stelzner, M., Dunn, J.C.Y., and Martín, M.G. Intestinal Subepithelial Myofibroblasts Support the Growth of Intestinal Epithelial Stem Cells. PLoS ONE 9, e84651, 2014.

[50] Tian, H., Biehs, B., Chiu, C., Siebel, C., Wu, Y., Costa, M., de Sauvage, F.J., and Klein, O.D. Opposing activities of Notch and Wnt signaling regulate intestinal stem cells and gut homeostasis. Cell reports 11, 33-42, 2015.

[51] van Es, J.H., van Gijn, M.E., Riccio, O., van den Born, M., Vooijs, M., Begthel, H., Cozijnsen, M., Robine, S., Winton, D.J., Radtke, F., and Clevers, H. Notch/[gamma]-secretase inhibition turns proliferative cells in intestinal crypts and adenomas into goblet cells. Nature 435, 959-963, 2005.

[52] Dahan, S., Rabinowitz, K.M., Martin, A.P., Berin, M.C., Unkeless, J.C., and Mayer, L. Notch-1 signaling regulates intestinal epithelial barrier function, through interaction with CD4+ T cells, in mice and humans. Gastroenterology 140, 550-559, 2011.

[53] Guezguez, A., Paré, F., Benoit, Y.D., Basora, N., and Beaulieu, J.-F. Modulation of stemness in a human normal intestinal epithelial crypt cell line by activation of the WNT signaling pathway. Experimental Cell Research 322, 355-364, 2014.

[54] Institute, R.K., and Germany, A.o.P.-b.C.R.i. Cancer in Germany 2009/2010. Berlin 9th edition, 1-149, 2014.

[55] Tan, S., and Barker, N. Epithelial stem cells and intestinal cancer. Seminars in Cancer Biology 32, 40-53, 2015.

[56] Danese, S., and Fiocchi, C. Ulcerative Colitis. New England Journal of Medicine 365, 1713-1725, 2011.

[57] Loftus Jr, E.V. Clinical epidemiology of inflammatory bowel disease: incidence, prevalence, and environmental influences. Gastroenterology 126, 1504-1517, 2004.

[58] Laass, M.W., Roggenbuck, D., and Conrad, K. Diagnosis and classification of Crohn's disease. Autoimmunity reviews 13, 467-471, 2014.

[59] de Mattos, B.R.R., Garcia, M.P.G., Nogueira, J.B., Paiatto, L.N., Albuquerque, C.G., Souza, C.L., Fernandes, L.G.R., Tamashiro, W.M.d.S.C., and Simioni, P.U. Inflammatory Bowel Disease: An Overview of Immune Mechanisms and Biological Treatments. Mediators of Inflammation 2015, 493012, 2015.

[60] Hwang, S.R., and Byun, Y. Advances in oral macromolecular drug delivery. Expert opinion on drug delivery 11, 1955-1967, 2014.

[61] Artursson, P., Ungell, A.L., and Lofroth, J.E. Selective paracellular permeability in two models of intestinal absorption: cultured monolayers of human intestinal epithelial cells and rat intestinal segments. Pharmaceutical research 10, 1123-1129, 1993.

[62] Lodish, H., Lange, C., Mahlke, K., Berk, A., Zipursky, S.L., Seidler, L., Träger, L., Matsudaira, P., Baltimore, D., and Darnell, J.E. Molekulare Zellbiologie: Spektrum Akademischer Verlag; 2001.

[63] Takano, M., Yumoto, R., and Murakami, T. Expression and function of efflux drug transporters in the intestine. Pharmacology & Therapeutics 109, 137-161, 2006.

[64] Stephens, R.H., O'Neill, C.A., Warhurst, A., Carlson, G.L., Rowland, M., and Warhurst, G. Kinetic Profiling of P-glycoprotein-Mediated Drug Efflux in Rat and Human Intestinal Epithelia. Journal of Pharmacology and Experimental Therapeutics 296, 584-591, 2001.

[65] Gordon, S., Daneshian, M., Bouwstra, J., Caloni, F., Constant, S., Davies, D.E., Dandekar, G., Guzman, C.A., Fabian, E., Haltner, E., Hartung, T., Hasiwa, N., Hayden, P., Kandarova, H., Khare, S., Krug, H.F., Kneuer, C., Leist, M., Lian, G., Marx, U., Metzger, M., Ott, K., Prieto, P., Roberts, M.S., Roggen, E.L., Tralau, T., van den Braak, C., Walles, H., and Lehr, C.M. Non-animal models of epithelial barriers (skin, intestine and lung) in research, industrial applications and regulatory toxicology. Altex 32, 327-378, 2015.

[66] Adler, S., Basketter, D., Creton, S., Pelkonen, O., van Benthem, J., Zuang, V., Andersen, K., Angers-Loustau, A., Aptula, A., Bal-Price, A., Benfenati, E., Bernauer, U., Bessems, J., Bois, F., Boobis, A., Brandon, E., Bremer, S., Broschard, T., Casati, S., Coecke, S., Corvi, R., Cronin, M., Daston, G., Dekant, W., Felter, S., Grignard, E., Gundert-Remy, U., Heinonen, T., Kimber, I., Kleinjans, J., Komulainen, H., Kreiling, R., Kreysa, J., Leite, S., Loizou, G., Maxwell, G., Mazzatorta, P., Munn, S., Pfuhler, S., Phrakonkham, P., Piersma, A., Poth, A., Prieto, P., Repetto, G., Rogiers, V., Schoeters, G., Schwarz, M., Serafimova, R., Tähti, H., Testai, E., van Delft, J., van Loveren, H., Vinken, M., Worth, A., and Zaldivar, J.-M. Alternative (non-animal) methods for cosmetics testing: current status and future prospects—2010. Arch Toxicol 85, 367-485, 2011.

[67] Macierzanka, A., Mackie, A.R., Bajka, B.H., Rigby, N.M., Nau, F., and Dupont, D. Transport of Particles in Intestinal Mucus under Simulated Infant and Adult Physiological Conditions: Impact of Mucus Structure and Extracellular DNA. PLoS ONE 9, e95274, 2014.

[68] Brun, E., Barreau, F., Veronesi, G., Fayard, B., Sorieul, S., Chanéac, C., Carapito, C., Rabilloud, T., Mabondzo, A., Herlin-Boime, N., and Carrière, M. Titanium dioxide nanoparticle impact and translocation through ex vivo, in vivo and in vitro gut epithelia. Particle and Fibre Toxicology 11, 13-13, 2014.

[69] Shah, R.B., and Khan, M.A. Regional permeability of salmon calcitonin in isolated rat gastrointestinal tracts: Transport mechanism using Caco-2 cell monolayer. The AAPS Journal 6, 36-40, 2004.

[70] Konkel, M.E., Mead, D.J., Hayes, S.F., and Cieplak, W. Translocation of Campylobacter jejuni across Human Polarized Epithelial Cell Monolayer Cultures. Journal of Infectious Diseases 166, 308-315, 1992.

[71] Muheem, A., Shakeel, F., Jahangir, M.A., Anwar, M., Mallick, N., Jain, G.K., Warsi, M.H., and Ahmad, F.J. A review on the strategies for oral delivery of proteins and peptides and their clinical perspectives. Saudi Pharmaceutical Journal.

[72] Lahar, N., Lei, N.Y., Wang, J., Jabaji, Z., Tung, S.C., Joshi, V., Lewis, M., Stelzner, M., Martín, M.G., and Dunn, J.C.Y. Intestinal Subepithelial Myofibroblasts Support in vitro and in vivo Growth of Human Small Intestinal Epithelium. PLoS ONE 6, e26898, 2011.

[73] Leonard, F., Collnot, E.-M., and Lehr, C.-M. A Three-Dimensional Coculture of Enterocytes, Monocytes and Dendritic Cells To Model Inflamed Intestinal Mucosa in Vitro. Molecular Pharmaceutics 7, 2103-2119, 2010.

[74] Kim, H.J., Huh, D., Hamilton, G., and Ingber, D.E. Human gut-on-a-chip inhabited by microbial flora that experiences intestinal peristalsis-like motions and flow. Lab on a Chip 12, 2165-2174, 2012.

[75] Pusch, J., Votteler, M., Gohler, S., Engl, J., Hampel, M., Walles, H., and Schenke-Layland, K. The physiological performance of a three-dimensional model that mimics the microenvironment of the small intestine. Biomaterials 32, 7469-7478, 2011.

[76] Date, S., and Sato, T. Mini-Gut Organoids: Reconstitution of Stem Cell Niche. Annu Rev Cell Dev Biol 2015.

[77] Artursson, P., and Karlsson, J. Correlation between oral drug absorption in humans and apparent drug permeability coefficients in human intestinal epithelial (Caco-2) cells. Biochemical and Biophysical Research Communications 175, 880-885, 1991.

[78] McCool, D.J., Marcon, M.A., Forstner, J.F., and Forstner, G.G. The T84 human colonic adenocarcinoma cell line produces mucin in culture and releases it in response to various secretagogues. Biochemical Journal 267, 491-500, 1990.

[79] Hubatsch, I., Ragnarsson, E.G.E., and Artursson, P. Determination of drug permeability and prediction of drug absorption in Caco-2 monolayers. Nat Protocols 2, 2111-2119, 2007.

[80] Balimane, P.V., and Chong, S. Cell culture-based models for intestinal permeability: A critique. Drug Discovery Today 10, 335-343, 2005.

[81] Ou, G., Baranov, V., Lundmark, E., Hammarström, S., and Hammarström, M.L. Contribution of Intestinal Epithelial Cells to Innate Immunity of the Human Gut – Studies on Polarized Monolayers of Colon Carcinoma Cells. Scandinavian Journal of Immunology 69, 150-161, 2009.

[82] Le Ferrec, E., Chesne, C., Artusson, P., Brayden, D., Fabre, G., Gires, P., Guillou, F., Rousset, M., Rubas, W., and Scarino, M.L. In vitro models of the intestinal barrier. The report and recommendations of ECVAM Workshop 46. European Centre for the

Validation of Alternative methods. Alternatives to laboratory animals : ATLA 29, 649-668, 2001.

[83] de Lau, W., Kujala, P., Schneeberger, K., Middendorp, S., Li, V.S.W., Barker, N., Martens, A., Hofhuis, F., DeKoter, R.P., Peters, P.J., Nieuwenhuis, E., and Clevers, H. Peyer's Patch M Cells Derived from Lgr5(+) Stem Cells Require SpiB and Are Induced by RankL in Cultured "Miniguts". Molecular and Cellular Biology 32, 3639-3647, 2012.

[84] Yeung, T.M., Chia, L.A., Kosinski, C.M., and Kuo, C.J. Regulation of self-renewal and differentiation by the intestinal stem cell niche. Cellular and molecular life sciences : CMLS 68, 2513-2523, 2011.

[85] Sato, T., Stange, D.E., Ferrante, M., Vries, R.G.J., van Es, J.H., van den Brink, S., van Houdt, W.J., Pronk, A., van Gorp, J., Siersema, P.D., and Clevers, H. Long-term Expansion of Epithelial Organoids From Human Colon, Adenoma, Adenocarcinoma, and Barrett's Epithelium. Gastroenterology 141, 1762-1772, 2011.

[86] Kauffman, A.L., Gyurdieva, A.V., Mabus, J.R., Ferguson, C., Yan, Z., and Hornby, P.J. Alternative functional in vitro models of human intestinal epithelia. Frontiers in Pharmacology 4, 79, 2013.

[87] Takenaka, T., Harada, N., Kuze, J., Chiba, M., Iwao, T., and Matsunaga, T. Human small intestinal epithelial cells differentiated from adult intestinal stem cells as a novel system for predicting oral drug absorption in humans. Drug Metab Dispos 42, 1947-1954, 2014.

[88] VanDussen, K.L., Marinshaw, J.M., Shaikh, N., Miyoshi, H., Moon, C., Tarr, P.I., Ciorba, M.A., and Stappenbeck, T.S. Development of an enhanced human gastrointestinal epithelial culture system to facilitate patient-based assays. Gut 64, 911-920, 2015.

[89] Yamaura, Y., Chapron, B.D., Wang, Z., Himmelfarb, J., and Thummel, K.E. Functional Comparison of Human Colonic Carcinoma Cell Lines and Primary Small Intestinal Epithelial Cells for Investigations of Intestinal Drug Permeability and First-Pass Metabolism. Drug Metab Dispos 44, 329-335, 2016.

[90] Zorn, A.M., and Wells, J.M. Vertebrate Endoderm Development and Organ Formation. Annual review of cell and developmental biology 25, 221-251, 2009.

[91] Spence, J.R., Mayhew, C.N., Rankin, S.A., Kuhar, M.F., Vallance, J.E., Tolle, K., Hoskins, E.E., Kalinichenko, V.V., Wells, S.I., Zorn, A.M., Shroyer, N.F., and Wells, J.M. Directed differentiation of human pluripotent stem cells into intestinal tissue in vitro. Nature 470, 105-109, 2011.

[92] D'Amour, K.A., Agulnick, A.D., Eliazer, S., Kelly, O.G., Kroon, E., and Baetge, E.E. Efficient differentiation of human embryonic stem cells to definitive endoderm. Nat Biotech 23, 1534-1541, 2005.

[93] Cao, L., Kuratnik, A., Xu, W., Gibson, J.D., Kolling, F., Falcone, E.R., Ammar, M., Van Heyst, M.D., Wright, D.L., Nelson, C.E., and Giardina, C. Development of intestinal organoids as tissue surrogates: Cell composition and the Epigenetic control of differentiation. Molecular Carcinogenesis 54, 189-202, 2015.

[94] Milano, J., McKay, J., Dagenais, C., Foster-Brown, L., Pognan, F., Gadient, R., Jacobs, R.T., Zacco, A., Greenberg, B., and Ciaccio, P.J. Modulation of Notch Processing by γ-

Secretase Inhibitors Causes Intestinal Goblet Cell Metaplasia and Induction of Genes Known to Specify Gut Secretory Lineage Differentiation. Toxicological Sciences 82, 341-358, 2004.

[95] Ogaki, S., Shiraki, N., Kume, K., and Kume, S. Wnt and Notch Signals Guide Embryonic Stem Cell Differentiation into the Intestinal Lineages. STEM CELLS 31, 1086-1096, 2013.

[96] Finkbeiner, S.R., Freeman, J.J., Wieck, M.M., El-Nachef, W., Altheim, C.H., Tsai, Y.-H., Huang, S., Dyal, R., White, E.S., Grikscheit, T.C., Teitelbaum, D.H., and Spence, J.R. Generation of tissue-engineered small intestine using embryonic stem cell-derived human intestinal organoids. Biology Open 2015.

[97] Wang, J., and Hou, T. Advances in computationally modeling human oral bioavailability. Advanced Drug Delivery Reviews 86, 11-16, 2015.

[98] Hans, M., Karl-Heinz, B., Thorsten, N., Thomas, K., and Bernard, P. Computational Approaches Towards the Rational Design of Drug-like Compound Libraries. Combinatorial Chemistry & High Throughput Screening 4, 453-475, 2001.

[99] Guerra, A., Campillo, N.E., and Páez, J.A. Neural computational prediction of oral drug absorption based on CODES 2D descriptors. European Journal of Medicinal Chemistry 45, 930-940, 2010.

[100] van de Waterbeemd, H., and Gifford, E. ADMET in silico modelling: towards prediction paradise? Nat Rev Drug Discov 2, 192-204, 2003.

[101] Filipa, A., Fernanda, A., Domingos, F., Hanne Mørck, N., and Bruno, S. Models to Predict Intestinal Absorption of Therapeutic Peptides and Proteins. Current Drug Metabolism 14, 4-20, 2013.

[102] Jung, E., Kim, J., Kim, M., Jung, D.H., Rhee, H., Shin, J.-M., Choi, K., Kang, S.-K., Kim, M.-K., Yun, C.-H., Choi, Y.-J., and Choi, S.-H. Artificial neural network models for prediction of intestinal permeability of oligopeptides. BMC Bioinformatics 8, 245-245, 2007.

[103] Larregieu, C.A., and Benet, L.Z. Drug Discovery and Regulatory Considerations for Improving In Silico and In Vitro Predictions that Use Caco-2 as a Surrogate for Human Intestinal Permeability Measurements. The AAPS Journal 15, 483-497, 2013.

[104] Gernot, H., Tomasz, J., Toby, D.B., Kathrin, H., Claus, M., Franz, J., Paul, D.D., and Jürgen, G. Additive manufacturing of scaffolds with sub-micron filaments via melt electrospinning writing. Biofabrication 7, 035002, 2015.

[105] Schacht, K., Jüngst, T., Schweinlin, M., Ewald, A., Groll, J., and Scheibel, T. Biofabrication of Cell-Loaded 3D Spider Silk Constructs. Angewandte Chemie International Edition 54, 2816-2820, 2015.

[106] Schanz, J., Pusch, J., Hansmann, J., and Walles, H. Vascularised human tissue models: A new approach for the refinement of biomedical research. Journal of Biotechnology 148, 56-63, 2010.

[107] Shahin, K., and Doran, P. Shear and Compression Bioreactor for Cartilage Synthesis. In: Doran P.M., ed. Cartilage Tissue Engineering: Springer New York; 2015. pp. 221-233.

[108] O'Connor, M.D. The 3R principle: advancing clinical application of human pluripotent stem cells. Stem Cell Research & Therapy 4, 21-21, 2013.

[109] Holzapfel, B.M., Reichert, J.C., Schantz, J.T., Gbureck, U., Rackwitz, L., Noth, U., Jakob, F., Rudert, M., Groll, J., and Hutmacher, D.W. How smart do biomaterials need to be? A translational science and clinical point of view. Adv Drug Deliv Rev 65, 581-603, 2013.

[110] Laschke, M.W., and Menger, M.D. Prevascularization in tissue engineering: Current concepts and future directions. Biotechnology advances 2015.

[111] (CDER), U.S.D.o.H.a.H.S.F.a.D.A.C.f.D.E.a.R. Waiver of In Vivo Bioavailability and Bioequivalence Studies for Immediate-Release Solid Oral Dosage Forms Based on a Biopharmaceutics Classification System. 2015.

[112] Kops, S.K., Lowe, D.K., Bement, W.M., and West, A.B. Migration of Salmonella typhi through Intestinal Epithelial Monolayers: An In Vitro Study. Microbiology and Immunology 40, 799-811, 1996.

[113] Brito Baleeiro, R., Schweinlin, M., Rietscher, R., Diedrich, A., Czaplewska, J.A., Metzger, M., Michael Lehr, C., Scherließ, R., Hanefeld, A., Gottschaldt, M., and Walden, P. Nanoparticle-Based Mucosal Vaccines Targeting Tumor-Associated Antigens to Human Dendritic Cells. Journal of Biomedical Nanotechnology 12, 1527-1543, 2016.

[114] Mertsching, H., Schanz, J., Steger, V., Schandar, M., Schenk, M., Hansmann, J., Dally, I., Friedel, G., and Walles, T. Generation and transplantation of an autologous vascularized bioartificial human tissue. Transplantation 88, 203-210, 2009.

[115] Miyoshi, H., and Stappenbeck, T.S. In vitro expansion and genetic modification of gastrointestinal stem cells in spheroid culture. Nat Protocols 8, 2471-2482, 2013.

[116] Zhao, C. Wnt Reporter Activity Assay. Bio-protocol 4(14): e1183. 2014.

[117] Prüfert, K., Vogel, A., and Krohne, G. The lamin CxxM motif promotes nuclear membrane growth. Journal of Cell Science 117, 6105-6116, 2004.

[118] Burk, O., Arnold, K.A., Nussler, A.K., Schaeffeler, E., Efimova, E., Avery, B.A., Avery, M.A., Fromm, M.F., and Eichelbaum, M. Antimalarial artemisinin drugs induce cytochrome P450 and MDR1 expression by activation of xenosensors pregnane X receptor and constitutive androstane receptor. Molecular pharmacology 67, 1954-1965, 2005.

[119] Wolbold, R., Klein, K., Burk, O., Nussler, A.K., Neuhaus, P., Eichelbaum, M., Schwab, M., and Zanger, U.M. Sex is a major determinant of CYP3A4 expression in human liver. Hepatology (Baltimore, Md) 38, 978-988, 2003.

[120] Schweinlin, M., Wilhelm, S., Schwedhelm, I., Hansmann, J., Rietscher, R., Jurowich, C., Walles, H., and Metzger, M. Development of an advanced primary human in vitro model of the small intestine. Tissue Engineering Part C: Methods 2016.

[121] Biesalski, H.K., and Grimm, P. Taschenatlas der Ernährung: Thieme; 2007.

[122] Moroz, E., Matoori, S., and Leroux, J.-C. Oral delivery of macromolecular drugs: Where we are after almost 100 years of attempts. Advanced Drug Delivery Reviews.

[123] Andrew, K. Systematic Reviews of Animal Experiments Demonstrate Poor Contributions Toward Human Healthcare. Reviews on Recent Clinical Trials 3, 89-96, 2008.

[124] Russell, W.M.S., Burch, R.L., and Hume, C.W. The principles of humane experimental technique. 1959.

[125] Artursson, P., Palm, K., and Luthman, K. Caco-2 monolayers in experimental and theoretical predictions of drug transport1. Advanced Drug Delivery Reviews 46, 27-43, 2001.

[126] Allen, D.D., Caviedes, R., Cárdenas, A.M., Shimahara, T., Segura-Aguilar, J., and Caviedes, P.A. Cell Lines as In Vitro Models for Drug Screening and Toxicity Studies. Drug Development and Industrial Pharmacy 31, 757-768, 2005.

[127] Hay, M., Thomas, D.W., Craighead, J.L., Economides, C., and Rosenthal, J. Clinical development success rates for investigational drugs. Nat Biotech 32, 40-51, 2014.

[128] Zhang, D., Luo, G., Ding, X., and Lu, C. Preclinical experimental models of drug metabolism and disposition in drug discovery and development. Acta Pharmaceutica Sinica B 2, 549-561, 2012.

[129] Leist, M., Hasiwa, N., Rovida, C., Daneshian, M., Basketter, D., Kimber, I., Clewell, H., Gocht, T., Goldberg, A., Busquet, F., Rossi, A.M., Schwarz, M., Stephens, M., Taalman, R., Knudsen, T.B., McKim, J., Harris, G., Pamies, D., and Hartung, T. Consensus report on the future of animal-free systemic toxicity testing. Altex 31, 341-356, 2014.

[130] van Breemen, R.B., and Li, Y. Caco-2 cell permeability assays to measure drug absorption. Expert opinion on drug metabolism & toxicology 1, 175-185, 2005.

[131] Sjöberg, Å., Lutz, M., Tannergren, C., Wingolf, C., Borde, A., and Ungell, A.-L. Comprehensive study on regional human intestinal permeability and prediction of fraction absorbed of drugs using the Ussing chamber technique. European Journal of Pharmaceutical Sciences 48, 166-180, 2013.

[132] Lundquist, P., and Artursson, P. Oral absorption of peptides and nanoparticles across the human intestine: Opportunities, limitations and studies in human tissues. Advanced Drug Delivery Reviews.

[133] Hofmann, C., Obermeier, F., Artinger, M., Hausmann, M., Falk, W., Schoelmerich, J., Rogler, G., and Grossmann, J. Cell-Cell Contacts Prevent Anoikis in Primary Human Colonic Epithelial Cells. Gastroenterology 132, 587-600.

[134] Simon-Assmann, P., Spenle, C., Lefebvre, O., and Kedinger, M. The role of the basement membrane as a modulator of intestinal epithelial-mesenchymal interactions. Progress in molecular biology and translational science 96, 175-206, 2010.

[135] Cukierman, E., Pankov, R., Stevens, D.R., and Yamada, K.M. Taking Cell-Matrix Adhesions to the Third Dimension. Science (New York, NY) 294, 1708-1712, 2001.

[136] Daley, W.P., Gervais, E.M., Centanni, S.W., Gulfo, K.M., Nelson, D.A., and Larsen, M. ROCK1-directed basement membrane positioning coordinates epithelial tissue polarity. Development (Cambridge, England) 139, 411-422, 2012.

[137] Kim, S.H., Chi, M., Yi, B., Kim, S.H., Oh, S., Kim, Y., Park, S., and Sung, J.H. Three-dimensional intestinal villi epithelium enhances protection of human intestinal cells from bacterial infection by inducing mucin expression. Integrative Biology 6, 1122-1131, 2014.

[138] Steinman, R.M. Dendritic cells: Understanding immunogenicity. European Journal of Immunology 37, S53-S60, 2007.

[139] Villadangos, J.A., and Schnorrer, P. Intrinsic and cooperative antigen-presenting functions of dendritic-cell subsets in vivo. Nat Rev Immunol 7, 543-555, 2007.

[140] Qu, C., Brinck-Jensen, N.-S., Zang, M., and Chen, K. Monocyte-derived dendritic cells: targets as potent antigen-presenting cells for the design of vaccines against infectious diseases. International Journal of Infectious Diseases 19, 1-5, 2014.

[141] Sprangers, S., de Vries, T.J., and Everts, V. Monocyte Heterogeneity: Consequences for Monocyte-Derived Immune Cells. Journal of Immunology Research 2016, 1475435, 2016.

[142] Schulz, O., Jaensson, E., Persson, E.K., Liu, X., Worbs, T., Agace, W.W., and Pabst, O. Intestinal CD103+, but not CX3CR1+, antigen sampling cells migrate in lymph and serve classical dendritic cell functions. J Exp Med 206, 3101-3114, 2009.

[143] Fujii, S.-i., Liu, K., Smith, C., Bonito, A.J., and Steinman, R.M. The Linkage of Innate to Adaptive Immunity via Maturing Dendritic Cells In Vivo Requires CD40 Ligation in Addition to Antigen Presentation and CD80/86 Costimulation. The Journal of Experimental Medicine 199, 1607-1618, 2004.

[144] Lelouard, H., Fallet, M., de Bovis, B., Méresse, S., and Gorvel, J.P. Peyer's Patch Dendritic Cells Sample Antigens by Extending Dendrites Through M Cell-Specific Transcellular Pores. Gastroenterology 142, 592-601.e593.

[145] Bermudez-Brito, M., Munoz-Quezada, S., Gomez-Llorente, C., Matencio, E., Romero, F., and Gil, A. Lactobacillus paracasei CNCM I-4034 and its culture supernatant modulate Salmonella-induced inflammation in a novel transwell co-culture of human intestinal-like dendritic and Caco-2 cells. BMC Microbiology 15, 79, 2015.

[146] Susewind, J., de Souza Carvalho-Wodarz, C., Repnik, U., Collnot, E.-M., Schneider-Daum, N., Griffiths, G.W., and Lehr, C.-M. A 3D co-culture of three human cell lines to model the inflamed intestinal mucosa for safety testing of nanomaterials. Nanotoxicology 10, 53-62, 2016.

[147] Scott, C.L., Wright, P.B., Milling, S.W.F., and Mowat, A.M. Isolation and Identification of Conventional Dendritic Cell Subsets from the Intestine of Mice and Men. In: Segura E., Onai N., eds. Dendritic Cell Protocols. New York, NY: Springer New York; 2016. pp. 101-118.

[148] Ko, H.-J., and Chang, S.-Y. Regulation of Intestinal Immune System by Dendritic Cells. Immune Network 15, 1-8, 2015.

[149] Rouch, J.D., Scott, A., Lei, N.Y., Solorzano-Vargas, R.S., Wang, J., Hanson, E.M., Kobayashi, M., Lewis, M., Stelzner, M.G., Dunn, J.C.Y., Eckmann, L., and Martín, M.G. Development of Functional Microfold (M) Cells from Intestinal Stem Cells in Primary Human Enteroids. PLoS ONE 11, e0148216, 2016.

[150] Nassar, T., Rom, A., Nyska, A., and Benita, S. Novel double coated nanocapsules for intestinal delivery and enhanced oral bioavailability of tacrolimus, a P-gp substrate drug. Journal of Controlled Release 133, 77-84, 2009.

[151] Joshi, M.D., Unger, W.J., Storm, G., van Kooyk, Y., and Mastrobattista, E. Targeting tumor antigens to dendritic cells using particulate carriers. Journal of Controlled Release 161, 25-37, 2012.

[152] Date, A.A., Hanes, J., and Ensign, L.M. Nanoparticles for oral delivery: Design, evaluation and state-of-the-art. Journal of Controlled Release.

[153] Alpar, H.O., Somavarapu, S., Atuah, K.N., and Bramwell, V.W. Biodegradable mucoadhesive particulates for nasal and pulmonary antigen and DNA delivery. Advanced Drug Delivery Reviews 57, 411-430, 2005.

[154] Danhier, F., Ansorena, E., Silva, J.M., Coco, R., Le Breton, A., and Preat, V. PLGA-based nanoparticles: an overview of biomedical applications. Journal of controlled release : official journal of the Controlled Release Society 161, 505-522, 2012.

[155] Burgdorf, S., Scholz, C., Kautz, A., Tampe, R., and Kurts, C. Spatial and mechanistic separation of cross-presentation and endogenous antigen presentation. Nat Immunol 9, 558-566, 2008.

[156] Roger, E., Kalscheuer, S., Kirtane, A., Guru, B.R., Grill, A.E., Whittum-Hudson, J., and Panyam, J. Folic acid-Functionalized Nanoparticles for Enhanced Oral Drug Delivery. Molecular pharmaceutics 9, 2103-2110, 2012.

[157] Desai, M.P., Labhasetwar, V., Walter, E., Levy, R.J., and Amidon, G.L. The mechanism of uptake of biodegradable microparticles in Caco-2 cells is size dependent. Pharmaceutical research 14, 1568-1573, 1997.

[158] Panyam, J., Sahoo, S.K., Prabha, S., Bargar, T., and Labhasetwar, V. Fluorescence and electron microscopy probes for cellular and tissue uptake of poly(D,L-lactide-co-glycolide) nanoparticles. Int J Pharm 262, 1-11, 2003.

[159] Hillgren, K.M., Kato, A., and Borchardt, R.T. In vitro systems for studying intestinal drug absorption. Medicinal research reviews 15, 83-109, 1995.

[160] Ensign, L.M., Cone, R., and Hanes, J. Oral Drug Delivery with Polymeric Nanoparticles: The Gastrointestinal Mucus Barriers. Advanced Drug Delivery Reviews 64, 557-570, 2012.

[161] Ismael, J.H. Assessing the Absorption of New Pharmaceuticals. Current Topics in Medicinal Chemistry 1, 385-401, 2001.

[162] Crapo, P.M., Gilbert, T.W., and Badylak, S.F. An overview of tissue and whole organ decellularization processes. Biomaterials 32, 3233-3243, 2011.

[163] Kleinman, H.K., McGarvey, M.L., Hassell, J.R., Star, V.L., Cannon, F.B., Laurie, G.W., and Martin, G.R. Basement membrane complexes with biological activity. Biochemistry 25, 312-318, 1986.

[164] Pinto, D., Gregorieff, A., Begthel, H., and Clevers, H. Canonical Wnt signals are essential for homeostasis of the intestinal epithelium. Genes & development 17, 1709-1713, 2003.

[165] Willert, K., Brown, J.D., Danenberg, E., Duncan, A.W., Weissman, I.L., Reya, T., Yates, J.R., and Nusse, R. Wnt proteins are lipid-modified and can act as stem cell growth factors. Nature 423, 448-452, 2003.

[166] Ke, J., Xu, H.E., and Williams, B.O. Lipid modification in Wnt structure and function. Current opinion in lipidology 24, 129-133, 2013.

[167] Bartfeld, S., and Clevers, H. Organoids as Model for Infectious Diseases: Culture of Human and Murine Stomach Organoids and Microinjection of Helicobacter Pylori. e53359, 2015.

[168] Mizutani, T., Nakamura, T., Morikawa, R., Fukuda, M., Mochizuki, W., Yamauchi, Y., Nozaki, K., Yui, S., Nemoto, Y., Nagaishi, T., Okamoto, R., Tsuchiya, K., and Watanabe, M. Real-time analysis of P-glycoprotein-mediated drug transport across primary intestinal epithelium three-dimensionally cultured in vitro. Biochemical and Biophysical Research Communications 419, 238-243, 2012.

[169] Zietek, T., Rath, E., Haller, D., and Daniel, H. Intestinal organoids for assessing nutrient transport, sensing and incretin secretion. Scientific reports 5, 16831, 2015.

[170] Samuel, S., Walsh, R., Webb, J., Robins, A., Potten, C., and Mahida, Y.R. Characterization of putative stem cells in isolated human colonic crypt epithelial cells and their interactions with myofibroblasts. American Journal of Physiology - Cell Physiology 296, C296-C305, 2009.

[171] Pinchuk, I.V., Mifflin, R.C., Saada, J.I., and Powell, D.W. Intestinal Mesenchymal Cells. Current Gastroenterology Reports 12, 310-318, 2010.

[172] Masaru, K. WNT Signaling in Stem Cell Biology and Regenerative Medicine. Current Drug Targets 9, 565-570, 2008.

[173] Ishizuya-Oka, A., and Hasebe, T. Sonic Hedgehog and Bone Morphogenetic Protein-4 Signaling Pathway Involved in Epithelial Cell Renewal along the Radial Axis of the Intestine. Digestion 77(suppl 1), 42-47, 2008.

[174] Yeung, T.M., Chia, L.A., Kosinski, C.M., and Kuo, C.J. Regulation of self-renewal and differentiation by the intestinal stem cell niche. Cellular and Molecular Life Sciences 68, 2513-2523, 2011.

[175] Moon, C., VanDussen, K.L., Miyoshi, H., and Stappenbeck, T.S. Development of a primary mouse intestinal epithelial cell monolayer culture system to evaluate factors that modulate IgA transcytosis. Mucosal Immunol 7, 818-828, 2014.

[176] Muendoerfer, M., Schaefer, U.F., Koenig, P., Walk, J.S., Loos, P., Balbach, S., Eichinger, T., and Lehr, C.-M. Online monitoring of transepithelial electrical resistance

(TEER) in an apparatus for combined dissolution and permeation testing. International Journal of Pharmaceutics 392, 134-140, 2010.

[177] Srinivasan, B., Kolli, A.R., Esch, M.B., Abaci, H.E., Shuler, M.L., and Hickman, J.J. TEER measurement techniques for in vitro barrier model systems. Journal of laboratory automation 20, 107-126, 2015.

[178] McLaren, W.J., Anikijenko, P., Thomas, S.G., Delaney, P.M., and King, R.G. In vivo detection of morphological and microvascular changes of the colon in association with colitis using fiberoptic confocal imaging (FOCI). Digestive diseases and sciences 47, 2424-2433, 2002.

[179] Shen, L., Weber, C.R., Raleigh, D.R., Yu, D., and Turner, J.R. Tight Junction Pore and Leak Pathways: A Dynamic Duo. Annual review of physiology 73, 283-309, 2011.

[180] Krug, S.M., Schulzke, J.D., and Fromm, M. Tight junction, selective permeability, and related diseases. Seminars in Cell & Developmental Biology 36, 166-176, 2014.

[181] Rebelo, S.P., Costa, R., Silva, M.M., Marcelino, P., Brito, C., and Alves, P.M. Three-dimensional co-culture of human hepatocytes and mesenchymal stem cells: improved functionality in long-term bioreactor cultures. Journal of tissue engineering and regenerative medicine 2015.

[182] Jeong, S.I., Kwon, J.H., Lim, J.I., Cho, S.-W., Jung, Y., Sung, W.J., Kim, S.H., Kim, Y.H., Lee, Y.M., Kim, B.-S., Choi, C.Y., and Kim, S.-J. Mechano-active tissue engineering of vascular smooth muscle using pulsatile perfusion bioreactors and elastic PLCL scaffolds. Biomaterials 26, 1405-1411, 2005.

[183] Ganong, W.F., and Auerswald, W. Medizinische Physiologie: Kurzgefaßtes Lehrbuch der Physiologie des Menschen für Studierende der Medizin und Ärzte: Springer Berlin Heidelberg; 2013.

[184] Bock, U., Flototto, T., and Haltner, E. Validation of cell culture models for the intestine and the blood-brain barrier and comparison of drug permeation. Altex 21 Suppl 3, 57-64, 2004.

[185] Kratz, J.M., Teixeira, M.R., Koester, L.S., and Simões, C.M.O. An HPLC-UV method for the measurement of permeability of marker drugs in the Caco-2 cell assay. Brazilian Journal of Medical and Biological Research 44, 531-537, 2011.

[186] Meir, M., Flemming, S., Burkard, N., Bergauer, L., Metzger, M., Germer, C.-T., and Schlegel, N. Glial cell line-derived neurotrophic factor promotes barrier maturation and wound healing in intestinal epithelial cells in vitro. American Journal of Physiology - Gastrointestinal and Liver Physiology 309, G613-G624, 2015.

[187] Vllasaliu, D., Falcone, F.H., Stolnik, S., and Garnett, M. Basement membrane influences intestinal epithelial cell growth and presents a barrier to the movement of macromolecules. Exp Cell Res 323, 218-231, 2014.

9 Appendix

9.1 Supplementary data

Table 21: List of donors (2014-2015)

Internal number	Date of Surgery	Segment	Gender	Age
PD 14-01	16.01.2014	duodenum	-	-
PD 14-02	22.01.2014	duodenum	-	-
PD 14-03	28.01.2014	duodenum	-	-
PD 14-04	17.02.2014	duodenum	w	51
PD 14-05	18.02.2014	duodenum	w	37
PD 14-06	19.02.2014	duodenum	-	-
PD 14-07	08.04.2014	duodenum	w	37
PD 14-08	10.04.2014	duodenum	w	43
PD 14-09	07.05.2014	duodenum	m	41
PD 14-10	08.05.2014	duodenum	-	-
PD 14-11	20.05.2014	duodenum	-	-
PD 14-12	11.06.2014	duodenum	w	58
PD 14-13	08.07.2014	duodenum	-	-
PD 14-14	17.07.2014	duodenum	w	35
PD 14-15	22.07.2014	duodenum	-	-
PD 14-16	29.07.2014	duodenum	w	45
PD 14-17	05.08.2014	duodenum	w	35
PD 14-18	07.08.2014	duodenum	w	46
PD 14-19	19.08.2014	duodenum	-	-
PD 14-20	07.10.2014	duodenum	w	21
PD 14-21	11.11.2014	duodenum	w	37
PD 14-22	28.11.2014	duodenum	w	34
PD 14-23	09.12.2014	duodenum	w	53
PD 14-24	10.12.2014	duodenum	w	40

PD 14-25	12.12.2014	duodenum	m	56
PD 15-01	28.01.2015	duodenum	m	52
PD 15-02	17.05.2015	duodenum	w	57
PD 15-03	10.03.2015	duodenum	w	37
PD 15-04	19.03.2015	duodenum	w	51
PD 15-05	23.04.2015	duodenum	m	66
PD 15-06	16.06.2015	duodenum	w	30
PD 15-07	05.08.2015	duodenum	w	65
PD 15-08	11.08.2015	duodenum	w	65
PD 15-09	22.09.2015	duodenum	w	24
PD 15-10	24.09.2015	duodenum	w	56
PD 15-11	30.09.2015	duodenum	w	58
PD 15-12	07.10.2015	duodenum	w	32

9.2 Curriculum Vitae

Matthias Oliver Schweinlin

Born on 26 November 1985 in Lörrach, Germany

Address: Rennweger Ring 14

97070 Würzburg (Germany)

matthias.schweinlin@uni-wuerzburg.de

Education

Since Jan 2012	University Hospital Würzburg, Germany
	Department of Tissue Engineering & Regenerative Medicine
	PhD-student (Dr. rer. nat.)
Oct 2006 – Dec 2011	University of Hohenheim
	Diploma with distinction in Nutrition Science
	Main subject: Cell biology/Tissue Engineering
Oct 2002 – Jun 2005	High School, Müllheim, Germany

Research Experience

Jan 2011 - Dec 2015	University Hospital Würzburg, Germany
	Department of Tissue Engineering & Regenerative Medicine
	Participant of the BMBF project PeTrA (platform for efficient epithelial transport of pharmaceutical applications by innovative particulate carrier system)
	PhD thesis: "Development of a human primary in vitro model of the small intestine"
	Supervision: Prof. Dr. Heike Walles
	Prof. Dr. Stefan Störk
	PD Dr. Beate Niesler

Jan 2010 – Sep 2010	Fraunhofer IGB, Stuttgart, Germany
	Diploma thesis: „Development and characterization of a porcine intestinal in vitro model"
	Supervision: Prof. Dr. Heike Walles
	Prof. Dr. Lutz Graeve

Professional Experience

Jan 2011 – present	University of Würzburg, Germany
	Advising and teaching students
2010	DSM, Basel, Switzerland
	Department for Analytics, Internship (9 weeks)
	Topic: Analysis of bacterial supernatant by HPLC
Oct 2005 – Jun 2006	Malteserschloßschule in Heitersheim, Germany
	Civilian service at a school for physically and mentally disabled Children

……………………………………….   ……………………………………………

 Place, Date   Signature

9.3 Publications and conference contributions

Articles

Sebastian Schuerlein, Thomas Schwarz, Steffan Krziminski, Sabine Gätzner, Anke Hoppensack, Ivo Schwedhelm, Matthias Schweinlin, Heike Walles, Jan Hansmann. A versatile modular bioreactor platform for Tissue Engineering. 5. August 2016.

Matthias Schweinlin, Sabine Wilhelm, Ivo Schwedhelm, Jan Hansmann, Rene Ritscher, Christian Jurowich, Heike Walles, Marco Metzger (2016). Development of an advanced primary human in vitro model of the small intestine. TISSUE ENGINEERING: Part C Volume 22, Number 9, 2016

Matthias Schweinlin, Angela Rossi, Nina Lodes, Christian Lotz, Stephan Hackenberg, Maria Steinke, Heike Walles, Florian Groeber (2016). Human barrier models for the in vitro assessment of drug delivery. Journal: "Drug Delivery and Translational Research (DDTR)". Published online 22. August 2016.

Baleeiro, R.B., Schweinlin, M., Rietscher, R., Diedrich, A., Czaplewska, J.A., Metzger, M., Lehr, C.M., Scherließ, R., Hanefeld, A., Gottschaldt, M. and Walden, P. (2015). Nanoparticle-based mucosal vaccines targeting tumor-associated antigens to human dendritic cells. Journal of Biomedical Nanotechnology. 12/p. 1-17/2016.

Kristin Schacht, ‡ , Tomasz Jüngst, ‡ , Matthias Schweinlin, Dr. Andrea Ewald, Prof. Dr. Jürgen Groll and Prof. Dr. Thomas Scheibe (2015). Biofabrication of Cell-Loaded 3D Spider Silk Constructs. Angew. Chem. Int. Ed. 2015, 54, S.1–6.

Angela Rossi, David Fecher, Sebastian Egner, Matthias Schweinlin, Maria Steinke (2014). Humane 3D-in vitro-Testsysteme für die präklinische Forschung. BIOspektrum | 04.14 | 20. Jahrgang

Oral presentations

M. Schweinlin, M. Steinke, F. Groeber, R. Gross, C. Reuter, K. Seidensticker, L. Schulte, M. Metzger, M. Engstler, H. Walles (2016, Linz, Austria). 3D in vitro tissue models for infection studies with human pathogens. European Society f. Alternatives to Animal Testing (EUSAAT2016 annual congress on 24-27 August 2016)

M. Schweinlin, L. Engelhardt, R. Seliger, F. Schmied, H. Walles, F. Groeber (2016, Regensburg, Germany). Impedance Spectroscopy: A new tool to characterize reconstructed human epidermis. 3rd Conference on Impedance-Based Cellular Assays.

M. Schweinlin; S.Wilhelm; H. Walles; M. Metzger (2015, Dresden, Germany). Improved primary 3D in vitro model of the human small intestine. Crossing Biological Barriers – Advances in Nanocarrier Design for Targeted Drug Delivery.

M. Schweinlin, M. Metzger et al. (2015, Würzburg, Germany). Development of an improved primary in vitro model of the human small intestine as alternative for cell line based models. 4th International Conference "Strategies in Tissue Engineering" in Würzburg.

M. Schweinlin, M. Metzger et al. (2013, Freising, Germany). Development of more predictive intestinal in vitro models. 20. Annual Meeting of the German Society of Neurogastroenterology and Motility (DGNM).

Posters

3th International Conferences: Strategies in Tissue Engineering, 23.-25.05.2012, Würzburg, Germany, title: "Establishment of primary human gut models in vitro"

EPOS 2012, 16.-17.10.2012, Würzburg, Germany, title: "Establishment of primary human gut models in vitro"

EMBO/ EMBL Symposium, 27.-30.08.2014, Heidelberg, Germany, title: „Development of an improved primary in vitro model of the human small intestine as alternative for cell line-based models"

Forum Life Science 2015, 11./12.03.2015, Garching, Germany, title: "Development of an improved primary in vitro model of the human small intestine as alternative for cell line-based models"

4th TERMIS World Congress, 08.-11.09.2015, Boston, USA, title: Development of an Improved Primary in vitro Model of the Human Small Intestine"

9th Seeon Conference, 24.-26.06.2016, Seeon, Germany, title: Microbiota, Probiotics and Host: "Development of an improved primary in vitro model of the human small intestine"

9.4 Danksagung

Den Mitarbeitern des Lehrstuhls TERM danke ich für die Unterstützung und tolle Arbeitsatmosphäre.

Angela Rossi danke ich für die tolle und lockere Atmosphäre in unserem kleinen Büro. Auf deine Rat, deine Unterstützung und Hilfe kann ich immer zählen. Unser Büro ist das BESTE!

Dr. Jan Hansmann und Ivo Schwedhelm danke ich für die Hilfe und den Rat in allen technischen Belangen und der Erstellung der Simulationen. Insbesondere bedanke ich mich bei Thomas Schwarz für seine Hilfe bei der Weiterentwicklung der Bioreaktoren und Offenheit für Vorschläge von Laien!

Danken möchte Mona Alzheimer für die stets fruchtbaren fachlichen Gespräche, ihren Rat und die Korrektur meiner Arbeit.

Ich danke der Volleyball Herrenmannschaft der TSV Jahn 1892 Würzburg für den Ausgleich und die Ablenkung.

Vielmals danken möchte ich Veronika Städele und Holger Kirch für das Korrekturlesen meiner Arbeit.

Meinen Eltern danke ich von ganzem Herzen für ihre uneingeschränkte Unterstützung und ihr Vertrauen auf meinem Weg. Auf euren Rückhalt, die Aufmunterungen und den Rat kann ich immer zählen. Von euch habe ich so viel gelernt. Ihr seid der Grund dass ich all dies erreichen konnte. Danke!

9.5 Affidavit

I hereby confirm that my thesis entitled "Development of advanced human intestinal in vitro models" is the result of my own work. I did not receive any help or support from commercial consultants. All sources and/or materials applied are listed and specified in the thesis.

Furthermore, I confirm that this thesis has not yet been submitted as part of another examination process neither in identical nor in similar form.

…………………………………………….   ……………………………………………

 Place, Date   Signature

9.6   Eidesstaatliche Erklärung

Hiermit erkläre ich an Eides statt, die Dissertation „Entwicklung von erweiterten humanen intestinalen in vitro Modellen" eigenständig, d.h. insbesondere selbständig und ohne Hilfe eines kommerziellen Promotionsberaters, angefertigt und keine anderen als die von mir angegebenen Quellen und Hilfsmittel verwendet zu haben.

Ich erkläre außerdem, dass die Dissertation weder in gleicher noch in ähnlicher Form bereits in einem anderen Prüfungsverfahren vorgelegen hat.

……………………………………… ……………………………………………

 Ort, Datum   Unterschrift